UNIVERSIDADE FEDERAL DE MINAS GERAIS
Instituto de Ciências Exatas
Programa de Pós-graduação em Física

Marcos Gabriel Alpino da Silva

MULTIPARTITE ENTANGLEMENT IN TENSOR NETWORKS

Belo Horizonte
2025

Marcos Gabriel Alpino da Silva

MULTIPARTITE ENTANGLEMENT IN TENSOR NETWORKS

Dissertação apresentada ao Programa de Pós-graduação em Física do Instituto de Ciências Exatas da Universidade Federal de Minas Gerais como requisito parcial para obtenção do título de Mestre em Ciências.

Orientador: Reinaldo Oliveira Vianna

Belo Horizonte

2025

Dados Internacionais de Catalogação na Publicação (CIP)

S586m Silva, Marcos Gabriel Alpino da.
Multipartite entanglement in tensor networks / Marcos Gabriel Alpino da Silva. – 2025.
99 f. : il.

Orientador: Reinaldo Oliveira Vianna.
Dissertação (mestrado) – Universidade Federal de Minas Gerais, Departamento de Física.
Bibliografia: f. 88-95.

1. Mecânica quântica. 2. Emaranhamento. 3. Transições de fases. I. Título. II. Vianna, Reinaldo Oliveira. III. Universidade Federal de Minas Gerais, Departamento de Física.

CDU – 530.145 (043)

Ficha catalográfica elaborada por Romário Martins Ribeiro – CRB6 3595
Biblioteca Professor Manoel Lopes de Siqueira – Departamento de Física - UFMG

UNIVERSIDADE FEDERAL DE MINAS GERAIS

ATA

ATA DA SESSÃO DE ARGUIÇÃO DA 765ª DISSERTAÇÃO DO PROGRAMA DE PÓS-GRADUAÇÃO EM FÍSICA, DEFENDIDA POR MARCOS GABRIEL ALPINO DA SILVA orientado pelo professor Reinaldo Oliveira Vianna para obtenção do grau de **MESTRE EM FÍSICA, área de concentração Física.** Às quatorze horas do dia dois de julho de dois mil e vinte e cinco reuniu-se, presencialmente, a Comissão Examinadora composta pelos professores **Reinaldo Oliveira Vianna** (Orientador - Departamento de Física/UFMG), **Carlos Henrique Monken** (Departamento de Física/UFMG) e **Emmanuel Araújo Pereira** (Departamento de Física/UFMG), para dar cumprimento ao Artigo 37 do Regimento Geral da UFMG, submetendo **MARCOS GABRIEL ALPINO DA SILVA** à arguição de seu trabalho de dissertação, que recebeu o título de **"Multipartite Entanglement In Tensor Networks".** O candidato fez uma exposição oral de seu trabalho durante aproximadamente 50 minutos. Após esta, os membros da comissão prosseguiram com a sua arguição, e apresentaram seus pareceres individuais sobre o trabalho, concluindo pela aprovação do candidato.

Belo Horizonte, 02 de julho de 2025.

Prof. Reinaldo Oliveira Vianna
Orientador do estudante
Departamento de Física/UFMG

Prof. Carlos Henrique Monken
Departamento de Física/UFMG

Prof. Emmanuel Araújo Pereira
Departamento de Física/UFMG

CANDIDATO: Marcos Gabriel Alpino da Silva

Documento assinado eletronicamente por **Emmanuel Araujo Pereira**, **Membro de comissão**, em 02/07/2025, às 16:31, conforme horário oficial de Brasília, com fundamento no art. 5º do Decreto nº 10.543, de 13 de novembro de 2020.

Documento assinado eletronicamente por **Marcos Gabriel Alpino da Silva**, **Usuário Externo**, em 02/07/2025, às 18:56, conforme horário oficial de Brasília, com fundamento no art. 5º do Decreto nº 10.543, de 13 de novembro de 2020.

Documento assinado eletronicamente por **Reinaldo Oliveira Vianna**, **Professor do Magistério Superior**, em 04/07/2025, às 10:14, conforme horário oficial de Brasília, com fundamento no art. 5º do Decreto nº 10.543, de 13 de novembro de 2020.

Documento assinado eletronicamente por **Carlos Henrique Monken**, **Professor do Magistério Superior**, em 09/07/2025, às 18:25, conforme horário oficial de Brasília, com fundamento no art. 5º do Decreto nº 10.543, de 13 de novembro de 2020.

A autenticidade deste documento pode ser conferida no site https://sei.ufmg.br/sei/controlador_externo.php?acao=documento_conferir&id_orgao_acesso_externo=0, informando o código verificador **4340221** e o código CRC **39C2D607**.

Referência: Processo nº 23072.240312/2025-72 SEI nº 4340221

Aqueles que partiram para Pasárgada
e deixaram para trás duas dores:
a sua, e a de quem ficou.
Esta dissertação é dedicada à memória dos que se foram e ao amor dos que permanecem.

Agradecimentos

- Às agências de fomento CNPq, CAPES e FAPEMIG, pelo incentivo à ciência brasileira;
- Ao meu orientador, Reinaldo O. Vianna, pelas conversas, pelo carinho e pelo ensino;
- À minha grande amiga, avó e mãe, Edna Passoni Alpino, pelo carinho, apoio e amor;
- À minha namorada, Júlia Paula Rabelo, pelo apoio nos momentos de dificuldade, pelas aulas de desenho que possibilitaram a entrega dos diagramas presentes neste texto, e pelo amor;
- Ao meu Senhor Jesus Cristo, que morreu na cruz pelos meus pecados.

Resumo

A caracterização de transições de fase quânticas por meio de métodos baseados em emaranhamento tem se consolidado como uma estrutura poderosa para a compreensão do comportamento crítico em sistemas unidimensionais. Nesta dissertação, foi investigada a estrutura do emaranhamento genuinamente multipartido em cadeias de spins-1/2 invariantes por translação, utilizando-se o algoritmo Variational Uniform Matrix Product States (VUMPS) para o cálculo do estado fundamental do modelo quântico de Ising com campo transversal no limite termodinâmico. Mostrou-se que a multinegatividade associada à célula unitária diverge de forma logarítmica na vizinhança do ponto crítico, configurando-se como um indicador sensível, baseado em emaranhamento de muitas partes, da transição de fase. Adicionalmente, propôs-se uma formulação alternativa para a redução de estados quânticos, na qual medições locais projetivas substituem o traço parcial convencional. No contexto dessa abordagem, introduziu-se a noção de *redução não tendenciosa*, definida como um procedimento que minimiza o viés informacional e preserva as propriedades estruturais do estado global. Essa ideia foi explorada por meio da análise da multinegatividade e da coerência quântica dos estados reduzidos sob diferentes direções de projeção. Resultados numéricos preliminares sustentam a conjectura de que projeções realizadas em bases ortogonais ao parâmetro de ordem induzem mínima perturbação e máxima coerência local, permitindo, assim, o acesso a propriedades globais por meio de dados locais pós-medição.

Palavras-chave: Teoria Quântica da Informação; Emaranhamento Multipartido; Transições de Fase Quânticas; Redes de Tensores; Redução Não Tendenciosa.

Abstract

The characterization of quantum phase transitions through entanglement-based methods has emerged as a powerful framework for understanding critical behavior in low-dimensional quantum systems. In this dissertation, the structure of genuinely multipartite entanglement in translationally invariant spin-1/2 chains is investigated using the Variational Uniform Matrix Product States (VUMPS) algorithm to compute the ground state of the quantum transverse-field Ising model in the thermodynamic limit. It is shown that the multipartite negativity associated with the unit cell diverges logarithmically at criticality, thus serving as a sensitive entanglement-based indicator of the quantum phase transition. Furthermore, an alternative framework for quantum state reduction is proposed, in which local projective measurements replace the conventional partial trace. Within this approach, a notion of *unbiased reduction* is introduced—defined as a procedure that minimizes informational bias and preserves the structural properties of the global state. This idea is operationalized by analyzing the behavior of multipartite negativity and quantum coherence of the reduced states under different local projection directions. Numerical evidence supports the conjecture that projections in bases orthogonal to the system's order parameter induce minimal disturbance and maximal coherence, thereby revealing global properties from post-measurement data. These findings point to new possibilities for inferring inaccessible features of quantum many-body states from local information.

Keywords: Quantum Information Theory; Multipartite Entanglement; Quantum Phase Transitions; Tensor Networks; Unbiased State Reduction.

Contents

1 INTRODUCTION 11
1.1 Foundations of Quantum Theory and Quantum Information 11
1.2 Information in Many-Body and Condensed Matter Systems 13

2 FUNDAMENTALS OF QUANTUM INFORMATION THEORY . . 17
2.1 Statistical Description of Quantum Theory: Density Operators . . 18
2.1.1 Spectral Decomposition and State Purity 19
2.2 Composite Systems and Tensor Product Structure 20
2.2.1 Bipartite Quantum Systems 21
2.2.2 Realization of Entangled States 25
2.3 Quantifying Bipartite Entanglement 26
2.3.1 Motivation and Axiomatic Requirements 26
2.3.2 Entanglement Measures for Pure States 27
2.3.3 Entanglement Measures for Mixed States 28
2.3.3.1 Entanglement of Formation 28
2.3.3.2 Concurrence and the Two-Qubit Case 29
2.3.3.3 Negativity and Logarithmic Negativity 31
2.3.4 Comparison Between Entanglement Measures and Operational Remarks . 32
2.4 Entanglement Witnesses for Bipartite Systems 33
2.4.1 Definition and Geometric Interpretation 33
2.4.2 Characterization and Construction 34
2.5 Multipartite Entanglement 36
2.5.1 Motivation and Conceptual Challenges 36
2.5.2 Classification of Multipartite States 36
2.5.3 Measures and Monotonicity in the Multipartite Setting 38
2.6 Multinegativity and Entanglement Witnesses in Many-Body Systems 40
2.6.1 Definition and Convex Roof Structure 40
2.6.2 Application to Many-Body Systems and Phase Transitions 40

3 PHASE TRANSITIONS 42
3.1 Classical Phase Transitions 42
3.1.1 Phase Transition on Ising Model (Classical) 44
3.2 Quantum Phase Transitions 46
3.2.1 Spin Chains 47
3.2.1.1 Solving one-dimensional Quantum Spin Chains 47
3.2.1.2 Boundary Terms and Periodic Conditions 51

3.2.1.3 Parity Sectors Diagonalization 54

4 TENSOR NETWORKING FORMALISM 59
4.1 Fundamental Concepts 59
4.1.1 Matrix Product State 59
4.1.1.1 Gauge Freedom and Canonical Form 61
4.1.2 Matrix Product Operator 63
4.2 Algorithms Based on Tensor Networks 65
4.2.1 Density Matrix Renormalization Group (DMRG) 66
4.2.2 Variational Uniform Matrix Product States (VUMPS) 69
4.2.2.1 Optimization Problem 71

5 ENTANGLEMENT ANALYSIS OF QUANTUM SPIN CHAINS . . 76
5.1 Model Definition 76
5.1.1 Numerical Results and Validation of the Simulation 77
5.2 Multipartite Entanglement Structure of the Unit Cell 80
5.3 Towards Unbiased Quantum State Reductions 82
5.4 Final Remarks and Perspectives 86

BIBLIOGRAPHY 88

APPENDIX 96

APPENDIX A – DIGRESSION ON THE COMPUTATIONAL PROBLEMS 97

1 Introduction

1.1 Foundations of Quantum Theory and Quantum Information

Since the earliest developments of quantum theory, foundational questions concerning its conceptual structure have sparked profound debates and enduring interest. From its inception, quantum mechanics challenged the classical worldview, confronting physicists with phenomena that resisted intuitive interpretation. Particularly striking were issues related to the completeness of the quantum description, the role of measurement, and the nature of reality itself. Among the most famous illustrations of these conceptual tensions is the Einstein–Podolsky–Rosen (EPR) paradox, proposed in 1935 [1], which aimed to demonstrate that quantum mechanics must be incomplete unless it could be reconciled with a theory possessing both realism and locality.

In response, Niels Bohr offered a vigorous defense of quantum theory, invoking his principle of complementarity to argue that the apparent contradictions highlighted by EPR stem from a misunderstanding of the quantum formalism [2]. Bohr emphasized that the properties of quantum systems are not independent of the experimental context in which they are measured, a view that stood in stark contrast to the classical notions of objective reality. This exchange marked a significant chapter in the foundational discourse of quantum mechanics, exemplifying the deep philosophical divide between the Copenhagen interpretation and Einstein's vision of a deterministic and local physical theory.

The debate between Einstein and Bohr persisted for decades, with Einstein famously remarking that "God does not play dice with the universe", expressing his discomfort with the inherent randomness and probabilistic nature of quantum mechanics [3, 4]. Bohr, in turn, is reported to have replied, "Einstein, stop telling God what to do". These dialogues underscore not only the depth of the conceptual tensions within quantum theory but also the richness of its philosophical implications—debates that continue to inspire inquiry and interpretation to this day [5–7].

In the same period, alternative interpretations emerged, e.g. Bohmian mechanics, which posits the existence of hidden variables that determine the outcomes of quantum measurements [8,9]. These early efforts were primarily philosophical in nature, motivated by the desire to restore a classical-like ontology to the emerging quantum formalism. However, the landscape changed dramatically with the advent of John Bell's theorem in the 1960s. In this work, Bell showed that no theory based on local hidden variables can reproduce all the predictions of quantum mechanics [10]. This result provided a concrete way to distinguish quantum mechanics from classical realist theories through experimentally testable inequalities.

In the decades that followed, experimental tests of Bell inequalities, culminating in loophole-free violations, confirmed the nonlocal nature of quantum correlations [11–13]. This provided strong evidence that quantum theory, as understood in its standard formulation, cannot be both local and

realistic in the sense defined by the EPR framework [14]. These breakthroughs not only resolved long-standing philosophical disputes, but also laid the foundation for a new understanding of entanglement as a fundamental and physically testable phenomenon. Indeed, the importance of these results was recognized in 2022 with the awarding of the Nobel Prize in Physics to Alain Aspect, John Clauser, and Anton Zeilinger, for their pioneering experiments on entangled photons and the violation of Bell inequalities [15].

Within this evolving intellectual and experimental landscape, quantum entanglement, once regarded as a paradoxical feature, has come to be recognized as one of the most fundamental aspects of quantum theory [16, 17]. Far from being a mere theoretical curiosity, entanglement is now understood as a defining property of quantum systems, responsible for nonclassical correlations that cannot be explained within any classical probabilistic framework [18]. Its formal study has produced rigorous criteria for distinguishing separable from entangled states [19], as well as operational measures for quantifying different forms of quantum correlations [20–23]. These advances have not only deepened of the conceptual understanding of quantum theory but also enabled practical applications in quantum communication, metrology, and computation [24–26].

More significantly, entanglement is now viewed through the lens of quantum information theory (QIT) as a physical resource (on par with energy) that enables tasks classically unattainable. Examples include:

- Quantum teleportation, which enables the transfer of an unknown quantum state between distant parties using previously shared entangled states, without any physical transmission of the state itself [24].
- Superdense coding, which allows the transmission of two classical bits by sending a single qubit, contingent on prior entanglement [25].
- Quantum key distribution (QKD), with protocols such as BB84 [27] and Ekert's [28] exploiting quantum correlations to achieve provably secure communication [26].
- Quantum-enhanced computation, where entanglement underpins algorithmic speed-ups (e.g., Shor's and Grover's algorithms), quantum error correction, and variational quantum algorithms [25].

Having examined the conceptual trajectory of entanglement and QIT, from its foundational origins to formal and operational maturity, it is now evident that the role of entanglement has evolved far beyond the confines of academic inquiry. In contemporary quantum science, entanglement has become a central resource for emerging technologies with tangible societal and economic impact. For instance, international initiatives such as the European Union's *Quantum Flagship* program and China's deployment of the *Micius* quantum satellite have positioned entanglement at the forefront of efforts to build scalable quantum infrastructures[1]. These initiatives aim to enable unconditionally secure com-

[1] For more information, see the *Quantum Flagship* portal at `https://qt.eu/` and the experimental demonstration in [29].

munication, distributed quantum computation, and non-classical synchronization—key elements of a future quantum internet.

In parallel, advances in experimental platforms (including superconducting circuits, trapped ions, and photonic processors) have culminated in milestone demonstrations of quantum computational advantage, where specific problems were solved exponentially faster than any known classical method [30, 31]. Such achievements critically rely on the ability to coherently generate, manipulate, and stabilize large-scale entangled states.

These developments mark a decisive transition: entanglement is no longer a theoretical abstraction, but a driving force behind applied quantum technologies. A particularly promising application domain is combinatorial and convex optimization, a class of problems ubiquitous in areas such as logistics, finance, and operations research. Quantum semidefinite programming solvers [32] and quantum interior-point methods [33] exemplify how entanglement and quantum parallelism can offer provable speed-ups for certain optimization tasks.

In the context of finance, this potential has spurred a growing literature on quantum-enhanced methods for portfolio optimization, option pricing, risk assessment, and Monte Carlo simulations [34–36]. For instance, variational quantum algorithms and quantum annealing have been investigated for solving the mean-variance optimization problem under realistic market constraints. These approaches exploit entanglement to explore large solution spaces more efficiently than classical heuristics, opening new pathways for high-frequency trading, asset allocation, and real-time decision-making in volatile markets.

1.2 Information in Many-Body and Condensed Matter Systems

In a more foundational perspective, QIT offers profound insights when its conceptual and mathematical tools are applied to condensed matter systems. At first glance, the task of describing interacting quantum many-body systems from first principles is notoriously difficult. The exponential growth of the Hilbert space with system size renders exact simulations intractable for all but the most trivial cases. Nevertheless, despite this computational complexity, it is often physically meaningful (indeed essential) to inquire how quantum correlations are distributed, structured, and constrained among the constituent parts of such systems.

This informational perspective underscores the relevance of correlation measures such as entanglement entropy, mutual information, and fidelity susceptibility [17, 37–39]. These quantities offer powerful tools for characterizing quantum states beyond the reach of conventional observables and order parameters. In particular, they can unveil universal features associated with criticality and phase transitions, as well as detect qualitative changes in the ground state structure that may not manifest in local observables.

A paradigmatic illustration of the power of informational tools arises in systems exhibiting

topological order, where no local order parameter suffices to distinguish between distinct phases [40]. In these cases, entanglement-based quantities, most notably the topological entanglement entropy [41], constitute the primary diagnostic tools for identifying the underlying phase structure. More generally, such measures have been instrumental in uncovering hidden orders, elucidating the physics of many-body localization, and characterizing critical scaling behavior in the vicinity of quantum phase transitions [42].

Crucially, the applicability of these approaches is not restricted to systems with topological or exotic phases. Even in well-established fermionic models, e.g. the Hubbard, $1D$-free fermions, and extended Hubbard models, entanglement measures have emerged as valuable indicators of quantum criticality and competing many-body effects. Specifically, the scaling of bipartite entanglement entropy and the fine structure of the entanglement spectrum provide sensitive probes of correlation-induced transitions and emergent long-range entanglement. Within this context, several studies have demonstrated how entropic diagnostics can identify phase boundaries and reveal qualitative features of the ground state that are not captured by conventional observables [43, 44].

These developments underscore a growing recognition: entanglement is not merely an abstract mathematical artifact of the quantum formalism, but a physically meaningful quantity that encodes structural and universal properties of complex quantum systems. As such, QIT offers a rigorous language and a powerful computational toolkit for addressing longstanding challenges in condensed matter physics from a fundamentally new perspective. This conceptual shift departs from the traditional scope of atomic, molecular, and optical physics (wich often focuses on few-body systems in finely controlled environments) moves toward a broader framework, increasingly referred to as *modern condensed matter physics*[2].

Having established the relevance of QIT within the broader context of many-body physics, the present dissertation proceeds to examine how distinct manifestations of entanglement (specifically, bipartite and genuinely multipartite forms) may be systematically employed to enhance the understanding of quantum correlations in low-dimensional systems. Particular emphasis is placed on the analysis of ground-state properties and critical behavior in one-dimensional spin-$1/2$ chains. Within this setting, the transverse-field quantum Ising model[3] is adopted as a paradigmatic case study. This model not only furnishes a minimal and conceptually transparent framework for investigating quantum phase transitions (QPts), but also admits both analytical and numerical tractability, thereby enabling the controlled exploration of entanglement measures across different quantum regimes.

As will be clear in the next chapter, the bipartite entanglement measures have long been employed as diagnostics for correlation and criticality, growing evidence suggests that these tools capture

[2] The designation *modern condensed matter physics* is increasingly used to distinguish contemporary approaches from canonical treatments of condensed matter. While traditional texts such as [45, 46] emphasize band theory, phonons, and symmetry-breaking orders, modern treatments, as exemplified by [47], incorporate concepts from quantum information, and non-equilibrium dynamics. Notably, entire textbooks now adopt this terminology, such as [48], which foregrounds topological phases, gauge structures, and long-range entanglement as central organizing principles.

[3] Or simple quantum Ising model (QIM).

only a fraction of the rich structure present in many-body quantum states. In particular, they may fail to detect nontrivial collective phenomena that arise from the interplay of correlations distributed across multiple parties. To address this limitation, the present work focuses on the emergence of genuinely multipartite entanglement in the ground state, its scaling behavior in the vicinity of the quantum critical point, and its potential role as a universal indicator of phase transitions. In doing so, entanglement is approached not merely as a mathematical construct, but as a physically grounded quantity capable to encoding the structural reorganizations that accompany fundamental changes in the phase of quantum matter.

To facilitate this investigation, the ground state of the system will be approximated using the framework of uniform Matrix Product States (uMPS), a variational class of states particularly well-suited for describing translationally invariant one-dimensional systems in the thermodynamic limit [49–51]. This tensor network-based approach not only enables the efficient representation of quantum states that obey the area law for entanglement[4], but also provides a natural setting in which entanglement measures can be computed with high precision. Since quantum phase transitions are, by definition, transitions that occur in the ground state as a function of a continuous parameter.

Furthermore, it is worth noting that, despite the apparent limitation of MPS representations to states with low entanglement, this restriction is not a drawback in practice. On the contrary, several rigorous results have demonstrated that physically relevant ground states of local Hamiltonians (those that are of interest for condensed matter) typically obey area laws and can be faithfully approximated by MPS of polynomial bond dimension [53, 54]. In particular, it has been shown that the set of MPS approximates the ground states of gapped one-dimensional systems with arbitrary precision, and that even critical (gapless) systems can be efficiently captured with moderate bond dimensions due to logarithmic corrections to the area law [55]. These findings justify the use of uMPS not only as a computationally efficient method but also as a physically grounded representation for analyzing quantum correlations in many-body systems.

The remainder of this dissertation is organized as follows:

Chapter 2 lays the conceptual groundwork by reviewing the mathematical formalism of QIT. The density matrix is introduced as a fundamental object for describing quantum states, followed by a detailed discussion of entanglement theory. Special attention is given to bipartite and multipartite entanglement measures such as the von Neumann entropy, negativity, and multinegativity.

Chapter 3 presents the theory of quantum phase transitions (QPTs), highlighting their distinctive features in comparison to classical phase transitions. It discusses how criticality arises from nonanalytic behavior in the ground-state energy and correlation functions, induced by quantum fluctuations.

[4] The *area law* refers to the scaling behavior of entanglement entropy in ground states of local Hamiltonians, where the entropy of a subsystem scales with the size of its boundary rather than its volume. In one-dimensional systems with gapped Hamiltonians, this implies that the entanglement entropy saturates to a constant, allowing for efficient representation via tensor networks such as Matrix Product State (MPS) [52]. In contrast, *volume law* states exhibit entropy that grows proportionally to the volume of the subsystem, as is typical for thermal states or highly excited eigenstates, rendering MPS-based descriptions inefficient.

The chapter introduces a selection of exactly solvable models—particularly the transverse-field Ising and XY models—as paradigmatic systems for understanding QPTs in one-dimensional settings.

Chapter 4 develops the tensor network formalism, with emphasis on the MPS representation. The efficiency of MPS in capturing ground states of gapped one-dimensional systems is discussed in light of area-law entanglement scaling. The chapter proceeds with a formal introduction to variational optimization techniques based on tensor networks, focusing on the Variational Uniform Matrix Product State (VUMPS) algorithm as a robust tool for studying infinite, translationally invariant systems in the thermodynamic limit.

Chapter 5 contains the core results of this dissertation. Building upon the theoretical and numerical tools introduced in the preceding chapters, the behavior of both bipartite and genuinely multipartite entanglement is investigated across the phase diagram of the transverse-field quantum Ising model. In particular, the multinegativity is employed as a quantifier of multipartite entanglement within the unit cell of the uniform MPS in the thermodynamic limit. A central finding is that the multinegativity diverges logarithmically near the quantum critical point, thereby serving as a robust, entanglement-based diagnostic of critical behavior in many-body systems. Furthermore, an alternative framework for quantum state reduction is proposed, in which partial trace is replaced by local projective measurements. This approach gives rise to the notion of *unbiased reduction*, defined as a procedure that preserves the structural and informational features of the global quantum state with minimal disturbance. The operational implications of this idea are explored through numerical simulations of quantum coherence and multipartite entanglement under different local projection schemes.

2 Fundamentals of Quantum Information Theory

Quantum mechanics (QM) is often first introduced through the concept of the *wave function*, typically in the context of single-particle systems in one-dimensional space. This approach, as presented in textbooks such as Eisberg and Resnick [56], relies on the interpretation of the squared modulus of the wave function, $|\psi(x)|^2$, as the probability density for finding the particle within the interval $[x, x + \mathrm{d}x]$. In this picture, the quantum state is described by a complex-valued function $\psi(x)$ defined over configuration space, satisfying a normalization condition and evolving under the Schrödinger equation.

While pedagogically valuable and historically foundational, this formulation is limited in scope. It is best suited for systems with continuous degrees of freedom and becomes increasingly inadequate when extended to more general quantum systems — such as spin chains, multipartite configurations, or scenarios involving entanglement and statistical uncertainty.

In more advanced and modern treatments of QM, students are introduced to a more abstract and general framework based on Dirac's notation, in which physical preparations are represented by normalized vectors $|\psi\rangle$ in a complex vectorial space with an internal product structure, in general denoted by $\mathscr{H}$ [57–60][1].

However, even this vector-based description is insufficient for many physically relevant scenarios. In particular, it fails to fully describe systems prepared in statistical mixtures, or those interacting with an environment — that is, systems which are not isolated. In such cases, a more complete notion of quantum state must be employed: the *density operator* [61–63]. This formalism is fully defined by the following postulates:

Postulate 2.1: Formal Description of Dynamical Variables [61]

To each dynamical variable $\mathscr{A}$, there corresponds a Hermitian operator A, whose eigenvalues represent the possible outcomes of a measurement of $\mathscr{A}$. The expectation value of $\mathscr{A}$ in a physical ensemble described by the density operator ρ is given by:

$$\langle A \rangle := \mathrm{Tr}(\rho A), \tag{2.1}$$

[1] Within this new approach, the wave function $\psi(x)$ is understood as the coordinate representation of the state vector in the position basis: $\psi(x) := \langle x|\psi\rangle$.

Postulate 2.2: Formal description of states [61]

To each physical state, ρ, there corresponds a unique state operator, which must be Hermitian ($\rho = \rho^\dagger$), nonnegative ($\rho \geq 0$), and of unit trace ($\mathrm{Tr}(\rho) = 1$).

2.1 Statistical Description of Quantum Theory: Density Operators

In this work, the primary focus lies on finite-dimensional Hilbert spaces. In this setting, the set of all physically valid quantum states is described by the set of *density matrices*:

Definition 2.1: The set of density operators

Let $\mathscr{B}(\mathscr{H})$ denote the set of bounded linear operators acting on a finite-dimensional Hilbert space $\mathscr{H}$. The set of density operators is defined as:

$$\mathscr{D}(\mathscr{H}) = \left\{\rho \in \mathscr{B}(\mathscr{H}) \;\middle|\; \rho \geq 0,\ \mathrm{Tr}(\rho) = 1, \rho^\dagger = \rho\right\}. \tag{2.2}$$

The elements of $\mathscr{D}(\mathscr{H})$ are typically classified into two distinct categories:

Definition 2.2: Pure states

A quantum state ρ is said to be *pure* if the physical preparation it represents corresponds to a completely known quantum state. Mathematically, this is the case when ρ has rank one, and it can be written in terms of a normalized vector $|\psi\rangle \in \mathscr{H}$ as:

$$\rho = |\psi\rangle\langle\psi|. \tag{2.3}$$

Definition 2.3: Mixed states

A state ρ is said to be *mixed* if it cannot be represented by a single vector in $\mathscr{H}$. This situation reflects statistical uncertainty or lack of complete information about the preparation procedure. Formally, a mixed state admits a convex decomposition of the form

$$\rho = \sum_i p_i |\psi_i\rangle\langle\psi_i|, \tag{2.4}$$

where $p_i \geq 0$, $\sum_i p_i = 1$, and $|\psi_i\rangle \in \mathscr{H}$ are not necessarily orthogonal nor linearly independent.

This decomposition highlights an important structural property of the space of quantum states: the set $\mathscr{D}(\mathscr{H})$ admits convex combinations of its elements. In fact, this set possesses the following fundamental geometric feature:

Lemma 2.1: Convexity of the set of density operators

The set $\mathscr{D}(\mathscr{H})$ of density operators is convex.

Proof. Let $\rho_1, \rho_2 \in \mathscr{D}(\mathscr{H})$, and let $\lambda \in [0, 1]$. Define

$$\rho = \lambda\rho_1 + (1 - \lambda)\rho_2.$$

Since both ρ_1 and ρ_2 are positive semidefinite operators, and the set of positive semidefinite operators is closed under convex combinations, it follows that $\rho \geq 0$. Moreover, using linearity of the trace:

$$\mathrm{Tr}(\rho) = \lambda\,\mathrm{Tr}(\rho_1) + (1 - \lambda)\,\mathrm{Tr}(\rho_2) = \lambda + (1 - \lambda) = 1.$$

Therefore, $\rho \in \mathscr{D}(\mathscr{H})$, and $\mathscr{D}(\mathscr{H})$ is convex. □

2.1.1 Spectral Decomposition and State Purity

A fundamental result in linear algebra, the *spectral theorem*, guarantees that any Hermitian operator acting on a finite-dimensional Hilbert space admits a diagonal representation in an orthonormal basis. Since every density operator $\rho \in \mathscr{D}(\mathscr{H})$ is Hermitian by definition, it follows that:

Theorem 2.1: Spectral Decomposition of Density Operators

Let $\rho \in \mathscr{D}(\mathscr{H})$ be a density operator on a Hilbert space $\mathscr{H}$. Then there exists an orthonormal basis $\{|e_i\rangle\} \subset \mathscr{H}$ and a probability distribution $\{\lambda_i\}$, i.e., $\lambda_i \geq 0$ and $\sum_i \lambda_i = 1$, such that:

$$\rho = \sum_i \lambda_i \, |e_i\rangle\langle e_i| \,. \tag{2.5}$$

The coefficients λ_i are the eigenvalues of ρ, and each $|e_i\rangle$ is the corresponding eigenvector.

This decomposition is unique up to degeneracies in the spectrum of ρ, and highlights the fact that every quantum state can be interpreted as a classical mixture of orthogonal pure states [61].

Thus, the spectral representation provides a natural setting for quantifying the degree of mixedness of a quantum state, as it reveals the eigenvalue spectrum $\{\lambda_i\}$, which directly encodes the statistical weights of the constituent pure states in the mixture. A commonly used measure for this purpose is the *purity*, defined as follows:

Definition 2.4: State purity

The *purity* of a quantum state ρ is defined as

$$\gamma(\rho) \coloneqq \mathrm{Tr}\left(\rho^2\right). \tag{2.6}$$

It satisfies $0 < \gamma(\rho) \leq 1$, with $\gamma(\rho) = 1$ if and only if ρ is pure, and $\gamma(\rho) < 1$ for mixed states [25].

Particularly, the purity reaches its minimum value $\gamma(\rho) = 1/d$ when $\rho = \mathbb{I}/d$, the maximally mixed state in a Hilbert space of dimension $d = \dim(\mathscr{H})$. In experimental quantum information processing, purity is commonly used as an indicator of decoherence or noise. For instance, a decrease in purity can signal the interaction of a system with its environment, resulting in the degradation of quantum coherence. Measuring purity is particularly relevant in quantum state tomography, where estimating $\mathrm{Tr}(\rho^2)$ can be more feasible than reconstructing the full state.

2.2 Composite Systems and Tensor Product Structure

One of the foundational aspects of quantum theory is its treatment of composite systems. When multiple quantum systems are considered jointly, the total Hilbert space is no longer given by a direct sum, as in classical probability theory, but rather by a *tensor product* of individual Hilbert spaces [62].

Definition 2.5: Tensor Product Structure

Let $\mathscr{H}_1, \mathscr{H}_2, \ldots, \mathscr{H}_n$ be the Hilbert spaces associated with subsystems $1, 2, \ldots, n$. The total Hilbert space of the composite system is given by

$$\mathscr{H}_{\text{tot}} = \mathscr{H}_1 \otimes \mathscr{H}_2 \otimes \cdots \otimes \mathscr{H}_n. \tag{2.7}$$

Example 2.1: Spin Chains as Composite Systems

Consider a quantum spin chain of L sites, where each local site corresponds to a two-level system (qubit), represented by $\mathbb{C}^2$. The total Hilbert space of the chain is then given by the tensor product

$$\mathscr{H}_{\text{chain}} = \bigotimes_{i=1}^{L} \mathbb{C}^2. \tag{2.8}$$

Each basis element of $\mathscr{H}_{\text{chain}}$ corresponds to a configuration such as $|0\rangle_1 \otimes |1\rangle_2 \otimes \cdots \otimes |0\rangle_L$, typically abbreviated as $|01\cdots0\rangle$.

This tensor product rule reflects the fact that quantum systems exhibit correlations — including entanglement[2] — that cannot be captured by classical probability distributions over Cartesian products.

In this formalism, the distinction between local and global properties becomes essential. Operators that characterize global properties of the quantum system typically cannot be expressed in a simple tensor product form, $A \otimes B \otimes \cdots$, reflecting intrinsic nonlocality. Moreover, quantum states can exhibit robust correlations that span spatially separated subsystems, known as quantum correlations. This intricate structure underlies fundamental questions within Quantum Information Theory (QIT), particularly those regarding the distribution and sharing of quantum information across subsystems. Such considerations naturally motivate the detailed analysis of bipartite systems, which constitute the foundational units for rigorously exploring concepts like entanglement, separability criteria, and the theoretical framework of local quantum operations and classical communication (LOCC)[3].

2.2.1 Bipartite Quantum Systems

The simplest nontrivial scenario in which quantum correlations manifest is that of a bipartite quantum system. Consider two subsystems, denoted as A and B, each associated with respective Hilbert spaces $\mathscr{H}_A$ and $\mathscr{H}_B$. The composite Hilbert space for the joint system AB is then defined as the tensor product

$$\mathscr{H}_{AB} = \mathscr{H}_A \otimes \mathscr{H}_B. \tag{2.9}$$

A density operator ρ_{AB}, describing the joint state of the system, resides within the set of density operators $\mathscr{D}(\mathscr{H}_{AB})$. A central question in QIT pertains to the distribution of quantum information between subsystems, specifically addressing whether the state ρ_{AB} can be decomposed into a mixture of product states, thereby determining its separability or entanglement properties:

[2] To be defined in the next subsection.

[3] Local Operations and Classical Communication (LOCC) refer to a class of physically implementable operations on quantum systems, where each party is allowed to perform quantum operations locally on their subsystem and communicate classically with the others. LOCC protocols form the standard framework for resource theories of entanglement, as entangled states cannot be created from separable ones using only LOCC.

Definition 2.6: Product and separable states

A pure state $|\psi_{AB}\rangle \in \mathscr{H}_{AB}$ is called a *product state* if it can be written as

$$|\psi_{AB}\rangle = |\psi_A\rangle \otimes |\psi_B\rangle \,, \tag{2.10}$$

for some $|\psi_A\rangle \in \mathscr{H}_A$ and $|\psi_B\rangle \in \mathscr{H}_B$. Otherwise, it is called an *entangled state*.
More generally, a mixed state $\rho_{AB} \in \mathscr{D}(\mathscr{H}_{AB})$ is said to be *separable* if it can be written as a convex combination of product states:

$$\rho_{AB} = \sum_i p_i \, \rho_A^{(i)} \otimes \rho_B^{(i)}, \tag{2.11}$$

where $p_i \geq 0$, $\sum_i p_i = 1$, and $\rho_A^{(i)} \in \mathscr{D}(\mathscr{H}_A)$, $\rho_B^{(i)} \in \mathscr{D}(\mathscr{H}_B)$. If no such decomposition exists, the state is said to be *entangled*.

The foregoing definition establishes a formal criterion for distinguishing between separable and entangled bipartite quantum states. However, this immediately gives rise to a fundamental and highly nontrivial question: given an arbitrary quantum state, how can it be determined whether the state is separable or entangled? Addressing this question has been one of the central challenges in QIT, prompting the development of a variety of operational and algebraic criteria aimed at characterizing separability.

Among the most prominent and extensively employed techniques in this context is the concept of *partial transposition*, which was first introduced by Peres and subsequently refined through the work of the Horodecki family. Before this notion can be formally introduced, an essential functional operation must be defined:

Definition 2.7: Partial Transposition

Let $\rho_{AB} \in \mathscr{D}(\mathscr{H}_A \otimes \mathscr{H}_B)$ be a density operator with matrix elements $\rho_{ij,kl} = \langle i_A j_B | \rho_{AB} | k_A l_B \rangle$. The *partial transpose* of ρ_{AB} with respect to subsystem B, denoted $\rho_{AB}^{T_B}$, is defined by

$$\langle i_A j_B | \rho_{AB}^{T_B} | k_A l_B \rangle = \langle i_A l_B | \rho_{AB} | k_A j_B \rangle. \tag{2.12}$$

In other words, the transposition is applied only to the indices corresponding to subsystem B.

The partial transposition was used to define the following separability criterion:

Theorem 2.2: Peres–Horodecki Separability Criterion (PPT Theorem)

Let $\rho_{AB} \in \mathscr{D}(\mathscr{H}_A \otimes \mathscr{H}_B)$ be a bipartite quantum state. If ρ_{AB} is separable, then its partial transpose $\rho_{AB}^{T_B}$ is positive semi-definite. Moreover, when $\dim(\mathscr{H}_A) \times \dim(\mathscr{H}_B) \leq 6$, that is, in 2×2 and 2×3 dimensional systems, the converse also holds: positivity of the partial transpose is both a necessary and sufficient condition for separability.

Proof. Suppose that the state $\rho_{AB} \in \mathscr{D}(\mathscr{H}_A \otimes \mathscr{H}_B)$ is separable. By definition, there exists a convex decomposition of the form

$$\rho_{AB} = \sum_i p_i \, \rho_A^{(i)} \otimes \rho_B^{(i)},$$

where $\rho_A^{(i)} \in \mathscr{D}(\mathscr{H}_A)$, $\rho_B^{(i)} \in \mathscr{D}(\mathscr{H}_B)$, and $\{p_i\}$ is a probability distribution. The partial transpose with respect to subsystem B is given by

$$\rho_{AB}^{T_B} = \sum_i p_i \, \rho_A^{(i)} \otimes \left(\rho_B^{(i)}\right)^{\mathsf{T}}.$$

Since the transpose operation preserves positivity for Hermitian matrices, each $\left(\rho_B^{(i)}\right)^{\mathsf{T}}$ is positive semi-definite. Then, the tensor product of two positive operators is positive, and convex combinations of positive operators remain positive. Hence, $\rho_{AB}^{T_B} \geq 0$.

To prove sufficiency for 2×2 and 2×3 systems, it must be shown that any state ρ_{AB} with a positive partial transpose in these dimensions is necessarily separable. This result was rigorously demonstrated by the Horodecki family [19], using advanced techniques from matrix theory and positive maps. The key idea involves characterizing positive but not completely positive maps and showing that, in these low-dimensional cases, the partial transposition captures the full structure of entanglement witnesses[4]. In higher dimensions, the existence of bound entangled states with positive partial transpose renders the PPT condition only necessary, but not sufficient. Therefore, the PPT criterion provides both a necessary and sufficient condition for separability if and only if $\dim(\mathscr{H}_A) \times \dim(\mathscr{H}_B) \leq 6$. □

Another fundamental construct in the study of composite quantum systems is the notion of *reduced states*—that is, the density operators associated with individual subsystems. These arise naturally through the mathematical operation known as the *partial trace*, which effectively eliminates the degrees of freedom corresponding to one or more components of the full system. The partial trace is essential when one is interested in the local properties of a subsystem or in describing situations where only partial information about the global system is accessible[5].

[4] This notion will be formal defined in few sections.

[5] Although most commonly introduced in the bipartite setting, the partial trace is not limited to two-party systems. It generalizes naturally to multipartite scenarios, where one traces out arbitrary subsets of subsystems to obtain reduced density operators on the remaining components.

Definition 2.8: Partial Trace

Given a bipartite quantum system described by the density operator $\rho_{AB} \in \mathscr{D}(\mathscr{H}_A \otimes \mathscr{H}_B)$, the *partial trace* over subsystem B is the linear map

$$\mathrm{Tr}_B : \mathscr{D}(\mathscr{H}_A \otimes \mathscr{H}_B) \to \mathscr{D}(\mathscr{H}_A), \tag{2.13}$$

characterized by the identity

$$\mathrm{Tr}\left[X_A \ \mathrm{Tr}_B(\rho_{AB})\right] = \mathrm{Tr}\left[(X_A \otimes \mathbb{I}_B)\,\rho_{AB}\right], \tag{2.14}$$

for all observables X_A acting on $\mathscr{H}_A$. The resulting state $\rho_A = \mathrm{Tr}_B(\rho_{AB})$ is called the *reduced state* of subsystem A. Analogously, one defines $\rho_B = \mathrm{Tr}_A(\rho_{AB})$.

Although the partial trace is a purely mathematical operation, it admits a clear operational interpretation: it corresponds to averaging over the outcomes of all possible measurements on the discarded subsystem. In laboratory terms, this reflects the typical experimental situation in which a part of the system is unobserved or inaccessible, and the state of the accessible subsystem is inferred from statistical measurement outcomes.

To elucidate the structure of bipartite entangled states, one of the most emblematic examples in QIT may be considered: the Bell state $|\Phi^+\rangle$[6]. By evaluating its reduced states, it becomes evident how entanglement is encoded in the local subsystems, despite the global state being pure.

Example 2.2: Reduced States of an Entangled Bell State

Let the Bell state be defined as

$$\left|\Phi^+\right\rangle = \frac{1}{\sqrt{2}}\left(|00\rangle + |11\rangle\right), \tag{2.15}$$

with associated density operator $\rho_{AB} = |\Phi^+\rangle\langle\Phi^+|$. The reduced state of subsystem A is obtained by performing the partial trace over subsystem B:

$$\rho_A = \mathrm{Tr}_B(\rho_{AB}) = \frac{1}{2}\left(|0\rangle\langle 0| + |1\rangle\langle 1|\right) = \frac{\mathbb{I}_2}{2}. \tag{2.16}$$

Hence, although the global state ρ_{AB} is pure, the reduced state ρ_A is maximally mixed. This property exemplifies a key feature of quantum entanglement: the incompatibility between global purity and local purity.

[6] The complete set of Bell states is given by $|\Phi^\pm\rangle = \frac{1}{\sqrt{2}}(|00\rangle \pm |11\rangle)$ and $|\Psi^\pm\rangle = \frac{1}{\sqrt{2}}(|01\rangle \pm |10\rangle)$. These states form an orthonormal basis for the bipartite Hilbert space $\mathscr{H}_2 \otimes \mathscr{H}_2$, and are maximally entangled. They constitute the Bell basis and play a fundamental role in quantum communication and computation protocols.

2.2.2 Realization of Entangled States

While entanglement is a central concept in the mathematical structure of quantum theory, it also plays a crucial role in experimental implementations of quantum technologies. The ability to generate, manipulate, and measure entangled states is a prerequisite for tasks such as quantum teleportation, quantum key distribution, and universal quantum computation [16, 24, 25].

In practice, entangled states can be realized across a variety of physical platforms. One of the most established and widely used is quantum optics, where entangled photons are routinely generated via nonlinear optical processes such as *spontaneous parametric down-conversion* (SPDC) [64]. In SPDC, a single photon entering a nonlinear crystal can spontaneously decay into two lower-energy photons—commonly referred to as *signal* and *idler* — whose polarizations, momenta, or frequencies exhibit strong quantum correlations. By appropriately filtering and post-selecting the photon pairs, one can produce high-quality entangled states such as the Bell state $|\Phi^+\rangle$ where $|0\rangle$ and $|1\rangle$ may correspond, for instance, to horizontal and vertical polarizations.

Beyond photonic systems, entanglement has also been demonstrated in trapped ions [65], superconducting qubits [66], cold atoms in optical lattices [67], and nitrogen-vacancy (NV) centers in diamond [68]. In these platforms, interactions between qubits — either engineered or naturally present — are used to implement quantum gates that generate entangled states from initially separable ones. A paradigmatic example is the controlled-NOT (CNOT) gate, which, when applied to the input $|+\rangle\,|0\rangle$, produces the entangled state $|\Phi^+\rangle$ [69]. The generation of such states via quantum logic gates forms the backbone of most architectures for quantum computing [70].

Importantly, the creation of entangled states is typically followed by verification protocols, such as quantum state tomography [71] or the violation of Bell inequalities [11], to confirm the presence and quality of entanglement. These experimental procedures not only certify the successful preparation of quantum resources but also enable the benchmarking of devices for quantum information processing.

2.3 Quantifying Bipartite Entanglement

2.3.1 Motivation and Axiomatic Requirements

In the previous section, the concept of entangled quantum states was formally introduced within the bipartite framework. A distinction was established between separable and entangled states, and operational tools such as the Peres–Horodecki criterion, based on partial transposition, were discussed to determine whether a given density operator $\rho_{AB} \in \mathscr{D}(\mathscr{H}_A \otimes \mathscr{H}_B)$ is entangled.

In this context, a natural question arises: *how much entangled a state is?* While the detection of entanglement is essential, it does not provide a complete characterization of the quantum resources encoded in the state. A quantitative assessment of entanglement allows for a more nuanced understanding of its operational significance and enables comparisons among different states. In particular, resource-based approaches in QIT rely on the amount of entanglement to determine the cost and feasibility of implementing communication protocols such as quantum teleportation, entanglement distillation, and entanglement-assisted computation [26].

In order to serve as a meaningful and physically consistent indicator of quantum correlations, any function $E : \mathscr{D}(\mathscr{H}_A \otimes \mathscr{H}_B) \to \mathbb{R}_{\geq 0}$ proposed as an *entanglement measure* is expected to satisfy a set of axiomatic requirements [20, 62]:

1. Vanishing on separable states: It is required that $E(\rho_{AB}) = 0$ whenever ρ_{AB} is separable. This ensures that only genuinely entangled states are assigned a nonzero value.

2. Monotonicity under LOCC: It must be ensured that entanglement cannot be increased by means of LOCC protocols, that is,

$$E(\Lambda_{\text{LOCC}}[\rho_{AB}]) \leq E(\rho_{AB}), \tag{2.17}$$

   for every LOCC operation Λ_{LOCC}. This condition reflects the physical intuition that entanglement cannot be generated through operations restricted to local agents.

3. Convexity: It is generally required that the entanglement measure be convex, so that classical mixing does not artificially increase entanglement:

$$E\left(\sum_i p_i \rho_{AB}^{(i)}\right) \leq \sum_i p_i E(\rho_{AB}^{(i)}), \tag{2.18}$$

   where $\{p_i\}$ denotes a probability distribution and $\rho_{AB}^{(i)}$ are density operators on the composite Hilbert space.

4. Reduction to the von Neumann entropy for pure states: For pure states $|\psi_{AB}\rangle$, the measure should reduce to the von Neumann entropy of the reduced state:

$$E(|\psi_{AB}\rangle\langle\psi_{AB}|) = S(\rho_A), \quad \text{where } \rho_A = \text{Tr}_B(|\psi_{AB}\rangle\langle\psi_{AB}|). \tag{2.19}$$

This condition ensures that the entanglement of pure bipartite states is uniquely characterized by the entropy of their marginal states.

Although not all measures satisfy all of the above properties simultaneously, these axioms serve as foundational guidelines by which the operational and mathematical validity of a proposed entanglement quantifier may be assessed. In the following subsections, several widely used entanglement measures will be introduced and analyzed in light of these requirements.

2.3.2 Entanglement Measures for Pure States

For bipartite quantum systems prepared in pure states, the quantification of entanglement is conceptually simpler and admits a unique characterization. Let $|\psi_{AB}\rangle \in \mathscr{H}_A \otimes \mathscr{H}_B$ denote a pure state of the composite system. Due to the Schmidt decomposition[7] , it can always be written in the canonical form

$$|\psi_{AB}\rangle = \sum_{i=1}^{r} \sqrt{\lambda_i}\, |e_i\rangle_A \otimes |f_i\rangle_B \,, \tag{2.20}$$

where $\{|e_i\rangle_A\}$ and $\{|f_i\rangle_B\}$ are orthonormal bases in $\mathscr{H}_A$ and $\mathscr{H}_B$, respectively, $\lambda_i > 0$ are the Schmidt coefficients, and $r \leq \min(\dim \mathscr{H}_A, \dim \mathscr{H}_B)$ is the Schmidt rank.

This decomposition implies that the reduced density matrices $\rho_A = \mathrm{Tr}_B(|\psi_{AB}\rangle\langle\psi_{AB}|)$ and $\rho_B = \mathrm{Tr}_A(|\psi_{AB}\rangle\langle\psi_{AB}|)$ share the same non-zero spectrum, namely $\{\lambda_i\}$. As a consequence, any entropy functional evaluated on the reduced state provides a consistent measure of the entanglement content of $|\psi_{AB}\rangle$.

To proceed with a quantitative characterization of bipartite entanglement in pure states, it is essential to first introduce the von Neumann entropy, a central functional in QIT that quantifies the degree of mixedness of a quantum state:

Definition 2.9: von Neumann Entropy

Given a density operator ρ acting on a finite-dimensional Hilbert space, the *von Neumann entropy* (vNE) associated with ρ is defined as

$$S(\rho) := -\,\mathrm{Tr}\,(\rho \log \rho)\,. \tag{2.21}$$

This quantity quantifies the uncertainty or mixedness of the quantum state ρ, and reduces to the Shannon entropy in the eigenbasis of ρ.

[7] The Schmidt decomposition of a pure bipartite state $|\psi_{AB}\rangle \in \mathscr{H}_A \otimes \mathscr{H}_B$ can be obtained by first tracing out one of the subsystems to compute the reduced density matrix, e.g., $\rho_A = \mathrm{Tr}_B(|\psi_{AB}\rangle\langle\psi_{AB}|)$. Since ρ_A is positive semi-definite and Hermitian, it admits a spectral decomposition $\rho_A = \sum_i \lambda_i |e_i\rangle\langle e_i|_A$, where $\{\lambda_i\}$ are the eigenvalues and $\{|e_i\rangle_A\}$ the corresponding orthonormal eigenvectors. The original state $|\psi_{AB}\rangle$ can then be written in the canonical Schmidt form $|\psi_{AB}\rangle = \sum_i \sqrt{\lambda_i}\, |e_i\rangle_A \otimes |f_i\rangle_B$, where $\{|f_i\rangle_B\}$ are orthonormal states in $\mathscr{H}_B$ obtained by projecting $|\psi_{AB}\rangle$ onto $\{|e_i\rangle_A\}$. The set $\{\lambda_i\}$ constitutes the *Schmidt spectrum*, and fully determines the entanglement properties of $|\psi_{AB}\rangle$.

This entropy functional plays a central role in quantum information theory, and, in particular, provides a natural measure of bipartite entanglement for pure states. Since the reduced density operators of a pure state $|\psi_{AB}\rangle$ share the same non-zero spectrum, the entropy of either subsystem fully characterizes the entanglement of the global state.

Definition 2.10: Entropy of Entanglement

The *entropy of entanglement* (EoE) of a bipartite pure state $|\psi_{AB}\rangle \in \mathscr{H}_A \otimes \mathscr{H}_B$ is defined as the von Neumann entropy of either of its reduced density matrices:

$$E(|\psi_{AB}\rangle\langle\psi_{AB}|) \coloneqq S(\rho_A) = S(\rho_B), \tag{2.22}$$

where $\rho_A = \mathrm{Tr}_B(|\psi_{AB}\rangle\langle\psi_{AB}|)$ and $\rho_B = \mathrm{Tr}_A(|\psi_{AB}\rangle\langle\psi_{AB}|)$.

The EoE satisfies all the axiomatic properties discussed in Section 2.3.1, and uniquely quantifies the amount of quantum correlations in $|\psi_{AB}\rangle$. It vanishes if and only if the state is separable, and reaches its maximal value $\log d$ when the reduced state is maximally mixed, with $d = \min(\dim \mathscr{H}_A, \dim \mathscr{H}_B)$.

2.3.3 Entanglement Measures for Mixed States

For mixed states $\rho_{AB} \in \mathscr{D}(\mathscr{H}_A \otimes \mathscr{H}_B)$, the quantification of entanglement is considerably more subtle. This increased complexity arises from the fact that mixed states can exhibit both classical and quantum correlations, which are not straightforwardly disentangled in general. Thus, unlike pure states, which are uniquely specified by their Schmidt coefficients, mixed states admit infinitely many convex decompositions into pure-state ensembles, leading to intrinsic ambiguities in attributing entanglement content.

While for pure states the vNE of the reduced density matrix offers a unique and unambiguous measure of entanglement, no single functional enjoys such a universally canonical status in the mixed-state regime. Instead, a variety of entanglement quantifiers have been introduced, each grounded in different physical motivations and exhibiting distinct operational and computational properties.

2.3.3.1 Entanglement of Formation

One of the most conceptually natural measures of mixed-state entanglement is the *entanglement of formation* (EoF). This measure captures the minimal entanglement cost — expressed in terms of pure entangled states — required to asymptotically prepare a given mixed state using only LOCC. For instance, if a mixed state ρ_{AB} arises as the reduced state of a noisy or decohered entangled system, the EoF quantifies the minimal number of Bell pairs needed, on average, to recreate ρ_{AB} through LOCC - based preparation. It is formally defined as follows:

Definition 2.11: Entanglement of Formation

The entanglement of formation of a mixed state ρ_{AB} is defined by

$$E_F(\rho_{AB}) \coloneqq \inf \sum_i p_i \, S(\rho_A^{(i)}), \tag{2.23}$$

where the infimum is taken over all pure-state ensembles $\rho_{AB} = \sum_i p_i \left|\psi_{AB}^{(i)}\right\rangle\!\left\langle\psi_{AB}^{(i)}\right|$, and $\rho_A^{(i)} = \mathrm{Tr}_B\left(\left|\psi_{AB}^{(i)}\right\rangle\!\left\langle\psi_{AB}^{(i)}\right|\right)$ denotes the reduced state of each pure component.

The EoF is a convex functional, vanishes on separable states, and reduces to the EoE when ρ_{AB} is pure. Despite its conceptual elegance and strong operational meaning, the evaluation of E_F is generally computationally intractable, as it requires an optimization over all possible pure-state ensemble decompositions of ρ_{AB}. This task is difficult because the set of such decompositions is uncountably infinite and lacks a closed parametrization, rendering standard variational methods inefficient or impractical in most cases.

2.3.3.2 Concurrence and the Two-Qubit Case

A notable simplification arises in the case of two-qubit systems ($\dim \mathscr{H}_A = \dim \mathscr{H}_B = 2$). In this setting, a closed-form expression for the entanglement of formation was derived by Wootters [22], based on an auxiliary quantity known as the *concurrence*, which captures the entanglement content of arbitrary mixed states in $\mathbb{C}^2 \otimes \mathbb{C}^2$.

Definition 2.12: Concurrence for Two-Qubit States

Let $\rho \in \mathscr{D}(\mathbb{C}^2 \otimes \mathbb{C}^2)$. The *concurrence* $C(\rho)$ is defined as

$$C(\rho) \coloneqq \max\{0, \lambda_1 - \lambda_2 - \lambda_3 - \lambda_4\}, \tag{2.24}$$

where $\{\lambda_i\}$ are the square roots, arranged in decreasing order, of the eigenvalues of the non-Hermitian matrix

$$\tilde{R} = \rho\,\tilde{\rho}, \qquad \text{with } \tilde{\rho} = (\sigma_y \otimes \sigma_y)\rho^*(\sigma_y \otimes \sigma_y), \tag{2.25}$$

and where ρ^* denotes complex conjugation in the computational basis. The concurrence takes values in the interval $[0, 1]$, vanishing for separable states and reaching unity for maximally entangled pure states.

Once the concurrence $C(\rho)$ has been determined, the entanglement of formation can be computed via a closed-form expression involving the binary entropy function. This provides a rare example of an exact and computable entanglement measure for mixed states.

Definition 2.13: Entanglement of Formation via Concurrence

For a two-qubit state $\rho \in \mathscr{D}(\mathbb{C}^2 \otimes \mathbb{C}^2)$, the *entanglement of formation* is given by

$$E_F(\rho) = h\left(\frac{1+\sqrt{1-C(\rho)^2}}{2}\right), \tag{2.26}$$

where $C(\rho)$ is the concurrence, and $h(x)$ is the binary entropy function

$$h(x) := -x\log_2 x - (1-x)\log_2(1-x). \tag{2.27}$$

This functional is monotonically increasing with $C(\rho)$, ranging from 0 to 1, and reflects the asymptotic entanglement cost of preparing ρ under LOCC protocols. The structure of the formula reveals a formal similarity with the so-called *linear entropy*, defined as $S_L(\rho) = 1 - \mathrm{Tr}(\rho^2)$, in that both quantify deviation from purity in terms of squared quantities. However, while linear entropy captures general mixedness, the concurrence is tailored specifically to entanglement.

Example 2.3: Entanglement of Formation of a Werner State

Consider the Werner state

$$\rho_W(p) = p\left|\Psi^-\right\rangle\!\left\langle\Psi^-\right| + (1-p)\frac{\mathbb{I}_4}{4}, \qquad 0 \le p \le 1, \tag{2.28}$$

where $|\Psi^-\rangle = \frac{1}{\sqrt{2}}(|01\rangle - |10\rangle)$ is a singlet state. For this family, the concurrence is given by

$$C(\rho_W) = \max\left\{0, \frac{3p-1}{2}\right\},$$

which implies that entanglement is present for $p > \frac{1}{3}$. The entanglement of formation is then obtained by substituting $C(\rho_W)$ into the formula above. At $p = 1$, the Werner state is pure and maximally entangled, yielding $E_F(\rho_W) = 1$, while for $p \le \frac{1}{3}$, one finds $E_F(\rho_W) = 0$.

This analytic result provides a powerful tool for evaluating entanglement in two-qubit systems, where most entanglement measures become difficult to compute. It also illustrates how operationally motivated quantities - such as the minimum cost of state preparation under LOCC - can be connected to mathematically well-defined and computationally tractable entanglement quantifiers.

Beyond concurrence and EoF, a variety of alternative measures have been developed to capture different geometric, algebraic, or informational aspects of entanglement. These include generalizations based on Rényi and Tsallis entropies [72–74], which introduce parametric families of entropic functionals sensitive to different features of the state's spectrum. Other proposals rely on distance - based measures such as the relative entropy of entanglement [21], fidelity - based metrics, and geometric distances to the set of separable states. Additionally, robustness-type measures quantify the mini-

mal noise required to destroy entanglement, as exemplified by the robustness of entanglement [75].

Each of these approaches emphasizes distinct structural properties of the state space and offers complementary perspectives on the nature of quantum correlations. However, many of them require full state tomography or involve complex numerical optimization, limiting their practical applicability in experimental settings.

To overcome such limitations, the next section will introduce the framework of *entanglement witnesses*, which provides a scalable and physically implementable method for detecting entanglement in mixed bipartite systems using only partial information about the state.

2.3.3.3 Negativity and Logarithmic Negativity

Among the entanglement measures applicable to mixed states, particular attention has been given to those derived from the partial transposition map. Within this class, the *negativity* and the *logarithmic negativity* have been extensively studied due to their ease of computation and clear operational interpretation in terms of distinguishability and entanglement distillation bounds.

Definition 2.14: Negativity

Let $\rho_{AB} \in \mathscr{D}(\mathscr{H}_A \otimes \mathscr{H}_B)$ be a bipartite density operator. The *negativity*, $\mathcal{N}(\rho_{AB})$, is defined as

$$\mathcal{N}(\rho_{AB}) := \frac{\left\|\rho_{AB}^{T_B}\right\|_1 - 1}{2}, \tag{2.29}$$

where $\rho_{AB}^{T_B}$ denotes the partial transpose of ρ_{AB} with respect to subsystem B, and $\|\cdot\|_1$ denotes the trace norm.

This measure quantifies the sum of the absolute values of the negative eigenvalues of the partially transposed state $\rho_{AB}^{T_B}$. In this sense, it directly characterizes the degree to which the Positive Partial Transpose (PPT) criterion is violated. For separable states, the partial transpose is guaranteed to remain positive semidefinite, and hence $\mathcal{N}(\rho_{AB}) = 0$. A nonzero value thus signals the presence of entanglement and can serve as a quantitative indicator of non-separability.

Definition 2.15: Logarithmic Negativity

The *logarithmic negativity* of a bipartite state ρ_{AB} is defined as

$$E_{\mathcal{N}}(\rho_{AB}) := \log_2 \left\|\rho_{AB}^{T_B}\right\|_1, \tag{2.30}$$

where $\|\cdot\|_1$ denotes the trace norm, $\|X\|_1 = \operatorname{Tr}\sqrt{X^\dagger X}$, equal to the sum of the singular values of X.

The logarithmic negativity is an entanglement monotone that provides an upper bound on

the amount of entanglement that can be extracted via distillation protocols under LOCC [23][8]. It is additive and satisfies monotonicity under LOCC, although it does not exhibit convexity. Its primary advantage lies in its computational simplicity: it can be efficiently evaluated for arbitrary mixed states by computing the trace norm of the partial transpose.

Both the negativity $\mathcal{N}(\rho_{AB})$ and the logarithmic negativity $E_{\mathcal{N}}(\rho_{AB})$ depend solely on the spectrum of the partially transposed state, making them numerically stable and tractable for systems of moderate size. Their practical relevance is particularly evident in experimental scenarios, where partial transposition serves as a foundational tool for constructing entanglement witnesses and certifying entanglement without full state tomography.

Although these measures are not faithful - since they fail to detect bound entangled states with positive partial transpose - they nonetheless provide reliable and computable lower bounds on the distillable entanglement. As such, they remain among the most accessible and widely used quantifiers of bipartite entanglement in mixed-state regimes.

2.3.4 Comparison Between Entanglement Measures and Operational Remarks

The variety of entanglement measures introduced above reflects the multifaceted nature of quantum correlations in mixed states. Each measure captures a distinct aspect of entanglement and is grounded in different operational or mathematical motivations. It is therefore instructive to compare these measures in terms of their properties, computational feasibility, and applicability in both theoretical and experimental contexts.

The *entropy of entanglement*, defined for pure states, provides an unambiguous and unique characterization. Its extension to mixed states via the *entanglement of formation* preserves some of this interpretational clarity, but at the cost of high computational complexity due to the required optimization over pure-state decompositions. In contrast, the *concurrence* offers a tractable solution for two-qubit systems, yielding an explicit formula for the entanglement of formation in that specific setting.

The *negativity* and *logarithmic negativity* stand out for their simplicity and computational accessibility. These measures rely on the spectral properties of the partially transposed density matrix and can be evaluated efficiently. While they may fail to detect bound entangled states (i.e., states with positive partial transpose that are nevertheless entangled), they remain valuable tools in scenarios where full state tomography or convex roof constructions are impractical.

From an operational perspective, different entanglement measures are associated with distinct information-theoretic or thermodynamic interpretations. For instance, the entanglement of formation quantifies the cost of creating a given mixed state from pure entangled pairs under LOCC, while the logarithmic negativity bounds the number of Bell pairs that can be distilled in an asymptotic set-

[8] Entanglement distillation refers to the process by which multiple copies of a weakly entangled mixed state are transformed, through LOCC operations, into a smaller number of highly entangled pure states, typically Bell pairs. This process is central to quantum communication and entanglement purification schemes.

ting. It should be emphasized, however, that no single measure universally captures all features of entanglement across all regimes.

Entanglement Measure	LOCC Monotone	Convex	Efficiently Computable
Entropy of Entanglement	Yes	Yes	Yes (pure states only)
Entanglement of Formation	Yes	Yes	No (except for 2×2)
Concurrence (2 qubits)	Yes	Yes	Yes
Negativity	Yes	Yes	Yes
Logarithmic Negativity	Yes	No	Yes

Table 1 – Qualitative comparison of selected bipartite entanglement measures. Criteria include monotonicity under LOCC, convexity, and computational tractability.

In light of these considerations, the choice of an appropriate entanglement measure must be guided by the specific physical scenario, the dimensionality of the system, and the available computational or experimental resources. In practice, it is often desirable not only to quantify entanglement but also to detect its presence reliably in situations where complete state knowledge is unavailable.

To address this challenge, a powerful and widely applicable approach is offered by the framework of *entanglement witnesses*. These are Hermitian observables tailored to detect the entanglement of specific states or families of states, and will be the subject of the next section.

2.4 Entanglement Witnesses for Bipartite Systems

In many practical scenarios, the full reconstruction of the density matrix via quantum state tomography is either infeasible or inefficient, especially as the system dimension increases. To circumvent this limitation, the concept of an *entanglement witness* was introduced as an operationally accessible method for identifying entangled states without requiring complete state knowledge.

2.4.1 Definition and Geometric Interpretation

The theoretical foundation for entanglement witnesses relies on the geometric properties of the state space. As shown earlier, the set of all density operators $\mathscr{D}(\mathscr{H}_A \otimes \mathscr{H}_B)$ is convex. In other words, the subset $\mathcal{S} \subset \mathscr{D}(\mathscr{H}_A \otimes \mathscr{H}_B)$ consisting of all separable states is also convex, since separability is defined via convex combinations of product states. In addition, $\mathcal{S}$ is closed, and the full state space is compact in finite dimensions. By the Hahn–Banach separation theorem, it follows that for every entangled state $\rho \notin \mathcal{S}$, there exists at least one Hermitian operator that defines a hyperplane separating ρ from $\mathcal{S}$. This observation motivates the following definition.

2.4.2 Characterization and Construction

Every entangled state admits at least one entanglement witness. However, constructing an appropriate witness operator W generally requires some prior knowledge of the target state or its class. In certain cases, families of witnesses can be systematically constructed using the theory of positive but not completely positive maps, as captured by the following general result.

Theorem 2.3: Horodecki Criterion via Witnesses

A mixed state $\rho_{AB} \in \mathscr{D}(\mathscr{H}_A \otimes \mathscr{H}_B)$ is entangled if and only if there exists a Hermitian operator W such that $\mathrm{Tr}(W\rho_{AB}) < 0$ and $\mathrm{Tr}(W\sigma) \geq 0$ for all separable states σ.

This theorem, due to the Horodecki family [19], guarantees that entanglement witnesses provide a universal framework for entanglement detection, even though they do not quantify entanglement. A practical construction method involves designing a witness tailored to a specific target state ρ_0, using the ansatz

$$W = \lambda \mathbb{I} - \rho_0, \tag{2.31}$$

where the scalar $\lambda = \sup_{\sigma \in \mathcal{S}} \mathrm{Tr}(\rho_0 \sigma)$ ensures that W is positive on all separable states, yet negative on ρ_0. Although this guarantees witness validity, the exact computation of λ generally constitutes a difficult convex optimization problem.

Example 2.4: Witness for the Bell State $|\Phi^+\rangle$

Consider the Bell state $|\Phi^+\rangle = \frac{1}{\sqrt{2}}(|00\rangle + |11\rangle)$. A corresponding entanglement witness is given by

$$W_{\Phi^+} = \frac{1}{2}\mathbb{I}_4 - |\Phi^+\rangle\langle\Phi^+|. \tag{2.32}$$

It can be verified that $\mathrm{Tr}(W_{\Phi^+}\sigma) \geq 0$ for all separable states σ, and $\mathrm{Tr}(W_{\Phi^+}\rho) < 0$ for any ρ sufficiently close to $|\Phi^+\rangle\langle\Phi^+|$. This construction demonstrates how a projector-based witness can detect entanglement in the neighborhood of a maximally entangled state.

Example 2.5: Reduction Map and the Reduction Criterion

Another general construction is obtained from the *reduction map*, leading to the witness operator

$$W = \mathbb{I}_A \otimes \rho_B - \rho_{AB}, \tag{2.33}$$

where $\rho_B = \mathrm{Tr}_A(\rho_{AB})$ is the reduced state of subsystem B. If $\rho_{AB} \not\leq \mathbb{I}_A \otimes \rho_B$, then ρ_{AB} must be entangled. This criterion is particularly useful for low-dimensional systems and is related to the positivity of certain positive but not completely positive maps.

Example 2.6: Entanglement Witness for the W State

The three-qubit W state is defined as

$$|W\rangle = \frac{1}{\sqrt{3}} \left(|001\rangle + |010\rangle + |100\rangle \right). \tag{2.34}$$

Although no two-qubit entanglement exists between any pair of subsystems, the state exhibits genuine multipartite entanglement. A witness that detects this property is

$$W_W = \frac{2}{3}\mathbb{I}_8 - |W\rangle\langle W|. \tag{2.35}$$

One can verify that $\mathrm{Tr}(W_W \sigma) \geq 0$ for all biseparable states σ, while $\mathrm{Tr}(W_W |W\rangle\langle W|) = -\frac{1}{3} < 0$. This illustrates the power of witness operators in certifying multipartite entanglement structures beyond simple bipartite separability.

Experimental Implementation and Comparative Remarks

A key advantage of entanglement witnesses lies in their experimental accessibility. Since every witness is a Hermitian operator, its expectation value can, in principle, be estimated via a finite set of measurements. In practice, this typically involves decomposing the witness W into a weighted sum of local observables,

$$W = \sum_j c_j \, A_j \otimes B_j,$$

where each A_j, B_j acts on subsystems A and B, respectively. Such decompositions enable direct measurement on experimental platforms such as trapped ions, photonic circuits, and superconducting qubits — circumventing the need for full quantum state tomography. For this reason, entanglement witnesses have become standard tools for certifying entanglement in noisy intermediate-scale quantum (NISQ) devices.

The table below summarizes a comparative perspective on widely used entanglement criteria:

Criterion	Computable	Complete Detection	Experimentally Accessible
PPT Criterion	Yes (partial transp.)	No (misses PPT - states)	Indirect
Reduction Criterion	Yes	No	Indirect
Ent. Witnesses	Partially (state-dependent)	Yes (in principle)	Yes (local measurements)

Table 2 – Comparison of common entanglement detection methods. While PPT and reduction criteria offer general-purpose algorithms, entanglement witnesses are often better suited for experimental detection and specific state families.

In summary, entanglement witnesses form a versatile framework for the detection of entanglement in both theoretical and practical settings. Their geometric foundation, coupled with experimental viability, makes them indispensable tools in the study and certification of quantum correlations.

2.5 Multipartite Entanglement

2.5.1 Motivation and Conceptual Challenges

While bipartite entanglement is relatively well understood and admits a coherent formal framework with canonical quantifiers and detection criteria, the transition to the multipartite setting introduces profound conceptual and technical challenges. This increased complexity stems not merely from the addition of subsystems, but from the qualitative richness of possible entanglement structures that emerge when three or more parties are involved.

In bipartite systems, entanglement is uniquely characterized by the impossibility of expressing a state as a tensor product, or more generally as a convex combination of such products. In contrast, multipartite systems admit various types of partial separability, leading to a hierarchy of entanglement classes that are not reducible to the bipartite case. For instance, a pure state of three qubits may be entangled across all three parties (genuine multipartite entanglement), or only between a subset of them, even though it is not fully separable. This distinction gives rise to subtle classifications that require refined mathematical tools for their analysis.

To illustrate this point, consider the paradigmatic three-qubit states:

$$|\mathrm{GHZ}\rangle = \frac{1}{\sqrt{2}}\left(|000\rangle + |111\rangle\right), \tag{2.36}$$

$$|W\rangle = \frac{1}{\sqrt{3}}\left(|001\rangle + |010\rangle + |100\rangle\right). \tag{2.37}$$

Although both are genuinely multipartite entangled, they belong to inequivalent entanglement classes under stochastic local operations and classical communication (SLOCC)[9] . The GHZ state displays maximal nonlocal correlations that disappear upon tracing out any subsystem, whereas the W state retains bipartite entanglement upon loss of a qubit. This dichotomy exemplifies the need for a more nuanced understanding of entanglement in multipartite settings.

The study of multipartite entanglement is thus not merely a generalization of the bipartite case, but rather the exploration of an inherently richer landscape. In what follows, a formal classification of multipartite states will be introduced, along with tools for their detection and quantification.

2.5.2 Classification of Multipartite States

In multipartite quantum systems, entanglement cannot be adequately characterized by a single criterion or measure. Instead, it becomes necessary to introduce a hierarchy of separability classes, reflecting the different ways in which quantum correlations may be distributed among the subsys-

[9] Stochastic Local Operations and Classical Communication (SLOCC) correspond to local quantum operations that succeed with nonzero probability, possibly conditioned on classical communication between the parties. Two pure states are said to be SLOCC-equivalent if one can be converted into the other via invertible local operations, even if the process is not deterministic. This notion induces a classification of entangled states into equivalence classes based on their interconvertibility under probabilistic LOCC.

tems. These distinctions are essential for understanding the structure and dynamics of entanglement beyond the bipartite regime.

Let $\mathscr{H} = \bigotimes_{i=1}^{n} \mathscr{H}_i$ denote the Hilbert space of an n-partite quantum system. The classification of a multipartite state $\rho \in \mathscr{D}(\mathscr{H})$ is typically based on the possibility of expressing it as a convex combination of product states over various partitions of the system.

Definition 2.16: Fully Separable State

A mixed state $\rho \in \mathscr{D}(\mathscr{H})$ is said to be *fully separable* if it can be written as a convex combination of product states across all subsystems:

$$\rho = \sum_i p_i \, \rho_1^{(i)} \otimes \rho_2^{(i)} \otimes \cdots \otimes \rho_n^{(i)}, \tag{2.38}$$

where each $\rho_j^{(i)} \in \mathscr{D}(\mathscr{H}_j)$, and $\{p_i\}$ is a probability distribution.

Definition 2.17: Biseparable State

A state ρ is called *biseparable* if it can be written as a convex mixture of pure states, each of which is separable with respect to some bipartition of the system:

$$\rho = \sum_i p_i \, |\psi_i\rangle\langle\psi_i| \,, \qquad |\psi_i\rangle = \left|\phi_A^{(i)}\right\rangle \otimes \left|\phi_B^{(i)}\right\rangle, \tag{2.39}$$

where $A \cup B = \{1, 2, \ldots, n\}$, $A \cap B = \emptyset$, and each bipartition $A|B$ may vary across the decomposition.

Definition 2.18: Genuine Multipartite Entanglement (GME)

A mixed state $\rho \in \mathscr{D}(\mathscr{H})$ is said to be *genuinely multipartite entangled* if it is not biseparable. That is, it cannot be written as a convex mixture of states that are separable with respect to any bipartition.

These definitions induce a natural inclusion hierarchy:

$$\text{Fully separable} \subset \text{Biseparable} \subset \text{Entangled}.$$

GME states lie outside the set of biseparable states and exhibit entanglement across all possible bipartitions.

Example 2.7: Three-Qubit Classification

In the case $n = 3$, the GHZ state

$$|\text{GHZ}\rangle = \frac{1}{\sqrt{2}}(|000\rangle + |111\rangle)$$

is genuinely multipartite entangled, as it cannot be written as a mixture of states separable across any bipartition. In contrast, the state

$$\rho_{\text{bisep}} = \frac{1}{2}\left(|0\rangle\langle 0|_1 \otimes \left|\Phi^+\right\rangle\left\langle\Phi^+\right|_{23} + |1\rangle\langle 1|_1 \otimes \left|\Phi^-\right\rangle\left\langle\Phi^-\right|_{23}\right),$$

where $|\Phi^\pm\rangle = \frac{1}{\sqrt{2}}(|00\rangle \pm |11\rangle)$, is biseparable, as each term is separable under the partition $1|23$, though the state as a whole is still entangled.

This classification reveals the intricate structure of multipartite entanglement and highlights the need for tools capable of identifying and quantifying these various forms of nonclassical correlations. In the next subsection, we discuss detection strategies based on multipartite witnesses and entropic criteria.

2.5.3 Measures and Monotonicity in the Multipartite Setting

Unlike the bipartite case, where the von Neumann entropy of the reduced state provides a natural and unique quantifier of entanglement for pure states, no universally accepted measure exists for genuine multipartite entanglement (GME). This increased complexity arises from the fact that entanglement can be distributed across various partitions and subsystems in structurally inequivalent ways. As a result, multiple measures have been proposed, each emphasizing a particular aspect of the entanglement structure.

Definition 2.19: Average Entropy of Marginals

For a pure state $|\psi\rangle \in \mathscr{H}_1 \otimes \cdots \otimes \mathscr{H}_n$, the *average entropy of marginals* is defined as

$$E_{\text{avg}}(|\psi\rangle) = \frac{1}{n}\sum_{i=1}^{n} S(\rho_i), \tag{2.40}$$

where $\rho_i = \text{Tr}_{\bar{i}}(|\psi\rangle\langle\psi|)$ is the reduced state of subsystem i. This functional quantifies the average delocalization of information and serves as a multipartite generalization of the entropy of entanglement.

Definition 2.20: Meyer–Wallach Measure

The *Meyer–Wallach measure* [76] for a pure state $|\psi\rangle \in (\mathbb{C}^2)^{\otimes n}$ is given by

$$Q(|\psi\rangle) = \frac{4}{n} \sum_{i=1}^{n} \left(1 - \mathrm{Tr}\left[\rho_i^2\right]\right), \tag{2.41}$$

where ρ_i denotes the reduced density matrix of qubit i. This quantity vanishes for product states and reaches its maximum for certain symmetric states exhibiting strong global entanglement.

Definition 2.21: Geometric Entanglement

The *geometric entanglement* of a pure state $|\psi\rangle$ is defined as

$$E_G(|\psi\rangle) = 1 - \max_{|\phi\rangle \in \mathrm{FS}} |\langle\phi|\psi\rangle|^2, \tag{2.42}$$

where FS denotes the set of fully separable pure states. This measure quantifies the minimal overlap with any separable configuration and is particularly amenable to numerical estimation via variational and tensor network methods.

When mixed states are considered, additional care must be taken to distinguish between global entanglement and entanglement confined to certain partitions. In such cases, convex roof extensions of pure-state measures are commonly employed, although their computation is typically intractable for large systems. It should be emphasized that multipartite entanglement measures are generally expected to satisfy monotonicity under stochastic local operations and classical communication (SLOCC)[10]. However, this condition is difficult to verify in practice, and many proposed functionals exhibit monotonicity only under restricted classes of operations.

The absence of a unique, universally accepted measure for multipartite entanglement reflects the structural richness of the phenomenon. Nevertheless, the measures presented here offer powerful tools for analyzing entanglement in complex systems—particularly when their behavior is interpreted within specific operational frameworks.

[10] Stochastic Local Operations and Classical Communication (SLOCC) correspond to local quantum operations that succeed with nonzero probability, possibly conditioned on classical communication between the parties. Two pure states are said to be SLOCC-equivalent if one can be converted into the other via invertible local operations, even if the process is not deterministic. This notion induces a classification of entangled states into equivalence classes based on their interconvertibility under probabilistic LOCC.

2.6 Multinegativity and Entanglement Witnesses in Many-Body Systems

A particularly useful tool for quantifying genuine multipartite entanglement in complex systems is the *genuine multipartite negativity* (GMN). Originally introduced as a monotonic entanglement measure computable via semidefinite programming [77], the GMN has since been analytically characterized for highly symmetric classes of states [78], and has proven useful in a variety of many-body settings, including the detection of quantum phase transitions [78, 79].

2.6.1 Definition and Convex Roof Structure

The GMN is defined through an optimization over fully decomposable entanglement witnesses. For an n-partite quantum state ρ, the renormalized GMN is given by

$$\mathcal{N}_g(\rho) = -\inf_W \mathrm{Tr}(W\rho), \tag{2.43}$$

subject to the constraint that for each bipartition $m|\bar{m}$, the witness W is fully decomposable:

$$W = P_m + Q_m^{T_m}, \quad P_m \geq 0, \quad Q_m \geq 0.$$

Here, T_m denotes partial transposition with respect to the subset m, and the constraints must be satisfied simultaneously for all bipartitions. This optimization can be cast as a semidefinite program (SDP), making $\mathcal{N}_g$ efficiently computable for moderate system sizes. Importantly, the GMN admits a convex roof-like structure:

$$\mathcal{N}_g(\rho) = \min_{\{p_k, \rho_k\}} \sum_k p_k \min_m \mathcal{N}_{m|\bar{m}}(\rho_k), \tag{2.44}$$

where $\mathcal{N}_{m|\bar{m}}(\rho)$ denotes the bipartite negativity across partition $m|\bar{m}$, and the minimization is performed over all convex decompositions of ρ. This interpretation justifies $\mathcal{N}_g$ as a genuine multipartite analogue of the bipartite negativity.

2.6.2 Application to Many-Body Systems and Phase Transitions

One of the most promising applications of the GMN is in the study of entanglement in many-body quantum systems, particularly near criticality. Because $\mathcal{N}_g$ can be efficiently computed via SDP and responds sensitively to changes in the structure of quantum correlations, it provides a practical tool for detecting the emergence of long-range entanglement and identifying critical points in quantum spin chains [79].

In this context, one typically evaluates the GMN on reduced density matrices of contiguous blocks extracted from ground states computed via tensor network methods[11]. The scaling behavior

[11] Tensor network methods are a class of numerical and analytical techniques that represent quantum many-body states using interconnected tensors arranged according to specific graph structures. These representations are particularly effective for describing systems with local entanglement and low entanglement entropy, such as the ground states of one-dimensional gapped Hamiltonians. Further details on the construction and application of these methods will be provided in the subsequent chapters.

and nonanalytic features of $\mathcal{N}_g$ across such blocks offer clear signatures of quantum phase transitions.

Moreover, the GMN can be directly linked to experimental observables through the measurement of its underlying entanglement witnesses. Since fully decomposable witnesses can be expressed as linear combinations of local observables, their expectation values are accessible via local tomography or entanglement certification protocols. This renders the GMN not only a theoretical diagnostic, but also an experimentally relevant figure of merit.

3 Phase Transitions

3.1 Classical Phase Transitions

The primary objective of statistical mechanics (SM) is to provide a rigorous description of macroscopic matter based on fundamental assumptions regarding its microscopic constituents. In the first approach to this problem, one can consider that the laboratory regime consists of a system of approximately 10^{23} interacting particles, whose dynamics are fully governed by a Hamiltonian function defined over the classical phase space (q, p) and evolving according to the Hamilton-Jacobi equations. However, this treatment is impractical, as it involves solving a coupled system in the order of 10^{23} ordinary differential equations, which is computationally infeasible for any quantum or classical computer‘ [80, 81].

In this scenario, the ensemble approach to microstates provides a more tractable and systematic framework for describing the macroscopic behavior of systems. In general, the core idea of the ensemble formalism is to consider a large collection of hypothetical copies of the system, each representing a possible microstate consistent with the given macroscopic constraints. In this context, for both classical and quantum systems in thermal equilibrium, the statistical properties and thermodynamic quantities of interest can be rigorously derived from the partition function. Formally, the connection between the system's Hamiltonian and the partition function is defined as[1]:

Definition 3.1: Partition Function [82]

Let $\{S_i\}$ denote the complete set of accessible microstates of a given physical system, and let $\mathcal{H}[S_i]$ be the Hamiltonian evaluated at microstate S_i. The *partition function* is defined as

$$Z[\{S_i\}] \coloneqq \mathrm{Tr}\left[\exp\left(-\beta\mathcal{H}[S_i]\right)\right], \tag{3.1}$$

where the trace operator $\mathrm{Tr}[\cdot]$ denotes the sum over all microstates S_i, and $\beta \coloneqq 1/T$ is the inverse temperature, with temperature T expressed in natural units (i.e., $k_B = 1$).

As stated in the previous discussion, the partition function fully encapsulates the mathematical and physical characteristics of the system of interest. However, a fundamental challenge remains unresolved: computing the partition function necessitates modeling the energy exchange across the entire system, which requires a well-defined Hamiltonian. In realistic physical systems, the interactions between individual particles are not directly controllable, making it infeasible to construct a complete and exact Hamiltonian. Consequently, from a theoretical perspective, it becomes essential to develop

[1] This expression can be generalized for quantum systems in the later chapters in terms of the transfer operator.

simplified models that effectively capture specific aspects of the system while allowing theoretical predictions to be tested against experimental observations.

In particular, one of the most extensively studied models in statistical physics is the ideal gas, which serves as a foundational framework for understanding thermodynamic behavior under dilute conditions. Despite its analytical simplicity and pedagogical value, the ideal gas model fails to account for phase transitions, as it assumes non-interacting particles that evolve independently within a fixed volume. The absence of interparticle interactions precludes the emergence of collective phenomena such as condensation or liquid-gas coexistence, which are hallmarks of phase transitions in real systems.

A fundamental extension to the ideal gas that incorporates phase transitions into its theoretical framework is the van der Waals model [83]. This model refines the ideal gas description by introducing an effective interparticle attraction and a finite volume exclusion, thereby accounting for the finite size of gas molecules. These modifications enable the emergence of critical behavior and phase coexistence, making the van der Waals model one of the simplest yet physically meaningful approaches to describing phase transitions in fluids.[2]

Talking about fluids, a defining characteristic of them is that their volume inherently depends on the shape and size of the confining container. This property suggests the possibility of modeling the spatial distribution of gas molecules using a discrete lattice structure, where the occupation of each site represents the presence or absence of a molecule. Within this framework, the system's Hamiltonian can be expressed in terms of occupation variables, which distinguish between occupied and unoccupied sites. Specifically, a fluid composed of N particles can be modeled by the Hamiltonian:

$$\mathcal{H}[\{n_i\}] = A\sum_{i=1}^{N} n_i + \frac{1}{2}\sum_{i,j} B_{ij} n_i n_j, \tag{3.2}$$

where A is an externally controllable parameter, B_{ij} represents the interaction strength between particles at sites i and j, and the occupation number n_i assumes values $n_i = 0, 1$, indicating the absence or presence of a particle at site i, respectively.

Defining an auxiliary pseudo-spin variable s_i, defined as $s_i = \pm 1$, such that the occupation variable is written as

$$n_i = \frac{1 + s_i}{2}.$$

The above Hamiltonian is represented in terms of s_i as

$$\mathcal{H}[\{s_i\}] = \frac{AN}{2} + \frac{A}{2}\sum_{i=1}^{N} s_i + \frac{1}{8}\sum_{i,j} B_{ij}(1 + s_i + s_j + s_i s_j). \tag{3.3}$$

[2] A modern and annotated reproduction of van der Waals' original work can be found in [84]. Moreover, it is important to say that the van der Waals model offers a reasonable description of real systems such as carbon dioxide (CO_2), ammonia (NH_3), and other simple molecular gases near the critical point.

By assuming that the interaction is symmetric, i.e., $B_{ij} = B_{ji} = B$, and that interactions occur only between nearest-neighbor sites, the Hamiltonian simplifies to

$$\mathcal{H}[\{s_i\}] = \left(\frac{AN}{2} + \frac{qBN}{8}\right) + \left(\frac{A}{2} + \frac{qB}{4}\right)\sum_{i=1}^{N} s_i + \frac{B}{8}\sum_{\langle i,j\rangle} s_i s_j, \tag{3.4}$$

where q denotes the coordination number, i.e., the number of nearest neighbors per site, and $< i, j >$ in the summation symbol means that the sum is over all nearest neighbors.

Within this formalism, s_i can be understood as describing a degree of freedom that aligns in two possible directions, analogous to a magnetic moment in the presence of an external field. This observation naturally leads to the formulation of the Ising model (IM), which describes a system of spins interacting through pairwise interactions and subjected to an external field.

Definition 3.2: Classical Ising Model

Let $\{s_i\}$ denote a set of spin variables, each taking values in $\{-1, +1\}$, arranged on the sites of a D-dimensional lattice. The *classical Ising model* is defined by the Hamiltonian

$$\mathcal{H}[\{s_i\}] = -J\sum_{\langle i,j\rangle} s_i s_j + h\sum_{i} s_i, \tag{3.5}$$

where $J \in \mathbb{R}$ is the coupling constant, $h \in \mathbb{R}$ denotes the strength of an external magnetic field, and $\langle i, j\rangle$ indicates a summation over nearest-neighbor pairs of lattice sites.

In this scenario, the isomorphism, i.e. mapping the net-gas model into a spin representation, is fully characterized assuming that $J = -\frac{B}{8}$ and $h = \left(\frac{A}{2} + \frac{qB}{4}\right)$.

3.1.1 Phase Transition on Ising Model (Classical)

Originally introduced by Wilhelm Lenz and later formalized by his doctoral student Ernst Ising [85], the Ising model (IM) has become a cornerstone of both Statistical Mechanics and Condensed Matter Physics [80–82]. It stands as one of the most fundamental and extensively studied models for understanding phase transitions and critical phenomena, offering a paradigmatic framework for analyzing cooperative behavior in many-body systems, both in classical and quantum regimes [47].

In recent years — and constituting the main perspective adopted in this work — the theoretical framework of Quantum Information Theory (QIT), particularly through the lens of Entanglement Theory (ET), has unveiled new insights into the critical properties and phase structure of the Ising model in the vicinity of its Quantum Critical Point (QCP) [17, 38, 86]. For completeness, a comprehensive and up-to-date treatment of the role of entanglement in spin chains, encompassing critical behavior, scaling properties, and quantum technological applications, can be found in [87].

The Ising model (IM) defined above admits an exact analytical solution in one spatial dimension ($D = 1$), for which no classical phase transition occurs, as thermal fluctuations preclude long-range order at any finite temperature [80]. In contrast, the two-dimensional model exhibits a genuine phase transition at finite temperature. In a seminal contribution, Onsager [88] derived, in 1944, an exact expression for the free energy of the two-dimensional Ising model on a square lattice in the absence of an external magnetic field. His solution rigorously demonstrated the presence of a second-order (continuous) phase transition, marked by the spontaneous vanishing of magnetization above a critical temperature T_c. For $T < T_c$, the system displays long-range ferromagnetic order; for $T > T_c$, thermal fluctuations dominate, leading to a paramagnetic disordered phase.

Onsager's exact solution stands as a milestone in the history of statistical physics, providing the first rigorous treatment of a nontrivial interacting many-body system at criticality. It not only illuminated the microscopic origins of phase transitions but also laid the foundation for the development of modern critical phenomena theory. Nevertheless, despite its success, obtaining exact analytical solutions for more general instances of the Ising model — such as the $D = 2$ case under finite magnetic fields or higher-dimensional versions ($D \geq 3$) [89] — remains an outstanding challenge in the field.

To tackle the general case, several approximate methods have been developed. One of the simplest approaches is the mean-field approximation, which assumes that each spin experiences an average effective field due to its neighbors. While this method provides qualitative insights, it fails to capture critical fluctuations and yields inaccurate results, particularly in lower dimensions. The mean-field approach is known to overestimate the critical temperature and neglects the role of correlations, leading to discrepancies when compared to exact solutions. In particular, it fails to describe the lower critical dimension D_l, below which no phase transition occurs, and the upper critical dimension D_u, above which mean-field predictions become accurate [82].

More sophisticated approaches to the study of phase transitions include perturbative methods such as Landau-Ginzburg theory (LGT) and the renormalization group (RG) technique [90, 91]. The LGT framework provides a phenomenological description by introducing an order parameter and constructing an effective free energy functional, enabling the analysis of symmetry-breaking phenomena. However, this formalism lacks a microscopic derivation and fails to accurately capture critical fluctuations beyond mean-field predictions. In contrast, the RG approach offers a powerful and systematic tool to investigate the behavior of systems near criticality by integrating out short-wavelength (high-momentum) degrees of freedom. This methodology has proven instrumental in classifying phase transitions, computing critical exponents, and revealing the universality underlying a wide class of models.

While the study of classical phase transitions is a rich and well-established field in its own right, it is not the primary focus of this work[3]. Instead, the main attention is directed toward quantum

[3] For readers interested in a modern and pedagogical exposition of the classical formalism, it is highly recommend the lecture notes by David Tong on Statistical Physics [92] and Statistical Field Theory [93]. These materials, freely available on his personal webpage, are part of a broader collection of high-quality lecture notes covering various topics in theoretical physics. See: https://www.damtp.cam.ac.uk/user/tong/.

systems at zero temperature, where quantum fluctuations, rather than thermal effects, drive critical behavior.

To motivate the study of quantum phase transitions, it is instructive to consider a formal correspondence between classical and quantum critical phenomena. Specifically, a d-dimensional quantum system at zero temperature can often be mapped onto a classical statistical system in $D = d+1$ dimensions. This mapping emerges naturally from the path integral formulation of quantum mechanics in imaginary time, where the quantum partition function at zero temperature is expressed as a functional integral over configurations defined on a $(d+1)$-dimensional space-time manifold [47].

In this construction, the additional dimension corresponds to the (imaginary) time axis, whose extent is governed by the inverse temperature $\beta = 1/T$. In the zero-temperature limit, $\beta \to \infty$, leading to an effectively infinite extent in the time direction and thus establishing a full equivalence with a classical system in one higher dimension. Quantum fluctuations in d spatial dimensions thereby play a role analogous to thermal fluctuations in $D = d+1$ dimensions. As a result, quantum phase transitions — driven by quantum fluctuations at zero temperature — can be analyzed using the mathematical and conceptual machinery originally developed for classical critical phenomena, such as scaling theory and the RG [47, 90, 91]. Furthermore, a pedagogical account of the mapping between classical and quantum systems, with explicit examples and technical detail, can be found in the project report by Hsieh [94].

A particularly illustrative example of this quantum-to-classical correspondence is found in the relation between the two-dimensional classical Ising model and the one-dimensional quantum Ising chain. In this case, the connection emerges naturally via the transfer matrix formalism: the partition function of the classical model can be recast as a trace over powers of a transfer operator T_m, which propagates configurations along one spatial direction and, at the thermodynamic limit, the dominant contribution to the free energy arises from the largest eigenvalue of T_m.

By interpreting T_m as an imaginary time evolution operator, one identifies a correspondence of the form $T_m \sim e^{-\delta\tau H}$, where H is the effective quantum Hamiltonian and $\delta\tau$ is a discretized time step. This identification is made precise through the Trotter-Suzuki decomposition, which allows the classical partition function to be expressed as a path integral over quantum configurations evolving in imaginary time [95]. This construction not only substantiates the structural equivalence between classical and quantum systems near criticality but also motivates the study of quantum critical phenomena using classical techniques and vice versa.

3.2 Quantum Phase Transitions

As previously discussed, quantum phase transitions (QPTs) manifest at zero temperature and are characterized by qualitative changes in the ground state of the system. Consequently, the accurate determination of ground-state properties for the relevant Hamiltonians is of fundamental importance. Although exact diagonalization offers a conceptually straightforward route to obtaining such ground

states, its applicability is severely limited by the exponential growth of the Hilbert space dimension with system size, which renders it computationally intractable for $N \gg 1$[4].

To overcome this limitation, a variety of efficient numerical techniques have been developed. Among these, variational tensor network methods have proven especially powerful for studying one-dimensional quantum systems. By exploiting the structure of entanglement in low-energy states, such methods are capable of approximating ground states with high fidelity while significantly reducing computational complexity. The density matrix renormalization group (DMRG), originally introduced by White [96, 97], stands as a landmark development in this context. Its later reinterpretation within the matrix product state (MPS) formalism [52, 98] has led to a deeper understanding of its variational nature and entanglement efficiency, firmly establishing MPS-based approaches as the standard toolkit for the study of one-dimensional quantum many-body systems.

These methods are particularly well-suited for analyzing quantum spin chains, which will constitute the focus of the following subsection.

3.2.1 Spin Chains

Spin chains are paradigmatic models in quantum many-body physics, widely employed to explore quantum phase transitions, the onset of long-range order, and the emergence of collective quantum phenomena such as entanglement and coherence — particularly near quantum critical points [17]. A spin chain consists of a set of localized quantum spins (typically spin-S) arranged on a discrete lattice, where neighboring spins interact via exchange couplings governed by the system's Hamiltonian. These models are especially relevant for describing low-dimensional magnetic materials, ultracold atoms in optical lattices [67], trapped ions [99], Rydberg atom arrays [100], and arrays of superconducting qubits [66], serving as powerful platforms for the quantum simulation of spin models.

The simplest and most studied geometry corresponds to a one-dimensional lattice, in which the spins are arranged linearly and interact predominantly with their nearest neighbors. Despite this apparent simplicity, one-dimensional spin chains exhibit rich and nontrivial behavior, making them a powerful theoretical laboratory for investigating critical phenomena, quantum correlations, and the structure of ground and excited states in strongly correlated systems.

3.2.1.1 Solving one-dimensional Quantum Spin Chains

As a representative example, consider a spin-$1/2$ system composed of N particles arranged on a one-dimensional lattice. Each spin is subject to nearest-neighbor couplings in the x- and y-directions, and influenced by an external magnetic field applied along the z-axis. The system is described by the anisotropic XY model, which interpolates between the Ising model and the isotropic XX model, depending on the relative values of the coupling constants.

[4] In this context, the Hamiltonian acts on a Hilbert space of the form $H \in \mathscr{B}(\bigotimes_{j=1}^{N} \mathscr{H}_j)$, with $\dim(\mathscr{H}_j) = 2$ for spin-$1/2$ systems.

Definition 3.3: Anisotropic XY Spin Chain

The Hamiltonian of the anisotropic XY model in a transverse magnetic field is defined as

$$H = -\sum_{i=1}^{L} \left[J_x \, \sigma_x^i \sigma_x^{i+1} + J_y \, \sigma_y^i \sigma_y^{i+1} + h \, \sigma_z^i \right], \tag{3.6}$$

where:

- σ_α^i denotes the Pauli operator along direction $\alpha = x, y, z$ acting on site i,
- J_α represents the coupling constant in the α-direction,
- h is the strength of the external magnetic field applied in the z-direction.

This model serves as a prototype for studying quantum criticality in low-dimensional systems and admits an exact solution through techniques such as Jordan-Wigner Transformation (JWT) and Bogoliubov rotation, which will be explored in this subsection.

Before proceeding with the formal solution of the XY-model, it is essential to ensure that the summation in Eq. (3.6) is well-defined. In particular, when $i = L$, the interaction term $\sigma_\alpha^i \sigma_\alpha^{i+1}$ depends on the choice of boundary conditions. The most common scenarios in this context are described as follows:

1. Open Boundary Conditions (OBC): In the case of an open chain, the interaction term is well-defined only for $i = 1$ to $i = L - 1$, leading to the Hamiltonian:

$$H_{\text{OBC}} = -\sum_{i=1}^{L-1} \left[J_x \sigma_x^i \sigma_x^{i+1} + J_y \sigma_y^i \sigma_y^{i+1} + h \sigma_z^i \right] + h \sigma_z^L. \tag{3.7}$$

   Under open boundary conditions, the system does not form a closed loop, meaning that the sites $i = 1$ and $i = L$ do not interact directly. This setup is particularly relevant for numerical simulations, including the DMRG and its thermodynamic limit extension, the infinite Density Matrix Renormalization Group (iDMRG), where open boundaries are often employed to mitigate finite-size effects.

2. Periodic Boundary Conditions (PBC): To model a system with translational symmetry, one can impose periodic boundary conditions, where the last site is coupled back to the first, effectively forming a closed chain:

$$H_{\text{PBC}} = -\sum_{i=1}^{L} \left[J_x \sigma_x^i \sigma_x^{i+1} + J_y \sigma_y^i \sigma_y^{i+1} + h \sigma_z^i \right], \tag{3.8}$$

[4] The Pauli matrices, expressed in the computational basis (σ_z-eigenbasis), are given by:

$$\sigma_x = \begin{pmatrix} 0 & 1 \\ 1 & 0 \end{pmatrix}, \quad \sigma_y = \begin{pmatrix} 0 & -i \\ i & 0 \end{pmatrix}, \quad \sigma_z = \begin{pmatrix} 1 & 0 \\ 0 & -1 \end{pmatrix}.$$

with the identification $\sigma_\alpha^{L+1} \equiv \sigma_\alpha^1$. This assumption ensures translational invariance in a finite system, facilitating analytical treatments, particularly those involving momentum-space representations via Fourier transformations.

3. Anti-Periodic Boundary Conditions (APBC): In certain contexts, particularly when mapping spin systems onto fermionic degrees of freedom through the JWT[5], it is advantageous to employ anti-periodic boundary conditions, which are defined as:

$$\sigma_\alpha^{L+1} = -\sigma_\alpha^1. \tag{3.9}$$

While PBC and APBC differ only by a relative phase factor, this phase shift plays a crucial role in modifying the spectrum of excitations. In the scenario of fermionic representations, such as those obtained via the JWT, the phase shift distinguishes between different boundary sectors, affecting the parity of the number of fermions. This aspect becomes particularly relevant in the study of topological effects and boundary-induced quantum phase transitions.

Moreover, to facilitate analytical treatment, the anisotropic XY Hamiltonian can be parametrized by an anisotropy parameter $\gamma \in [0, 1]$. In this representation, the coupling constants are defined as:

$$J_x = J\left(\frac{1+\gamma}{2}\right), \qquad J_y = J\left(\frac{1-\gamma}{2}\right). \tag{3.10}$$

This parametrization allows the interpolation between important limiting cases, as presented below.

Definition 3.4: The XX Model

The XX model is recovered by setting $\gamma = 0$ in the XY Hamiltonian. It describes an isotropic planar spin interaction, and its Hamiltonian is given by:

$$H_{XX} = -\frac{J}{2}\sum_{i=1}^{L}\left(\sigma_x^i\sigma_x^{i+1} + \sigma_y^i\sigma_y^{i+1}\right) - h\sum_{i=1}^{L}\sigma_z^i. \tag{3.11}$$

Definition 3.5: The Quantum Ising Model (QIM)

The quantum Ising model corresponds to the case $\gamma = 1$, where only $\sigma_x^i\sigma_x^{i+1}$ interactions remain. The Hamiltonian takes the form:

$$H_{QIM} = -J\sum_{i=1}^{L}\sigma_x^i\sigma_x^{i+1} - h\sum_{i=1}^{L}\sigma_z^i. \tag{3.12}$$

[5] A more detailed discussion of the Jordan-Wigner transformation and its implications will be presented in the following discussion.

These limiting cases underscore the versatility of the XY model, which serves as a unifying framework for exploring a range of physical regimes in one-dimensional quantum spin systems. In the isotropic limit ($\gamma = 0$), corresponding to the XX model, the system exhibits a continuous $U(1)$ symmetry and supports gapless excitations in the absence of a magnetic field. On the other hand, the extreme anisotropic limit ($\gamma = 1$) yields the quantum Ising model, characterized by a discrete $\mathbb{Z}_2$ symmetry and a well-known quantum phase transition separating ordered and disordered phases.

Finally, to analytically solve such class of spin Hamiltonians, one employs the JWT. This formalism establishes an exact, nonlocal mapping between spin operators — obeying the $SU(2)$ algebra — and fermionic creation and annihilation operators, akin to the second quantization framework in many-body physics.

Spin operators satisfy the canonical commutation relations:

$$[\sigma_\alpha, \sigma_\beta] = 2i\,\epsilon_{\alpha\beta\gamma}\,\sigma_\gamma,$$

where $\alpha, \beta, \gamma \in \{x, y, z\}$ and $\epsilon_{\alpha\beta\gamma}$ is the fully antisymmetric Levi-Civita symbol. In contrast, fermionic operators c_i and $c_i^\dagger$ satisfy the canonical anticommutation relations:

$$\{c_i, c_j^\dagger\} = \delta_{i,j}, \quad \{c_i, c_j\} = \{c_i^\dagger, c_j^\dagger\} = 0.$$

The JWT provides an algebra-preserving correspondence between these operator sets, enabling the reformulation of spin chains as fermionic systems with nonlocal string interactions.

Definition 3.6: Jordan-Wigner Transformation

Let σ_α^i be the Pauli operators acting on site i, and let $\sigma_\pm^i = (\sigma_x^i \pm i\sigma_y^i)/2$ denote the spin raising and lowering operators. The Jordan-Wigner transformation is defined as:

$$c_i = \left(\prod_{j=1}^{i-1} -\sigma_z^j\right) \sigma_-^i, \tag{3.13a}$$

$$c_i^\dagger = \left(\prod_{j=1}^{i-1} -\sigma_z^j\right) \sigma_+^i, \tag{3.13b}$$

$$-\sigma_z^i = \prod_{n=1}^{i} e^{i\pi c_n^\dagger c_n}. \tag{3.13c}$$

The nonlocal string operator $\prod_{j=1}^{i-1} -\sigma_z^j$ ensures that the anticommutation relations of the fermionic operators are preserved.

Given the operator identities established by the Jordan-Wigner transformation, it becomes possible to rewrite the spin Hamiltonian in terms of fermionic degrees of freedom. As an intermediate step, it is convenient to first express the spin operators in terms of the ladder operators σ_+ and σ_-,

using the identities:

$$\sigma_z^i = 2\sigma_+^i\sigma_-^i - \mathbb{1}_2, \tag{3.14a}$$
$$= 2c_i^\dagger c_i - \mathbb{1}_2, \tag{3.14b}$$
$$c_i^\dagger c_{i+1}^\dagger = \sigma_+^{i+1}\sigma_+^i. \tag{3.14c}$$

Applying these relations to the XY Hamiltonian expressed in terms of ladder operators yields:

$$\begin{aligned} H = &-\sum_{i=1}^{L-1}\left[J\left(\sigma_+^i\sigma_-^{i+1} + \sigma_-^i\sigma_+^{i+1}\right) + J\gamma\left(\sigma_+^{i+1}\sigma_+^i + \sigma_-^i\sigma_-^{i+1}\right)\right] \\ &- 2h\sum_{i=1}^{L}\sigma_+^i\sigma_-^i + hL + H'_{\text{BC}}, \end{aligned} \tag{3.15}$$

where H'_{BC} includes boundary terms that depend on the choice of boundary conditions.

Upon applying the Jordan-Wigner transformation, this spin Hamiltonian is mapped into a quadratic fermionic Hamiltonian:

$$\begin{aligned} H = &-\sum_{i=1}^{L-1}\left[J\left(c_i^\dagger c_{i+1} + c_{i+1}^\dagger c_i\right) + J\gamma\left(c_i^\dagger c_{i+1}^\dagger + c_{i+1}c_i\right)\right] \\ &- 2h\sum_{i=1}^{L}c_i^\dagger c_i + hL + H_{\text{BC}}, \end{aligned} \tag{3.16}$$

where H_{BC} encapsulates the boundary contributions resulting from the nonlocal string structure of the transformation.

3.2.1.2 Boundary Terms and Periodic Conditions

In the fermionic representation of spin chains, particular care must be taken with boundary terms, especially under periodic boundary conditions (PBC). These terms encode the global topological structure of the chain and play a nontrivial role due to the nonlocal nature of the Jordan-Wigner transformation. In the context of the XY model, the boundary contribution to the Hamiltonian can be written, in terms of ladder operators, as:

$$H_{\text{PBC}} = -J\left(\sigma_+^L\sigma_-^1 + \sigma_-^L\sigma_+^1\right) - J\gamma\left(\sigma_+^1\sigma_+^L + \sigma_-^L\sigma_-^1\right). \tag{3.17}$$

To incorporate this term into the fermionic formalism, it is necessary to manipulate it using the algebraic properties of the Pauli operators. Specifically, the following identities will prove essential:[6]

$$\sigma_+ = -(-\sigma_z)\sigma_+, \qquad \sigma_+ = \sigma_+(-\sigma_z),$$
$$\sigma_- = (+\sigma_z)\sigma_-, \qquad \sigma_- = -\sigma_-(-\sigma_z).$$

[6] These identities follow from the commutation relations of the Pauli matrices and can be verified using their matrix representations in the computational basis.

These relations enable the insertion and manipulation of Jordan–Wigner string operators across boundary terms, which is crucial for preserving the fermionic anticommutation relations. In particular, they allow the boundary coupling to be rewritten in a form compatible with the nonlocal fermionic structure imposed by the Jordan–Wigner transformation (JWT). The transformations that follow will make explicit how such boundary terms depend on the global fermion parity sector of the chain, and how periodic (or antiperiodic) boundary conditions affect the resulting fermionic Hamiltonian. In this context, it can be shown that:

$$c_L^\dagger c_1 = \prod_{j=1}^{L-1}(-\sigma_z^j)\sigma_z^L\sigma_-^1 \tag{3.18a}$$

$$= -\prod_{j=1}^{L}(-\sigma_z^j)\sigma_+^L\sigma_-^1 \tag{3.18b}$$

$$= -\prod_{j=1}^{L}\exp\left(i\pi c_j^\dagger c_j\right)\sigma_+^L\sigma_-^1. \tag{3.18c}$$

$$c_1^\dagger c_L = \prod_{j=1}^{L-1}(-\sigma_z^j)\sigma_-\sigma_+ \tag{3.18d}$$

$$= \prod_{j=1}^{L}\exp\left(i\pi c_j^\dagger c_j\right)\sigma_-^L\sigma_+^1. \tag{3.18e}$$

$$c_L^\dagger c_1^\dagger = \prod_{j=1}^{L-1}(-\sigma_z^j)\sigma_+^L\sigma_+^1 \tag{3.18f}$$

$$= -\prod_{j=1}^{L}\exp\left(i\pi c_j^\dagger c_j\right)\sigma_+^L\sigma_+^1. \tag{3.18g}$$

$$c_L c_1 = \prod_{j=1}^{L-1}(-\sigma_z^j)\sigma_-^L\sigma_-^1 \tag{3.18h}$$

$$= \prod_{j=1}^{L}\exp\left(i\pi c_j^\dagger c_j\right)\sigma_-^L\sigma_-^1. \tag{3.18i}$$

These transformations emphasize the critical role of boundary conditions, particularly the phase factor introduced by the Jordan-Wigner string, when reformulating the problem in terms of fermionic operators.

To further refine the fermionic representation, one introduces the total number operator:[7]

$$N \coloneqq \sum_{i=1}^{L} c_i^\dagger c_i = \sum_{i=1}^{L}\frac{\mathbb{1}_2 + \sigma_z^i}{2}. \tag{3.19}$$

[7] Physically, the number operator counts the total number of fermions in the chain. Additionally, from the above transformations, it is evident that the number operator is directly proportional to the total magnetization along the z-axis.

By substituting the number operator into Eqs. (3.18) and using the properties $\sigma_z^2 = \mathbb{1}_2$ along with the canonical anticommutation relations of fermionic operators, the boundary terms can be rewritten as:

$$\begin{aligned} \sigma_+^L \sigma_-^1 &= -(-1)^N c_L^\dagger c_1, \quad \sigma_-^L \sigma_+^1 = -(-1)^N c_1^\dagger c_L, \\ \sigma_+^L \sigma_+^1 &= -(-1)^N c_L^\dagger c_1^\dagger, \quad \sigma_-^L \sigma_-^1 = -(-1)^N c_1 c_L. \end{aligned}$$

Finally, incorporating these transformations, the full fermionic representation of the Hamiltonian is expressed as:

$$\begin{aligned} H = &-J \sum_{i=1}^{L-1} \left(c_i^\dagger c_{i+1} + c_{i+1}^\dagger c_i + \gamma (c_i^\dagger c_{i+1}^\dagger + c_{i+1} c_i) \right) - 2h \sum_{i=1}^{L} c_i^\dagger c_i + hL \\ &+ (-1)^N J \left(c_L^\dagger c_1 + c_1^\dagger c_L + \gamma (c_L^\dagger c_1^\dagger + c_1 c_L) \right). \end{aligned} \tag{3.20}$$

Moreover, the last terms in Eq. (3.20), proportional to the parity operator $(-1)^N$, can be further decomposed according to the parity eigenvalues. Since the parity operator satisfies $(-1)^N = 1$ for even N and $(-1)^N = -1$ for odd N, the Hamiltonian can be effectively separated into distinct parity sectors. This motivates the introduction of the projection operators $P_\pm$, which project onto the eigenspaces corresponding to parity eigenvalues ± 1:

$$\mathbb{1} H \mathbb{1} = P_+ H P_+ + P_- H P_- \coloneqq P_+ H_+ P_+ + P_- H_- P_-. \tag{3.21}$$

Within each parity sector, the Hamiltonian takes the form:

$$\begin{aligned} H_\pm = &-J \sum_{i=1}^{L-1} \left(c_i^\dagger c_{i+1} + c_{i+1}^\dagger c_i + \gamma (c_i^\dagger c_{i+1}^\dagger + c_{i+1} c_i) \right) - 2h \sum_{i=1}^{L} c_i^\dagger c_i + hL \\ &\pm J \left(c_L^\dagger c_1 + c_1^\dagger c_L + \gamma (c_L^\dagger c_1^\dagger + c_1 c_L) \right). \end{aligned} \tag{3.22}$$

This decomposition of the Hamiltonian into even and odd parity subspaces significantly simplifies its diagonalization and subsequent analysis. By treating each parity sector independently, one can impose anti-periodic boundary conditions for H_+ and periodic boundary conditions for H_-, ensuring that the Hamiltonian retains the same form in both sectors. At this point one remark is important: according to the Lee-Yang theorem, phase transitions in this model can only occur in the thermodynamic limit. Since the thermodynamic properties of the system remain unaffected by the choice between periodic and anti-periodic boundary conditions, both conditions yield the same physical results in this regime. After this procedure, the Hamiltonians are written as:

$$H_\pm = -J \sum_{i=1}^{L} \left(c_i^\dagger c_{i+1} + c_{i+1}^\dagger c_i + \gamma (c_i^\dagger c_{i+1}^\dagger + c_{i+1} c_i) \right) - 2h \sum_{i=1}^{L} c_i^\dagger c_i + hL \tag{3.23}$$

3.2.1.3 Parity Sectors Diagonalization

The diagonalization of H_+ is most efficiently performed in momentum space. To achieve this, one applies the Fourier transformation, assuming that L is even:

$$c_n = \frac{\exp(-i\pi/4)}{\sqrt{L}} \sum_k \exp(ikn) c_k, \tag{3.24}$$

where $k \in K_+$ represents the discrete momentum modes, and c_k denotes the fermionic annihilation operators in momentum space.

To determine the appropriate momentum domain, one enforces the anti-periodic boundary condition, given by $c_{L+1} = -c_1$. Substituting this condition into Eq. (3.24):

$$\frac{\exp(-i\pi/4)}{\sqrt{L}} \sum_k \exp[ik(L+1)] c_k = -\frac{\exp(-i\pi/4)}{\sqrt{L}} \sum_k \exp(ik) c_k. \tag{3.25}$$

Rearranging, it is possible to find that the allowed momentum values must satisfy:

$$\exp(ikL) = -1, \quad \forall k \in K_+. \tag{3.26}$$

Solving for k, this condition defines the discrete momentum set:

$$K_+ := \left\{ k = \pm \frac{(2l+1)\pi}{L} \mid l = 0, 1, \ldots, \frac{L}{2} - 1 \right\}. \tag{3.27}$$

Thus, using the orthonormality and completeness[8] of the Fourier basis, one can express the summations in the Hamiltonian as follows:

$$\begin{aligned} \sum_n c_n^\dagger c_{n+a} &= \sum_{kq} \left(\frac{1}{L} \sum_n \exp(i(k-q)n) \right) \exp(iqa) c_k^\dagger c_q \\ &= \sum_k \exp(ika) c_k^\dagger c_k. \end{aligned} \tag{3.28}$$

Similarly, for the pairing terms:

$$\sum_n c_{n+a} c_n = -i \sum_k \exp(-ika) c_{-k} c_k. \tag{3.29}$$

Therefore, the summation terms in the Hamiltonian can be rewritten as:

[8] Symbolically, the orthonormality and completeness relations are given by:

$$\frac{1}{L} \sum_{k \in K_+} \exp(ik(n-n')) = \delta_{n,n'}, \quad \frac{1}{L} \sum_{n=1}^{L} \exp(i(k-k')n) = \delta_{k,k'}.$$

$$\sum_{i=1}^{L}(c_i^\dagger c_{i+1} + c_{i+1}^\dagger c_i) = 2\sum_{k\in K_+}\cos(k)c_k^\dagger c_k; \tag{3.30a}$$

$$= 2\sum_{k\in K_{>0}^+}\cos(k)(c_k^\dagger c_k + c_{-k}^\dagger c_{-k}) \tag{3.30b}$$

$$\sum_{i=1}^{L} c_i^\dagger c_i = \sum_{k\in K_+} c_k^\dagger c_k; \tag{3.30c}$$

$$= \sum_{k\in K_{>0}^+}(c_k^\dagger c_k + c_{-k}^\dagger c_{-k}). \tag{3.30d}$$

$$\sum_{i=1}^{L} c_{i+1}c_i = -i\sum_{k\in K_+}\exp(-ik)c_{-k}c_k; \tag{3.30e}$$

$$= \sum_{k\in K_{>0}^+}(\exp(-ik)c_{-k}c_k + \exp(ik)c_k c_{-k})$$

$$= 2\sum_{k\in K_{>0}^+}\sin(k)c_{-k}c_k. \tag{3.30f}$$

Here, $k \in K_{>0}^+$ denotes positive momentum values within K_+. Finally, using the above relations, one can rewrite the Hamiltonian H_+ as:

$$H_+ = -2\sum_{k\in K_{>0}^+}\Big\{\big[h + J\cos(k)\big]\big(c_k^\dagger c_k + c_{-k}^\dagger c_{-k}\big) \quad - J\gamma\sin(k)\big(c_k^\dagger c_{-k}^\dagger + c_{-k}c_k\big)\Big\}. \tag{3.31}$$

Note, the constant term hL is omitted, as in a physical scenario, the initial Hamiltonian must be renormalized in the thermodynamic limit, where $L \to \infty$ implies $H \to \infty$.

The above expression reveals that the odd-parity sector of the Hamiltonian consists of pairwise interactions between the modes k and $-k$. Moreover, observing Eq. (3.31), one notes that the first term is diagonal in this basis. However, for a general γ, the second term introduces off-diagonal terms that prevent direct diagonalization. In this case, to fully diagonalize the Hamiltonian, one must determine a unitary transformation that eliminates the off-diagonal terms while preserving the physical structure of the system.

Definition 3.7: Bogoliubov Transformation

To diagonalize the Fourier-transformed fermionic Hamiltonian H_+, it is necessary to eliminate the pairing terms of the form $c_k^\dagger c_{-k}^\dagger + \text{H.c.}$ that arise from the anisotropic part of the interaction. This is achieved by performing a Bogoliubov rotation, which defines a new set of fermionic quasiparticle operators η_k and $\eta_k^\dagger$ via:

$$c_k \coloneqq u_k \eta_k - v_k \eta_{-k}^\dagger, \tag{3.32a}$$

$$c_{-k} \coloneqq u_k \eta_{-k} + v_k \eta_k^\dagger, \tag{3.32b}$$

where u_k and v_k are complex coefficients satisfying $|u_k|^2 + |v_k|^2 = 1$ for all momentum modes k.

The operators η_k and $\eta_k^\dagger$ represent fermionic quasiparticles and satisfy the canonical anticommutation relations:

$$\{\eta_k, \eta_{k'}^\dagger\} = \delta_{k,k'}, \qquad \{\eta_k, \eta_{k'}\} = \{\eta_k^\dagger, \eta_{k'}^\dagger\} = 0,$$

for all $k, k' \in K_\pm$. The Bogoliubov transformation brings the Hamiltonian into a diagonal form, allowing the system to be interpreted as a collection of noninteracting quasiparticles with momentum-dependent dispersion relations.

For the purposes of this work, one can assume that the Bogoliubov coefficients take the form:

$$u_k \coloneqq \cos(\theta_k/2), \quad v_k \coloneqq \sin(\theta_k/2), \tag{3.33}$$

where θ_k is a parameter to be determined such that the Hamiltonian is diagonalized. For the specific case of the XY-model, the angle θ_k is well known and is given by:

$$\tan(\theta_k/2) \coloneqq \frac{J\gamma \sin(k)}{h + J\cos(k)}. \tag{3.34}$$

Substituting this transformation, the Hamiltonian H_+ can be rewritten as:

$$H_+ = \sum_{k \in K_{>0}^+} \Big\{ -2\big(h + J\cos(k)\big) - 2\epsilon_k + 2\epsilon_k \big(\eta_k^\dagger \eta_k + \eta_{-k}^\dagger \eta_{-k}\big) \Big\}, \tag{3.35}$$

which simplifies to the fully diagonalized form:

$$H_+ = \varepsilon_0^+ + 2 \sum_{k \in K^+} \epsilon_k \eta_k^\dagger \eta_k. \tag{3.36}$$

Here, ϵ_k represents the quasiparticle energy spectrum, and ε_0^+ corresponds to the ground-state energy contribution defined, respectively, as:

$$\epsilon_k = \sqrt{(h + J\cos(k))^2 + J^2\gamma^2 \sin^2(k)} \tag{3.37a}$$

$$\varepsilon_0^+ = -2 \sum_{k \in K_{>0}^+} (h + J\cos(k) + \epsilon_k) \tag{3.37b}$$

For the sector corresponding to the odd fermion parity, the treatment proceeds analogously. Upon applying the Fourier transform and imposing the periodic boundary condition, the allowed momenta are given by the set $k \in K_-$, where:

$$K_- := \left\{ k = \pm\frac{2\pi l}{L}, \pi \,\middle|\, l = 0, 1, \ldots, \frac{L}{2} - 1 \right\}. \tag{3.38}$$

By employing the Fourier transform together with the completeness relation, the fermionic operators in momentum space are defined as:

$$c_k = \frac{e^{i\pi/4}}{\sqrt{2}} \sum_n e^{-ikn} c_n,$$
$$c_{-k} = \frac{e^{i\pi/4}}{\sqrt{2}} \sum_n e^{ikn} c_n.$$

It is observed that for the special momenta $k \in K_-$ with $k = 0$ or $k = \pi$, the operators c_k and c_{-k} coincide. As a consequence, the anisotropic interaction term vanishes for these values. In this sense, to properly account this behavior, a restricted set of momenta is defined by

$$K_\star^- := \{k \in K_- \,|\, k \neq 0, \pi\}. \tag{3.39}$$

Accordingly, the Hamiltonian in the odd fermion-number sector can be expressed as:

$$\begin{aligned} H_- = -2 \sum_{k \in K_\star^-} & \left\{ [h + J\cos(k)] \left(c_k^\dagger c_k + c_{-k}^\dagger c_{-k} \right) - J\gamma \sin(k) \left(c_k^\dagger c_{-k}^\dagger + c_{-k} c_k \right) \right\} \\ & - 2(h + J) c_0^\dagger c_0 - 2(h - J) c_\pi^\dagger c_\pi. \end{aligned} \tag{3.40}$$

In this scenario, the same Bogoliubov rotation as in the even-parity case H_+ can be performed. Consequently, in terms of the new quasiparticle operators, the Hamiltonian becomes diagonal and takes the form:

$$H_- = \varepsilon_0^- + 2 \sum_{k \in K_\star^-} \epsilon_k \, \eta_k^\dagger \eta_k - 2(h + J) c_0^\dagger c_0 - 2(h - J) c_\pi^\dagger c_\pi, \tag{3.41}$$

where the ground-state energy contribution is given by:

$$\varepsilon_0^- = -2 \sum_{k \in K_\star^-} (h + J\cos(k) + \epsilon_k). \tag{3.42}$$

Remark 3.1: Parity sectors and criticality

Although the Hamiltonians H_+ and H_- correspond to distinct fermionic parity sectors — associated with different sets of allowed quasimomenta $K_\pm$ — they share the same functional form after Bogoliubov diagonalization. In both cases, the spectrum consists of noninteracting fermionic quasiparticles with dispersion relation ϵ_k, and the only distinction lies in the ground state energy, which depends on the specific summation over k. This structural equivalence enables a unified analysis of the system's dynamical and thermodynamic properties.
Importantly, the quasiparticle dispersion relation takes the form

$$\epsilon_k = \sqrt{(h + J\cos k)^2 + J^2\gamma^2 \sin^2 k},$$

from which it follows that the system becomes gapless — i.e., $\min_k \epsilon_k = 0$ — if and only if $|J - h| = 0$ for $\gamma = 1$, which represents QIM. This condition uniquely determines the quantum critical point (QCP) of the model, separating the ferromagnetic and paramagnetic phases. On other words, the presence of a vanishing energy gap at $h = J$ signals a second-order quantum phase transition, characterized by divergent correlation length, for example.

4 Tensor Networking Formalism

4.1 Fundamental Concepts

Tensor Networks (TNs) constitute a powerful computational framework of central importance in modern quantum physics and related fields. They emerged as a response to the challenge of efficiently representing and simulating complex quantum many-body systems. The conceptual foundation of TNs is closely tied to the development of the *Density Matrix Renormalization Group* (DMRG), introduced by White in the early 1990s as a highly accurate variational technique for investigating the low-energy sector of one-dimensional quantum systems [96]. It was later recognized that DMRG can be naturally understood in terms of the Matrix Product State (MPS) formalism, a specific subclass of TNs [98].

This insight motivated a broader theoretical program aimed at generalizing tensor network structures beyond one dimension. Notable examples include the Projected Entangled Pair States (PEPS), introduced as a natural extension of MPS to higher-dimensional lattices [101]; the Multi-scale Entanglement Renormalization Ansatz (MERA), specifically designed to efficiently capture scale invariance and critical behavior [102]; and the Tree Tensor Network (TTN) architecture, which provides a hierarchical decomposition of quantum correlations with logarithmic scaling in depth [103].

Beyond their foundational role in many-body theory, tensor network methods have also found impactful applications in a range of other domains. In quantum computing, they offer a framework for simulating and analyzing quantum circuits [104,105]; in statistical mechanics, they provide insights into classical partition functions and critical phenomena [106,107]; and in machine learning, they furnish efficient representations for structured, high-dimensional data [108,109].

4.1.1 Matrix Product State

Let $|\psi\rangle \in \bigotimes_{i=1}^{N} \mathscr{H}_i$, where each $\mathscr{H}_i$ denotes a local Hilbert space (LHS) of finite dimension d. For each site j, let $\left\{ \left|\sigma_k^{(j)}\right\rangle \right\}_{k=1}^{d}$ be a fixed orthonormal basis for $\mathscr{H}_j$. Then, the set of product states

$$\left\{ |\vec{\sigma}_{\vec{i}}\rangle := \bigotimes_{j=1}^{N} \left|\sigma_{i_j}^{(j)}\right\rangle \right\}_{\vec{i}\in I^N}$$

forms a complete orthonormal basis for the global Hilbert space $\mathscr{H} = \bigotimes_{i=1}^{N} \mathscr{H}_i$[1]. Consequently, any pure state $|\psi\rangle \in \mathscr{H}$ admits a unique decomposition as a linear combination of these basis elements:

[1] Here, the index set $I = \{1, 2, \ldots, d\}$ labels the basis vectors of each local Hilbert space.

$$
\begin{aligned}
|\psi\rangle &= \sum_{i_1,i_2,\ldots,i_N} C_{i_1 i_2 \cdots i_N} \left|\sigma^1_{i_1}\right\rangle \otimes \left|\sigma^2_{i_2}\right\rangle \otimes \cdots \otimes \left|\sigma^N_{i_N}\right\rangle \\
&= \sum_{i_1,i_2,\ldots,i_N} C_{i_1 i_2 \cdots i_N} \left|\sigma^1_{i_1}, \sigma^2_{i_2}, \ldots, \sigma^N_{i_N}\right\rangle, \qquad (4.1)
\end{aligned}
$$

where $C_{i_1 i_2 \cdots i_N}$ is a complex-valued tensor with N physical indices, commonly referred to as the expansion coefficient tensor. In this formalism, all physical information about the quantum state $|\psi\rangle$ is fully encoded in the components of C.

However, directly manipulating the full N-index tensor quickly becomes computationally intractable as the system size N increases, due to the exponential growth in the number of components, which scales as d^N. To overcome this challenge, one seeks more compact and structured representations that efficiently capture the entanglement structure of physically relevant quantum states. One particularly successful approach is the MPS representation, which expresses the coefficient tensor $C_{i_1 i_2 \cdots i_N}$ as a product of lower-rank tensors, as described below.

Definition 4.1: Matrix Product State (MPS)

A pure quantum state $|\psi\rangle \in \bigotimes_{k=1}^{N} \mathscr{H}_k$, with expansion coefficients $C_{i_1 i_2 \cdots i_N}$, is said to admit a *Matrix Product State* (MPS) representation if the tensor C can be decomposed as

$$
C_{i_1 i_2 \cdots i_N} = \sum_{\{\alpha_k\}} A^{[1]}_{i_1 \alpha_1} A^{[2]}_{\alpha_1 i_2 \alpha_2} A^{[3]}_{\alpha_2 i_3 \alpha_3} \cdots A^{[N]}_{\alpha_{N-1} i_N}, \qquad (4.2)
$$

where each $A^{[k]}$ is a site-dependent tensor with one physical index i_k and up to two auxiliary (bond) indices α_{k-1}, α_k, which are contracted between neighboring sites. The dimensions of the bond indices, $\chi_k = \dim(\alpha_k)$, determine the amount of entanglement supported between partitions of the system.

Naturally, this leads to a fundamental question: how can one obtain the MPS form of an arbitrary tensor $C_{i_1 i_2 \cdots i_N}$? In practice, the set of tensors $\{A^{[k]}\}$ defining the MPS can be systematically constructed through a sequence of Singular Value Decompositions (SVDs)[2] applied to the original coefficient tensor. This procedure involves successively reshaping and decomposing C into matrices, which are then factorized to extract the local tensors while preserving the global structure of the quantum state.

Diagrammatically, the expansion coefficient tensor C can be represented as an N-leg object, with each leg corresponding to one of the physical indices i_k (see Fig. 1). The decomposition proceeds

[2] The singular value decomposition (SVD) of a matrix transforms it into a product $M = USV^\dagger$, where U and V are left - and right - isometric matrices, respectively, and S is a diagonal matrix containing the non-negative singular values. These singular values correspond to the square roots of the nonzero eigenvalues of both $MM^\dagger$ and $M^\dagger M$, which are Hermitian and positive semi-definite.

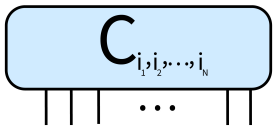

Figure 1 – Diagrammatic representation of the expansion tensor C. Each leg corresponds to a local degree of freedom.

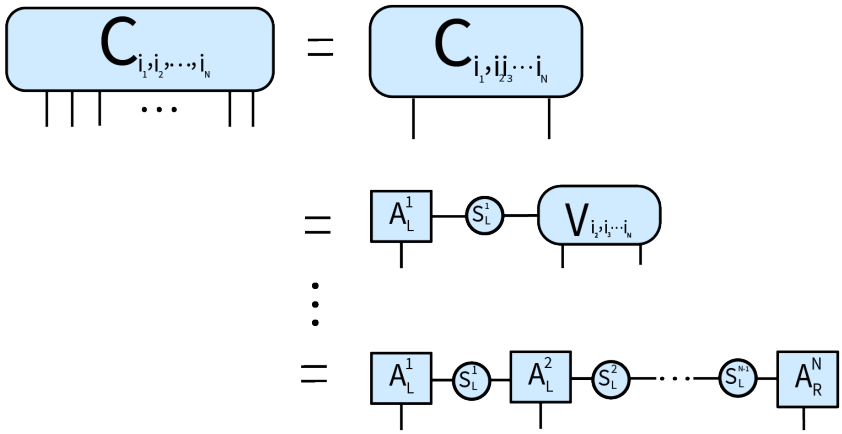

Figure 2 – Diagrammatic representation of the tensor decomposition process that yields the MPS form. The initial coefficient tensor $C_{i_1,i_2,\ldots,i_N}$, represented as a single node with N physical legs, is successively reshaped into matrices by grouping indices. At each step, a SVD is performed, factorizing the reshaped matrix into a product of two tensors: one associated with a site tensor $A^{[k]}_{L/R}$, and the other carrying the remaining degrees of freedom, which is further decomposed in the subsequent steps. The intermediate singular value tensors S (often absorbed into neighboring tensors or retained to enforce canonical forms)appear as circular nodes in the diagram. This recursive decomposition results in a chain of local tensors $\{A^{[k]}_{L/R}\}$, where L (R) means left (right) isometric tensor, connected via contracted auxiliary indices, forming the MPS representation of the original quantum state.

by reshaping the tensor $C_{i_1,i_2,\cdots,i_N}$ into a matrix $C_{i_1,i_2\cdots i_N}$, grouping subsets of physical indices, and applying the SVD. This process is repeated iteratively, sweeping through the system from left to right (or right to left), yielding the low-rank tensors $A^{[k]}$ that define the MPS representation (see Fig.2).

4.1.1.1 Gauge Freedom and Canonical Form

A fundamental property of MPS is their inherent *gauge freedom*, which originates from the non-uniqueness of their tensor network decomposition. This redundancy implies that the same physical state can be represented by infinitely many equivalent sets of local tensors. Specifically, as long as the virtual indices connecting neighboring tensors span finite-dimensional auxiliary Hilbert spaces, it is always possible to insert resolutions of the identity in the form of pairs of invertible matrices and their inverses along the virtual bonds, leaving the global state unchanged. This property underpins the concept of gauge freedom, formally defined as follows:

Definition 4.2: Gauge Freedom in MPS

Let $|\psi\rangle$ be a quantum state represented by a set of local tensors $\{A^{[n]}\}$ defining a MPS. The MPS is said to possess *gauge freedom* if, for any sequence of invertible matrices $\{X_n\}$, the local tensors can be transformed as

$$A^{[n]} \mapsto (X_{n-1})^{-1} A^{[n]} X_n, \tag{4.3}$$

without altering the physical state, that is, the transformed set of tensors still represents the same wavefunction $|\psi\rangle$.

This structural redundancy naturally motivates the introduction of a *canonical form* for MPS, in which the local tensors are brought into specific isometric conditions through an appropriate choice of gauge. Adopting such a form not only simplifies the mathematical representation of the quantum state but also plays a critical role in enhancing the numerical stability and efficiency of tensor network algorithms. In particular, bringing the MPS into this form allows for the direct computation of entanglement properties because, in this gauge, the Schmidt decomposition across any bipartition is explicitly encoded in the singular values of the corresponding bond[3].

Moreover, this structure enables the systematic truncation of bond dimensions in a controlled and physically meaningful manner, as the least significant Schmidt coefficients (those contributing least to the entanglement) can be discarded with a quantifiable and well-defined truncation error. This mechanism is central to maintaining computational efficiency without compromising the accuracy of the quantum state description. Consequently, MPS-based algorithms, such as DMRG and the *Variational Uniform Matrix Product State* (VUMPS) method (see next section), fundamentally rely on the canonical form to ensure well-posed local optimization problems and preserve the variational consistency of the MPS ansatz.

The notion of a *mixed-canonical form* arises naturally when considering a one-dimensional tensor network representation of a quantum state. Conceptually, one may visualize the MPS as a chain of interconnected tensors and freely select one of these tensors to serve as the *center of orthogonality*. This choice partitions the system into a left and a right block relative to the chosen site. A tensor network is said to be in mixed-canonical form when all tensors to the left of the orthogonality center satisfy the *left-orthonormality* condition, all tensors to its right satisfy the *right-orthonormality* condition, and the central tensor remains unconstrained.

[3] The orthonormalization conditions inherent to the canonical form guarantee that these singular values correspond precisely to the Schmidt coefficients, from which quantities such as the entanglement entropy can be readily computed.

Definition 4.3: Mixed-Canonical Form of an MPS

Consider an MPS with the orthogonality center located at site n. The network is said to be in *mixed-canonical form* if:

- Tensors to the left of site n satisfy the left-orthonormality condition:

$$\sum_s (A_L^s)^\dagger A_L^s = \mathbb{I}, \tag{4.4}$$

- Tensors to the right of site n satisfy the right-orthonormality condition:

$$\sum_s A_R^s (A_R^s)^\dagger = \mathbb{I}, \tag{4.5}$$

- The central tensor at site n remains unconstrained and captures the entanglement spectrum across the chosen bipartition.

Importantly, this central tensor explicitly encodes the entanglement properties of the bipartition defined by the orthogonality center. Adopting the mixed-canonical form not only clarifies the entanglement structure but also simplifies both variational optimizations and the computation of physical observables, as it provides a natural decomposition of the system into subsystems.

For a more formal and diagrammatic presentation of these concepts, the reader is referred to the comprehensive Tensor Network tutorials by Glen Evenbly, available at `https://www.tensors.net`. These resources provide not only rigorous graphical notation for tensor contractions but also detailed algorithmic explanations of canonical forms, Schmidt decompositions, and their applications in practical tensor network simulations. In particular, Evenbly's materials cover key procedures such as bringing an MPS into canonical form, performing entanglement cuts, and understanding how gauge transformations affect the numerical stability and physical interpretation of tensor network states. Additional authoritative references on this subject include the review by Orús [110] and the foundational book by Schollwöck [52], both of which extensively discuss the role of canonical forms in tensor network methods.

4.1.2 Matrix Product Operator

Having established that the complete physical content of a pure quantum state $|\psi\rangle$ is fully encoded in its expansion coefficients, naturally organized as an N-index tensor, it is conceptually and practically advantageous to extend this tensorial perspective to more general quantum objects — most notably, to density operators and linear maps.

Given a pure state $|\psi\rangle$, represented by an N-leg tensor C, the corresponding density operator $\rho := |\psi\rangle\langle\psi|$ is naturally described by an $2N$-leg tensor (see Fig. 3a). Within this framework, several physically meaningful operations can be formulated in an intuitive graphical language. For example,

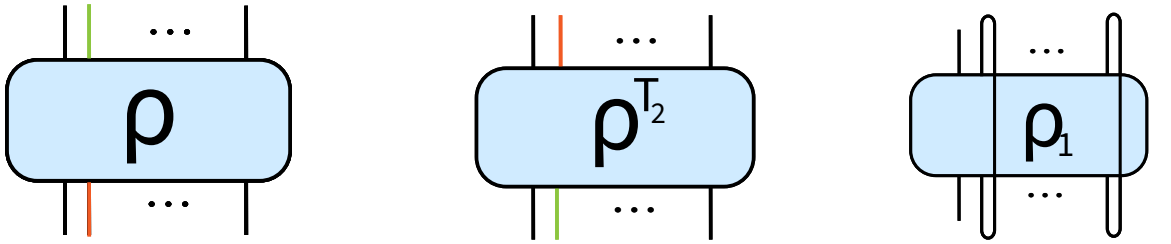

(a) ρ – full multipartitie state

(b) ρ^{T_2} – partial transpose on subsystem 2

(c) ρ_1 – one site reduced state

Figure 3 – Tensor network diagrams representing operations on multipartite quantum states. In 3a, the global density operator ρ, with input and output legs for each subsystem. In 3b, the partial transposition of the second site ρ^{T_2} which is obtained by swapping the input and output legs of subsystem 2. In3c, the one site reduced state is computed by contracting over the degrees of freedom.

the *partial transposition* (Fig. 3b) — a key ingredient in the evaluation of entanglement measures such as the multinegativity — is implemented by interchanging the output and input indices associated with a designated subsystem. Similarly, the *partial trace*, which yields reduced states for subsystems (Fig. 3c), is represented by contracting the corresponding tensor legs associated with the degrees of freedom to be traced out.

More generally, this perspective lays the foundation for expressing linear operators acting on many-body systems in terms of tensor networks. In particular, the class of *Matrix Product Operators* (MPOs) provides a compact and scalable representation for operators with local or quasi-local structure:

Definition 4.4: Matrix Product Operator (MPO)

Let $O \in \mathscr{B}(\mathscr{H}^{\otimes L})$ be an operator acting on a chain of L sites each with local dimension d, is said to admit an MPO representation if it can be written as

$$O = \sum_{\substack{\{i_k\},\\ \{j_k\}}} \sum_{\{\alpha_k\}} W^{[1]\,i_1 j_1}_{\alpha_0 \alpha_1} W^{[2]\,i_2 j_2}_{\alpha_1 \alpha_2} \cdots W^{[L]\,i_L j_L}_{\alpha_{L-1} \alpha_L} |i_1 i_2 \cdots i_L\rangle \langle j_1 j_2 \cdots j_L| , \tag{4.6}$$

where each tensor $W^{[k]\,i_k j_k}_{\alpha_{k-1}\alpha_k}$ is of rank four: it has two physical indices i_k, j_k (input and output), and two virtual (or bond) indices α_{k-1}, α_k that are contracted between neighboring sites. The outer indices α_0 and α_L determine the boundary conditions:

- For *open boundary conditions*, one sets $\alpha_0 = \alpha_L = 1$, so that the first and last tensors are vectors in the virtual space.
- For *periodic boundary conditions*, the virtual indices are contracted cyclically, and a trace over the product of local tensors is taken.

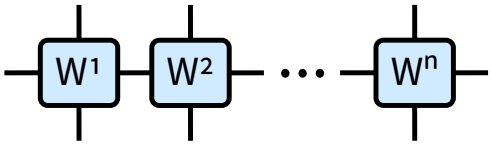

Figure 4 – Diagrammatic representation of a generic Matrix Product Operator (MPO) with open boundary conditions, illustrating the structure $O = \bigotimes_{i=1}^{N} W^{[i]}$. Each tensor $W^{[i]}$ is connected to its neighbors via virtual indices (horizontal lines) and to the physical input-output Hilbert spaces via vertical legs.

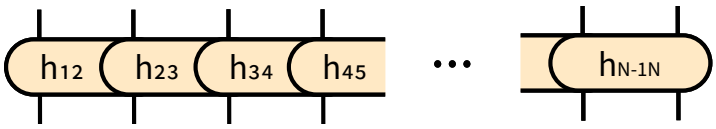

Figure 5 – Diagrammatic representation of a nearest-neighbor Hamiltonian as an MPO. The operator is decomposed as a sum of two-site interactions, $H = \sum_{i=1}^{N-1} h_{i,i+1}$, each of which is embedded into the MPO structure using local tensors.

The abstract definition of a MPO provided above admits an intuitive and powerful graphical representation within the tensor network formalism. In this diagrammatic language, each local tensor $W^{[k]}$ is depicted as a box with four legs — two corresponding to the physical input and output indices, and two connecting to neighboring sites via virtual bonds. Figure 4 illustrates the structure of a generic MPO representing an operator $O = \bigotimes_{i=1}^{n} W^{[i]}$, where the local tensors are arranged sequentially along a one-dimensional chain and contracted along their virtual indices.

Furthermore, a particularly relevant application of MPOs arises in the representation of local Hamiltonians, especially those composed of nearest-neighbor interactions, i.e. $H = \sum_i h_{i,i+1}$. In such cases, each local term acts nontrivially only on adjacent sites, and the total Hamiltonian is expressed as a sum of these pairwise contributions (as discussed in the later chapter). Figure 5 displays the diagrammatic form of such a Hamiltonian, where the local structure of the operator is encoded efficiently in the MPO ansatz.

4.2 Algorithms Based on Tensor Networks

The formalism of tensor networks not only provides a compact representation of quantum many-body states and operators, but also enables the development of highly efficient numerical algorithms for simulating and analyzing such systems. The essential idea is that both the objects of interest (e.g., states, observables, Hamiltonians) and the transformations acting on them (e.g., optimizations, time evolution, diagonalization) can be naturally represented as contractions of structured tensors. By exploiting the entanglement structure of low-energy states (typically obeying an area law) tensor network algorithms avoid the exponential growth of the Hilbert space and remain tractable even for large systems.

From this perspective, a computational algorithm is understood as a sequence of well-defined tensor operations, including contractions, decompositions (such as singular value decomposition or

QR factorization), projections, and iterative updates of tensor components. The guiding principle underlying such procedures is to carry out operations locally, typically by contracting one or two tensors at a time, while preserving a globally consistent network structure that faithfully encodes the physical state or operator of the system.

In practice, this entails defining an ansatz for the state (e.g., MPS) and iteratively optimizing its constituent tensors in a variational manner. The cost function to be minimized is often the energy expectation value with respect to a given Hamiltonian, represented as an MPO. The variational optimization, in turn, reduces to a series of local problems which can be efficiently solved by standard linear algebra methods.

The representation of algorithms as tensor networks is particularly powerful when paired with graphical notation. Each computational step — such as updating a tensor, applying a gate, or computing an expectation value — corresponds to a local transformation in the diagram, preserving the overall connectivity and structure of the network. This graphical calculus is not only visually intuitive, but also serves as a blueprint for implementing the algorithm in numerical code.

In the following subsections, two foundational algorithms that leverage the power of tensor networks are presented: the DMRG and VUMPS algorithms. Both methods are formulated in the MPS/MPO framework, yet each addresses different physical settings — finite systems in the case of DMRG, and infinite translationally invariant systems in the case of VUMPS.

4.2.1 Density Matrix Renormalization Group (DMRG)

In this framework, the ground state $|\psi_0\rangle$ of a given Hamiltonian H is sought. As a prototypical example, one may consider a quantum spin chain composed of N sites, where each site is associated with a local Hilbert space $\mathscr{H}_i$ of finite dimension d. The total Hilbert space of the system is given by the tensor product $\mathscr{H} = \bigotimes_{i=1}^{N} \mathscr{H}_i$, whose dimension scales exponentially with system size, namely as d^N.

In principle, the ground state of H can be obtained through exact diagonalization, i.e. solving the eigenvalue problem. However, as the number of sites N increases, the exponential growth of the Hilbert space renders such a procedure computationally intractable. In practice, exact methods are limited to relatively small systems, typically with $N \lesssim 20$ for spin-$1/2$ chains. Thus, more efficient approximation strategies are required for the study of larger systems.

To circumvent this limitation, the DMRG algorithm is employed. Rather than working directly in the full Hilbert space, the ground state is approximated within the class of MPS. In this MPS representation, the state vector $|\psi\rangle$ (ansatz) is encoded by a sequence of low-rank tensors, each associated with a site, and contracted along virtual bonds of bounded dimension.

Within the DMRG algorithm, a variational optimization is performed over the space of MPS with fixed bond dimension χ. This is achieved by locally updating a subset of the tensors — typically one or two neighboring sites — while keeping the remaining tensors fixed. The optimization process

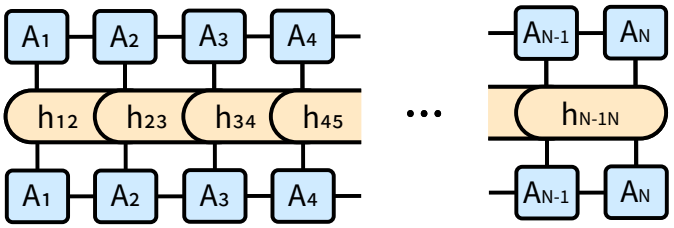

Figure 6 – Diagrammatic representation of the energy expectation value $\langle\psi|H|\psi\rangle$, where the state $|\psi\rangle$ is expressed as a MPS and the Hamiltonian H is encoded as a MPO. Each horizontal layer of tensors corresponds to one copy of the MPS or its adjoint, and the middle layer corresponds to the MPO. Virtual bonds connect neighboring tensors, encoding entanglement and operator structure. This diagram illustrates the central object minimized during the DMRG algorithm in order to approximate the ground state of a one-dimensional quantum system. The contraction of this network yields the total energy, which is optimized over the MPS manifold by iteratively updating local tensors.

is iterated along the entire chain in a sweeping fashion: the local tensors are successively updated from left to right and then from right to left, gradually converging toward the MPS that minimizes the energy expectation value $\langle\psi|H|\psi\rangle$ (see Fig. 6).

The key ingredient that gives the method its name is the use of the reduced density matrix. During each update step, the environment surrounding the local tensors is effectively incorporated via the construction of an effective Hamiltonian. The Hilbert space of the local tensors is then truncated by retaining only the most significant components, as determined by the spectrum of the reduced density matrix. This ensures that the most entangled and physically relevant degrees of freedom are preserved (more details in Ref. [52]).

In the following, the variational structure of the MPS ansatz and the local update strategy underlying the DMRG algorithm are formalized, accompanied by diagrammatic illustrations that emphasize the tensor network architecture at the core of the method.

Variational Principle and Local Optimization

The MPS ansatz, constrained by a fixed maximum bond dimension χ, is expressed in the following canonical form:

$$|\psi[A]\rangle = \sum_{\{i_k\}} A^{[1]i_1} A^{[2]i_2} \cdots A^{[N]i_N} \, |i_1 i_2 \cdots i_N\rangle \,,$$

where each tensor $A^{[k]i_k}$ carries one physical index $i_k \in \{1, \ldots, d\}$ and two virtual indices of dimension at most χ, except at the boundaries. The full state is thus specified by a sequence of tensors $\{A^{[k]}\}$, whose entries are optimized subject to the normalization constraint $\langle\psi|\psi\rangle = 1$.

Due to the high-dimensional nature of the global optimization landscape, the MPS tensors are not updated simultaneously. Instead, a local variational principle is applied, wherein a subset of tensors — typically one or two neighboring sites — is optimized while the remaining tensors are kept

fixed. This yields a local energy minimization problem of the form

$$\min_{|\psi^{\text{loc}}\rangle} \frac{\langle \psi^{\text{loc}} | H_{\text{eff}} | \psi^{\text{loc}} \rangle}{\langle \psi^{\text{loc}} | \psi^{\text{loc}} \rangle},$$

where H_{eff} denotes an effective Hamiltonian that results from contracting all fixed tensors in the network with the global Hamiltonian H, yielding a reduced operator that acts only on the local degrees of freedom being optimized.

In the two-site DMRG scheme, two consecutive tensors, say at sites k and $k+1$, are grouped into a joint object $M^{[k,k+1]}$, which is optimized as a whole. After the optimal local state has been found by solving the associated eigenvalue problem, a SVD is performed:

$$M^{[k,k+1]} = U\, S\, V^{\dagger},$$

and the tensors $A^{[k]}$ and $A^{[k+1]}$ are updated accordingly by reshaping U and $SV^{\dagger}$, with possible truncation of the smallest singular values to preserve the prescribed bond dimension. This SVD step corresponds, in physical terms, to a truncation based on the Schmidt decomposition, ensuring that only the most entangled components are retained.

The sweeping procedure is then carried out by successively applying this local optimization and truncation step along the entire chain, moving from left to right and back. Convergence is monitored by tracking the energy difference between successive sweeps or by evaluating the norm of the residual effective Hamiltonian action. A detailed diagrammatic representation of this local update step is shown in Figure 7

Thermodynamic Limit and Limitations of Finite DMRG

Although the DMRG algorithm is formulated for finite systems, important insights into the bulk behavior of quantum many-body models can be extracted by performing simulations for increasing chain lengths N, and subsequently extrapolating observables to the thermodynamic limit via *finite-size scaling* techniques. In this approach, quantities such as the ground-state energy density, correlation lengths, and entanglement entropy are computed for several system sizes and analyzed as functions of $1/N$, allowing thermodynamic properties to be estimated with controlled precision.

To bypass the need for multiple simulations and to directly target the thermodynamic limit, the *infinite DMRG* (iDMRG) algorithm has been developed. In iDMRG, the lattice is grown iteratively by adding sites to a repeating unit cell, and the MPS is updated at each step using a two-site DMRG update. As the system grows, convergence to a translationally invariant state is sought. This procedure enables a direct treatment of infinite systems and has been successfully applied to a variety of one-dimensional models.

However, several drawbacks are inherent to iDMRG. The algorithm depends sensitively on the size of the unit cell, and convergence may be slow or unstable near quantum critical points due to

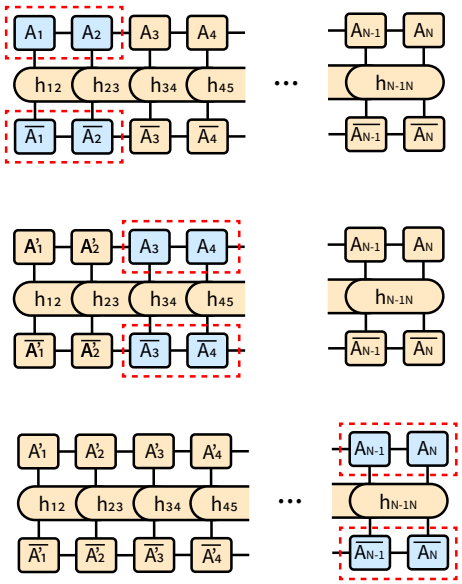

Figure 7 – Schematic depiction of a local update step in the two-site DMRG algorithm. The full tensor network contraction representing the energy expectation value $\langle\psi|H|\psi\rangle$ is decomposed into three parts: (i) the effective Hamiltonian H_{eff} acting on two active sites (highlighted in yellow), and (ii) the variational block $|\psi_{\text{loc}}\rangle$ spanning the two active sites (enclosed in red). This effective problem is solved to determine the optimal local tensor pair. The solution is then reshaped and reabsorbed into the MPS structure via a truncated singular value decomposition, as indicated in the lower part of the figure. The entire procedure is iterated across the chain through successive sweeps.

the entanglement growth and long correlation lengths. Furthermore, the growth process and boundary effects can complicate the interpretation of intermediate states and introduce numerical artifacts in the early stages of the iteration.

To overcome these limitations, the VUMPS algorithm has been proposed as a more robust and efficient alternative. By formulating the problem directly in terms of fixed-point equations for an infinite and translationally invariant MPS, VUMPS achieves rapid convergence and improved numerical stability [49, 50].

4.2.2 Variational Uniform Matrix Product States (VUMPS)

The VUMPS algorithm provides a variationally optimal and computationally efficient framework for determining the ground state of one-dimensional quantum lattice models directly in the thermodynamic limit. Originally introduced by Zauner-Stauber *et al.* in 2018 [49], this method refines and extends the infinite-system iDMRG by eliminating the necessity of system size growth and instead operating directly with a uniform or periodically repeating MPS ansatz.

In this framework, the many-body ground state is approximated by an infinite MPS composed of a tensor $A \in \mathbb{C}^{D\times d\times D}$, where d is the dimension of the local Hilbert space and D is the

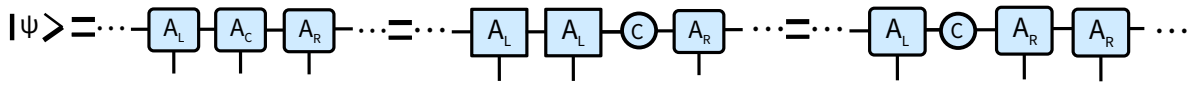

Figure 8 – Diagrammatic representation of the uniform MPS ansatz employed within the VUMPS algorithm. The state $|\psi\rangle$ is expressed in the mixed-canonical form, where the tensors A_L and A_R are left - and right - isometric, respectively, and A_C is the center tensor connecting both canonical forms. Several equivalent representations are illustrated: the leftmost expression corresponds to the standard mixed-canonical form involving A_L, A_C, and A_R; the middle expression introduces a factorization of the center tensor into an isometric tensor and a diagonal matrix C encoding the Schmidt coefficients; and the rightmost expression displays a periodic repetition of the canonical tensors, highlighting the translational invariance of the state in the thermodynamic limit.

bond dimension. Therefore the state can be expressed as

$$|\psi(A)\rangle = \sum_{\vec{\sigma}} \left(\cdots A^{[n-1]} A^{[n]} A^{[n+1]} \cdots \right) |\vec{\sigma}\rangle \,, \tag{4.7}$$

where the tensor A is repeated uniformly across all lattice sites [4].

By exploiting the inherent gauge freedom of the MPS representation, the state can always be brought into a convenient canonical form that facilitates the variational optimization process. In particular, a gauge can be chosen such that the MPS tensors satisfy the orthonormalization conditions specified by Eq. (2) of Ref. [49]. This corresponds explicitly to bringing the MPS into the *mixed-canonical form*, in which the orthogonality center is identified with the unit cell tensor, while the left and right environments are represented by sets of left - and right - isometric tensors, respectively. These tensors are required to satisfy the following conditions:

$$\sum_s (A_L^s)^\dagger A_L^s = \mathbb{I}, \qquad \sum_s A_L^s R (A_L^s)^\dagger = R, \tag{4.8a}$$

$$\sum_s A_R^s (A_R^s)^\dagger = \mathbb{I}, \qquad \sum_s (A_R^s)^\dagger L A_R^s = L, \tag{4.8b}$$

where the first condition in each line enforces the isometric property of the tensors with respect to their physical index, and the second condition guarantees that the fixed-point properties of the left (L) and right (R) transfer operators are preserved.

In this setting, the state can be expressed as

$$|\psi(A)\rangle = \sum_{\vec{\sigma}} \left(\cdots A_L^{[n-1]} A_C^{[n]} A_R^{[n+1]} \cdots \right) |\vec{\sigma}\rangle \,, \tag{4.9}$$

where $A_C^{[n]}$ denotes the tensor at the orthogonality center. Additionally, imposing the condition

$$A_C^{[n]} \equiv A_L^{[n]} C = C A_R^{[n]}, \tag{4.10}$$

[4] This corresponds to a one-site unit cell, but more generally, the unit cell may consist of multiple distinct tensors $\{A^{(1)}, A^{(2)}, \ldots, A^{(N)}\}$, defining a periodic structure with unit cell size N.

with C, a matrix, containing the Schmidt coefficients associated with the bipartition at the center bond, explicitly enforces translational invariance at the level of the MPS representation (see Fig. 8 for a diagrammatic representation). This condition ensures that the center tensor remains invariant under translations across the unit cell, thereby characterizing the true thermodynamic regime of the system. As a result, bulk properties can be computed free from boundary effects, and the MPS efficiently captures the infinite-lattice behavior using only a finite set of parameters.

Having established the uniform MPS ansatz, the next step is to determine the ground state of a given Hamiltonian H within this variational class. Analogously to the procedure employed in DMRG, the ground state is obtained by minimizing the energy expectation value over the manifold of uniform MPS, that is, by solving the variational problem

$$\min_{|\psi\rangle} \frac{\langle\psi|H|\psi\rangle}{\langle\psi|\psi\rangle}. \tag{4.11}$$

In this context, the trial state $|\psi\rangle$ is constrained to the set of translationally invariant MPS characterized by a fixed bond dimension. Due to the explicit parametrization of $|\psi\rangle$ in terms of the center tensor A_C and the isometric tensors A_L, A_R, the variational problem reduces to an effective local optimization over A_C, with the surrounding tensors and environments treated as fixed.

4.2.2.1 Optimization Problem

The optimization problem within the VUMPS framework has been introduced in the previous discussion as the minimization of the energy expectation value over the manifold of translationally invariant uniform MPS. Specifically, for Hamiltonians composed of local two-site terms of the form

$$H = \sum_n h_{n,n+1},$$

the total energy expectation value is expressed as the sum of the expectation values of the individual local terms. When the unit cell is positioned at site $n = 0$, the energy density can be decomposed into three contributions: the local interactions $h_{-1,0}$ and $h_{0,1}$, and the contributions from the left and right infinite environments. These environments correspond to the collections of terms $h_{n,n+1}$ with $n < -1$ and $n > 1$, respectively.

Within this framework, the degrees of freedom subject to optimization are the tensors that define the unit cell, as the energy minimization is effectively formulated in terms of the action of the Hamiltonian H on the variational state $|\psi\rangle$. Given the translationally invariant structure of the ansatz, this variational problem reduces to determining how the effective Hamiltonian acts on the unit cell tensors. In other words, the global variational problem is reformulated as a local one, where the goal is to adjust the unit cell tensors such that the updated tensors A'_C and C' satisfy the local fixed-point condition

$$A'_C = H_{\text{eff}} A_C, \qquad C' = H_{\text{eff}} C, \tag{4.12}$$

where H_{eff} represents the effective Hamiltonian projected onto the unit cell, incorporating contributions from the local two-site terms as well as the left and right infinite environments.

In this sense, the optimization proceeds by obtaining the pair $\{A'_C, C'\}$ that minimizes the energy density under the constraint of translational invariance. This constraint is enforced by requiring the updated tensors to satisfy the consistency condition

$$\|A'_C - A'_L C'\| = \|A'_C - C' A'_R\|, \tag{4.13}$$

which ensures that the left and right canonical forms remain compatible with the updated unit cell tensors. Through this procedure, a new set of isometric tensors $\{A_L, A_R\}$ is obtained, fully characterizing the updated MPS in the canonical form. This approach encapsulates the key iterative step of the VUMPS algorithm, wherein the global variational optimization is reduced to a sequence of local updates governed by the effective Hamiltonian acting on the unit cell.

In order to explicitly formulate the effective Hamiltonian H_{eff} that governs the local variational problem, it is necessary to rigorously characterize the contribution of the infinite environments surrounding the unit cell. Crucially, due to the translational invariance of the system, the expectation value of any local Hamiltonian term $h_{n,n+1}$ for $n < -1$ (or analogously for $n > 1$) does not depend on the specific choice of n, but rather on the asymptotic properties of the state captured by the transfer matrix structure. This observation allows the infinite sum over the environment contributions to be reformulated in terms of the spectral properties of the transfer matrices associated with the left - and right - isometric tensors.

In this scenario, the definition of the environment naturally arises from the spectral properties of the transfer matrix associated with the isometric tensors. The left - and right - isometric tensors, A_L and A_R, define transfer matrices that act as completely positive (CP) maps on the space of $D \times D$ operators. Formally, the transfer matrices associated with the left and right isometric tensors are defined as:

$$T_L \coloneqq \sum_s \overline{A_L^s} \otimes A_L^s, \tag{4.14}$$

$$T_R \coloneqq \sum_s \overline{A_R^s} \otimes A_R^s, \tag{4.15}$$

where the overline denotes element-wise complex conjugation without transposition.

As CP maps, these transfer matrices admit spectral decompositions characterized by a unique leading eigenvalue $\lambda_0 = 1$, associated with the steady-state eigenspace, and a set of subleading eigenvalues $\{\lambda_j\}$ satisfying $|\lambda_j| < 1$ for all $j > 0$. Accordingly, any operator T in this space can be decomposed as

$$T = P_0(T) + \sum_{j=1}^{D^2-1} \lambda_j P_j(T), \tag{4.16}$$

where P_0 denotes the projector onto the dominant eigenspace, while P_j are the projectors associated with the subleading eigenspaces.

In particular, the following identity holds:

$$\mathbb{I} - \tau = P_0(T) + \sum_{j>0} (1 - \lambda_j) P_j(T), \tag{4.17}$$

where $\tau \coloneqq T - P_0(T)$ represents the projection of the transfer matrix onto the subspace orthogonal to the steady state. Consequently, the inverse of this operator can be formally expressed as

$$(\mathbb{I} - \tau)^{-1} = P_0(T) + \sum_{j>0} \frac{1}{1-\lambda_j} P_j(T), \tag{4.18}$$

which is well-defined within the subspace orthogonal to the dominant eigenspace.

This decomposition allows for the resummation of infinite geometric series over powers of the transfer matrix:

$$\begin{aligned} \sum_{n=0}^{\infty} T^n &= |\mathbb{N}|\, P_0(T) + \sum_{j=1}^{D^2-1} \frac{1}{1-\lambda_j} P_j(T) \\ &= |\mathbb{N}|\, P_0(T) + (\mathbb{I} - P_0(T))(\mathbb{I} - \tau)^{-1}, \end{aligned} \tag{4.19}$$

where the divergent term proportional to $P_0(T)$ encapsulates the extensive contribution due to the infinite system size.

In this scenario, it is natural to express the contribution of the infinite left (or right) environment in terms of an *environment Hamiltonian*, denoted $(H_L|$ (or $|H_R)$), respectively. These are linear functionals acting over the operator space, formally defined as

$$(H_L| = (h_L| \sum_{k=0}^{\infty} [T_L]^k\,, \tag{4.20}$$

$$|H_R) = \sum_{k=0}^{\infty} [T_R]^k\, |h_R)\,, \tag{4.21}$$

where $(h_L|$ and $|h_R)$ encode the contributions of the individual local interaction terms $h_{n,n+1}$ for sites $n < -1$ and $n > 1$, respectively[5].

Leveraging the spectral decomposition of the transfer matrix, this problem can instead be reformulated, following Eq. (4.19), as the solution of a *linear but inhomogeneous system* restricted to the subspace orthogonal to the steady-state eigenspace. This leads directly to the closed-form equation system

$$(H_L|\,[\mathbb{I} - T_L + |R)\,(\mathbb{I}|] = (h_L| - (h_L|R)\,(\mathbb{I}|\,, \tag{4.22}$$

$$[\mathbb{I} - T_R + |\mathbb{I})\,(L|]\,|H_R) = |h_R) - |\mathbb{I})\,(L|h_R)\,. \tag{4.23}$$

Recasting the problem into this linear algebraic form not only regularizes the divergences associated with the dominant eigenspace but also enables the application of well-established computational techniques from numerical linear algebra. In particular, the resulting linear systems are

[5] Throughout this formulation, objects of the form $|X)$ and $(X|$ represent *vectorized operators*. Specifically, an operator acting on a D-dimensional Hilbert space is reshaped into a vector in a D^2-dimensional space, following the standard mapping $\mathrm{vec}(O) = \sum_{i,j} O_{ij}|i\rangle \otimes |j\rangle$.

typically high-dimensional but sparse or structured, making them amenable to iterative Krylov subspace methods such as GMRES, BiCGSTAB, or Conjugate Gradient for normal equations. These algorithms are widely implemented in robust and high-performance numerical libraries, including `IterativeSolvers.jl` and `Krylov.jl` in the Julia ecosystem. Such solvers are specifically optimized for handling large-scale linear systems where matrix-free formulations are advantageous—a natural fit given that transfer matrices $T_{L/R}$ are usually implemented as linear maps rather than explicitly constructed matrices in tensor network algorithms.

It is important to emphasize that the divergent term, which scales proportionally to the system size $|\mathbb{N}|$, corresponds to the extensive contribution of the *bulk energy density*. This term arises from the steady-state component of the transfer matrix, specifically from the projector $P_0(T)$ associated with the dominant eigenvalue $\lambda_0 = 1$. Physically, it reflects the contribution of an infinite number of identical local terms distributed throughout the bulk of the lattice.

Crucially, this divergent contribution is *independent* of the variational degrees of freedom encoded in the MPS tensors. As such, it constitutes a constant energy shift that affects the total energy uniformly across all candidate states within the variational manifold. Discarding this term does not impact the physical validity of the variational procedure, as the optimization depends exclusively on energy differences and gradients with respect to the parameters, not on absolute energy offsets.

This is entirely consistent with standard practices in statistical physics and condensed matter, where the thermodynamic limit naturally leads to divergences in extensive quantities like total energy. What remains physically meaningful are intensive quantities, such as the energy density, and finite corrections arising from boundaries or local perturbations.

Therefore, the physically relevant, finite contribution to the environment Hamiltonian corresponds precisely to the solution of the linear systems derived above, formulated over the vectorized operator space and projected onto the subspace orthogonal to the steady-state eigenspace. This finite part fully captures the influence of the infinite environment on the variational optimization, while the divergent bulk term can be systematically ignored without any loss of physical information or accuracy in determining the ground state properties.

All the mathematical structure and physical insights discussed so far are elegantly encapsulated in the tensor network diagrams presented in Figs. 9 to 12. Specifically, Fig. 9 illustrates the definition of the transfer matrices T_L and T_R, which encode how local tensors propagate correlations along the infinite lattice. Figure 10 depicts the diagrammatic construction of the environment Hamiltonians H_L (and analogously H_R), expressed as infinite geometric sums over the transfer matrices, weighted by the local interaction term $h_{i,i+1}$. This diagram concisely captures how the environment contribution is formally resummed and how its divergent and finite components are disentangled within the thermodynamic limit framework.

Building on these ingredients, the action of the effective Hamiltonian H_{eff} on the unit cell is graphically summarized in Figs. 11 and 12. Figure 11 illustrates the application of the effective Hamil-

tonian H_{A_C} on the center tensor A_C, producing the updated tensor A'_C. Complementarily, Fig. 12 represents the action of the effective Hamiltonian H_C on the bond tensor C, yielding the updated tensor C'. Together, these two operations constitute the core variational loop of the VUMPS algorithm, providing a computationally efficient and physically transparent route to accurately determine ground states directly in the thermodynamic limit.

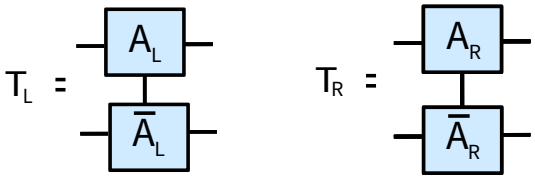

Figure 9 – Graphical representation of the left and right transfer operators T_L and T_R, constructed from the isometric tensors A_L and A_R.

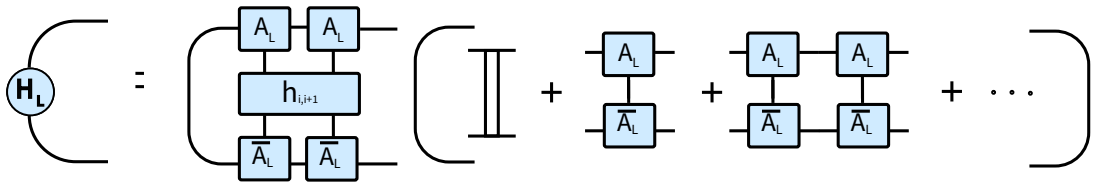

Figure 10 – Diagrammatic construction of the left environment Hamiltonian H_L based on the infinite sum over the transfer matrix and the local Hamiltonian term $h_{i,i+1}$.

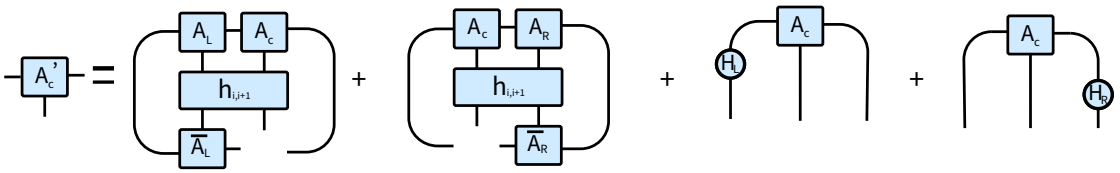

Figure 11 – Action of the effective Hamiltonian H_{eff} on the center tensor A_C, producing the updated tensor A'_C.

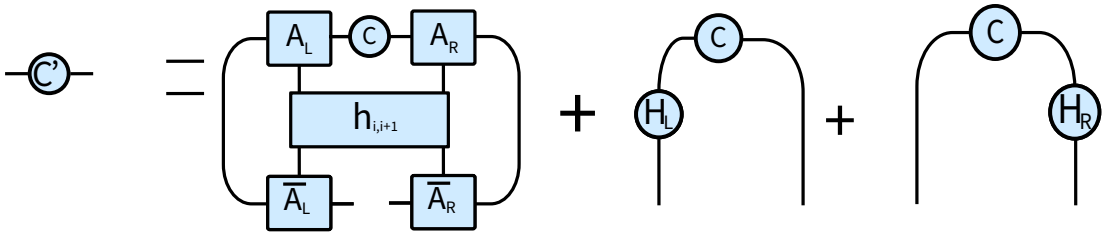

Figure 12 – Action of the effective Hamiltonian H_{eff} on the bond tensor C, yielding the updated tensor C'.

5 Entanglement Analysis of Quantum Spin Chains

In the preceding chapters, a comprehensive theoretical foundation was established by introducing key concepts from *Quantum Information Theory*, the fundamental aspects of *Quantum Phase Transitions*, and the *Tensor Network Formalism* employed for the efficient description and simulation of many-body quantum systems. These topics collectively provide the necessary conceptual and computational tools for the analysis of entanglement properties in quantum spin chains and their role in characterizing distinct quantum phases. Building upon these foundations, this chapter is devoted to presenting the specific methodologies and computational procedures adopted in this work to investigate the entanglement structure of one-dimensional QIM (Quantum Ising Model) in the thermodynamic limit.

5.1 Model Definition

In this work, the QIM is employed as the primary physical system for investigating the role of entanglement in characterizing quantum phase transitions. In such scenario, the Hamiltonian under consideration is defined as:

$$H(\lambda) \coloneqq -\frac{1}{2}\left(\lambda \sum_i \sigma_x^i \sigma_x^{i+1} + \sum_i \sigma_z^i\right), \tag{5.1}$$

where λ is a dimensionless coupling parameter controlling the strength of spin-spin interactions relative to the external transverse magnetic field, and σ_α^i $(\alpha = x, z)$ denote the Pauli matrices acting on site i.

As previously discussed in Chapter 3, this model exhibits a well-known quantum phase transition at the critical point $\lambda_c = 1$. For $\lambda < 1$, the system is in a *ferromagnetic phase*, characterized by an ordered[1] ground state dominated by the external magnetic field. Conversely, for $\lambda > 1$, the system undergoes spontaneous symmetry breaking, entering a *paramagnetic phase* where long-range order emerges due to the dominance of spin-spin interactions in x-direction. It is important to emphasize that this phase transition occurs exclusively at the ground-state level. Consequently, the accurate determination of the ground state becomes a fundamental step in the analysis of critical behavior. To this end, the VUMPS algorithm (see subsection 4.2.2 for a method review) was employed, allowing for the direct computation of ground-state properties in the thermodynamic limit.

Moreover, as discussed in the previous chapter, the VUMPS algorithm requires the explicit definition of a unit cell. For the case of a one-site unit cell, a dedicated implementation was developed

[1] Here, ordered means full aligned in the z-direction.

specifically for this work (see appendix). However, for more general scenarios involving larger unit cells, the `ITensor.jl` library[2] was utilized to perform the numerical computations efficiently.

An important feature of the QIM is that its ground state can be efficiently computed for any value of the coupling parameter λ. This capability enables a systematic investigation of the ground-state properties across the entire parameter space. For each fixed value of λ, the corresponding ground state is obtained, allowing the evaluation of physical quantities and entanglement measures at that specific point. By repeating this procedure for a continuous range of λ, it becomes possible to study the scaling behavior of these quantities as functions of the coupling parameter, thereby revealing critical signatures and universal properties associated with the phase transition.

Once the global ground state has been obtained in the thermodynamic limit under the assumption of translational invariance, the reduced density matrix corresponding to the unit cell is extracted. Specifically, if the unit cell contains N sites, the reduced state ρ_{cell} is computed by tracing out the degrees of freedom external to this block (as represented in Fig. 3c). Within this reduced state, the tools introduced in Chapter 2 are employed to analyze the entanglement structure. In this context, two main approaches can be pursued. The first involves calculating the vNE (von Neumann entropy) of ρ_{cell}, which quantifies the bipartite entanglement between the unit cell and the remainder of the infinite chain. This quantity serves as a physically meaningful measure of the entanglement contribution associated with the chosen partition. Alternatively, one can investigate the internal entanglement structure of the unit cell by applying multipartite entanglement measures directly to ρ_{cell}.

5.1.1 Numerical Results and Validation of the Simulation

Before presenting the main numerical results, it is crucial to validate the consistency and physical reliability of the obtained ground states. To this end, a series of diagnostic checks was performed to ensure that the simulations correctly capture the essential features of the QIM in the thermodynamic limit. In the present, the ground-state wavefunction was obtained using the VUMPS algorithm for unit cells of different sizes $N = [1, 2, 3, 4]$, and for each case, a smooth scan over the coupling parameter $\lambda \in [0.1, 3.0]$ was carried out.

For this simulations, the maximum bond dimension was set to `maxdim` = 80, meaning that the dimension of the virtual (auxiliary) indices connecting neighboring tensors in the MPS representation was restricted to a maximum of 80. A truncation cutoff of $\epsilon = 10^{-6}$ was used to discard singular values below this threshold during the subspace expansion steps. This ensures that only the most relevant Schmidt components are retained in the representation, effectively controlling the approximation error introduced during the iterative update process. To monitor the stability of the algorithm, an energy convergence tolerance of 10^{-5} was enforced, such that the VUMPS iterations were halted when the relative variation in the energy density between successive steps fell below this threshold. In

[2] ITensor is a high-performance tensor network library available for Julia, C++, and Python. The Julia version was adopted due to its high-level syntax, execution speed comparable to low-level languages, and native support for advanced linear algebra operations, providing an ideal balance between code readability and computational efficiency, more details can be found in Ref. [111, 112].

addition to energy convergence, an invariance tolerance parameter $\texttt{tol} = 10^{-5}$ was imposed to assess the fidelity of translational invariance in the final uniform MPS. Specifically, the consistency condition

$$\left\| \left(\prod_{i=1}^{N} A_L^{[i]} \right) C^{[N]} - C^{[1]} \left(\prod_{i=1}^{N} A_R^{[i]} \right) \right\| < \texttt{tol}$$

was required to hold at the end of the optimization. This ensures that the canonical form of the uMPS remains preserved across iterations and that the infinite chain is described by a state invariant under translations by the unit cell.

In particular, Figure 13 presents the numerical evaluation of the translational consistency condition for the case $N = 1$. As expected, the deviation remains below the imposed tolerance (10^{-5}) for all λ, with a small peak observed near the critical point $\lambda_c = 1$, where entanglement is maximal and convergence becomes intrinsically more challenging.

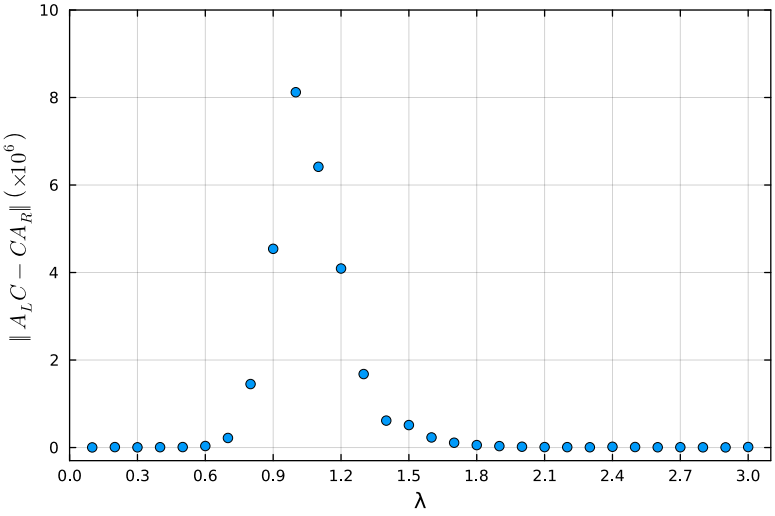

Figure 13 – Numerical evaluation of the translational invariance condition in the ground state obtained via VUMPS times 10^6. The plot shows the norm (i.e. 2-norm) of the deviation $\left\| \left(\prod_{i=1}^{N} A_L^{[i]} \right) C - C \left(\prod_{i=1}^{N} A_R^{[i]} \right) \right\|$ as a function of λ, for the case of a one-site unit cell, i.e. $N = 1$.

It is important to emphasize that convergence of the energy expectation value alone does not necessarily imply that the variational state faithfully approximates the true ground state. While the energy is obtained as a functional expectation value $E[\psi] = \langle\psi|H|\psi\rangle \,/\, \langle\psi|\psi\rangle$, it depends only on the projection of $|\psi\rangle$ onto the low-energy eigenspace of H. In particular, a state with high overlap with the ground state $|E_0\rangle$ can yield an energy close to E_0, but so can other states with substantial contributions from low-lying excitations. Thus, the energy may appear converged even if the full set of physical correlations encoded in the true ground-state vector is not accurately captured. This reflects the fact that computing eigenvalues is generally more stable and numerically less demanding than accurately resolving eigenvectors, which require capturing the correct entanglement structure and long-range correlations. Consequently, additional diagnostic checks — such as examining the preservation

of translational invariance or evaluating physical observables — are necessary to ensure the physical fidelity of the variational solution.

Given the aforementioned concern that energy convergence alone does not guarantee the physical reliability of the variational state, particular attention was paid to verifying whether the relevant quantum correlations were faithfully captured. To this end, the von Neumann entropy $\mathcal{S}(\rho_{\text{cell}})$ of the reduced density matrix associated with the unit cell was computed. This quantity serves as an indicator of how strongly the sites (or particles) comprising the unit cell are entangled with the remainder of the infinite chain, and thus provides a meaningful measure of bipartite quantum correlations across the chosen partition. The results are shown in Figure 14, where the entropy is observed to increase as the critical point $\lambda_c = 1$ is approached, followed by a saturation[3].

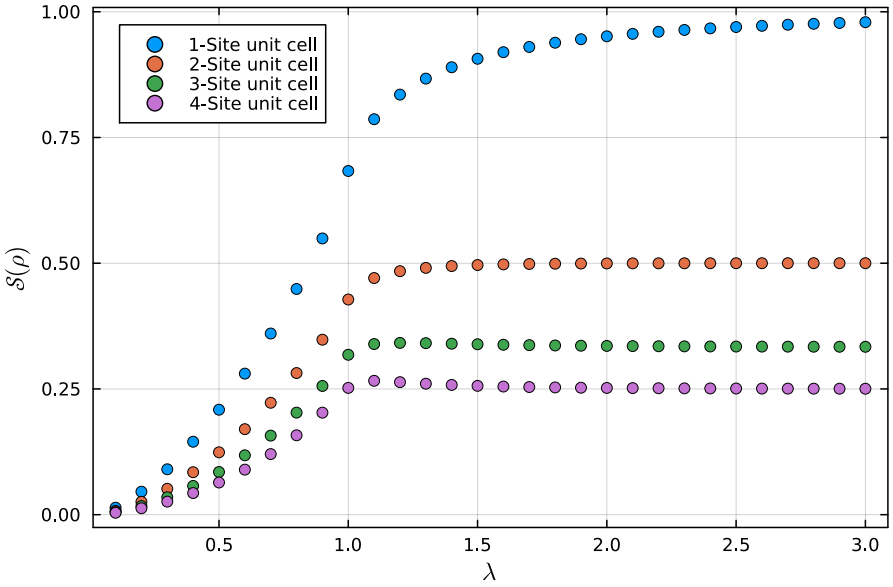

Figure 14 – Von Neumann entropy $\mathcal{S}(\rho)$ of the reduced density matrix ρ associated with the unit cell, computed as a function of the transverse field λ for different unit cell sizes $N = 1, 2, 3, 4$. This quantity measures the bipartite entanglement between the unit cell and the rest of the infinite chain.

Although the vNE, $\mathcal{S}(\rho_{\text{cell}})$, is inherently a bipartite quantity, it is important to emphasize that increasing the number of sites within the unit cell enriches the informational content of the bipartition. By enlarging the block size, a more representative cross-section of the many-body ground state is retained, allowing for a finer resolution of the underlying entanglement structure. This is particularly evident in the case $N = 4$, for which the signature of criticality near $\lambda = 1$ becomes significantly more pronounced. The emergence of a sharper entanglement peak in this regime highlights the advantages of employing larger partitions when extracting physical information from entropic observables, especially in the vicinity of QPT, where long-range correlations dominate.

[3] Note that, the numerical value of the vNE depends on the Hilbert space dimension of the reduced state. Consequently, direct comparisons of entanglement between unit cells of different sizes (e.g., between $N = 1$ and $N > 1$) become nontrivial. To address this, the logarithm appearing in the entropy definition was taken with base 2^N, such that the maximally mixed state of a system with dimension 2^N attains unit entropy.

5.2 Multipartite Entanglement Structure of the Unit Cell

Building upon the ensemble of reduced density matrices ρ_{cell} obtained in the previous subsection, an analysis was carried out to investigate the structure of multipartite entanglement within the unit cell. While the vNE provides insight into bipartite entanglement between the cell and its environment, it does not capture the intricate correlations that may exist among the individual constituents of the cell itself. To address this limitation, one can look to *multinegativity*.

As discussed in Chapter 2 (see Section 2.6), the multinegativity serves as a quantitative indicator of genuinely multipartite entanglement, defined operationally through the framework of fully decomposable entanglement witnesses. For a given density matrix ρ, this measure is obtained by minimizing the expectation value of ρ over the set of all fully decomposable witnesses. A negative value of this expectation certifies the presence of entanglement that cannot be accounted for by any bipartite entanglement across a single partition[4].

The results corresponding to a four-site unit cell are shown in Figure 15, where the multinegativity $\mathcal{N}(\rho_{\text{cell}})$ is defined as in Section 2.6. This plot provides a direct quantification of the genuinely multipartite correlations present within the unit cell and complements the bipartite characterization offered by the vNE. A pronounced peak is observed near the critical point $\lambda = 1$, where the multi-

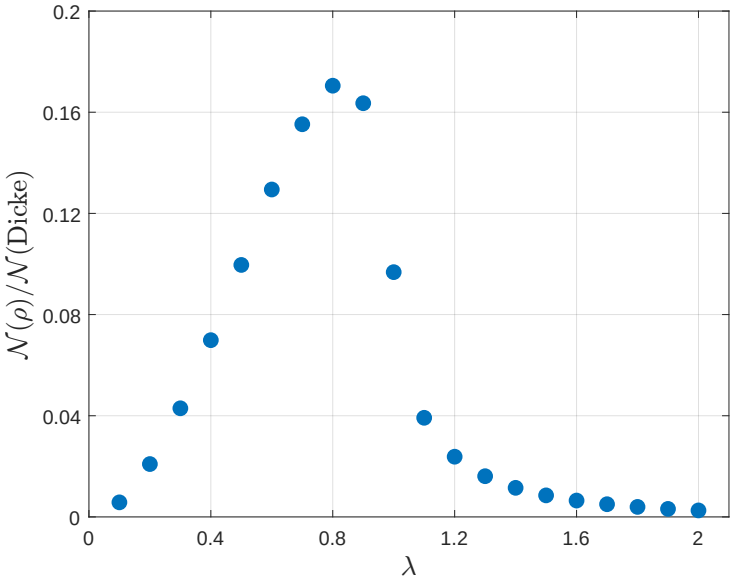

Figure 15 – Normalized genuine multipartite negativity $\mathcal{N}(\rho)/\mathcal{N}(\text{Dicke})$ as a function of the Hamiltonian parameter λ. Each data point corresponds to the value of multinegativity computed for the reduced state $\rho_{\text{cell}}(\lambda)$, obtained as the ground state of a translationally invariant spin chain for the specified parameter. Normalization was performed with respect to the value obtained for the Dicke state with two excitations among four qubits, defined as: $\left|D_4^{(2)}\right\rangle = \frac{1}{\sqrt{6}}(|0011\rangle + |0101\rangle + |0110\rangle + |1001\rangle + |1010\rangle + |1100\rangle)$, which is known to exhibit maximal genuine multipartite entanglement under the fully decomposable witness criterion.

[4] The multinegativity was computed numerically using a MATLAB implementation based on the `YALMIP` framework for semidefinite programming.

negativity sharply increases before rapidly decaying[5]. This non-monotonic behavior indicates that genuinely multipartite entanglement encode essential features of the system's quantum phase transition.

This observation raises the possibility of a divergent trend in $\mathcal{N}(\rho_{\text{cell}})$, consistent with the critical scaling behavior often exhibited by entanglement-sensitive observables. To explore this hypothesis, the numerical derivative of the multinegativity with respect to the Hamiltonian parameter λ was computed. This analysis aims to determine whether the observed peak corresponds to a true divergence and, if so, whether it follows a logarithmic scaling law analogous to that reported for bipartite entanglement measures in earlier studies [37].

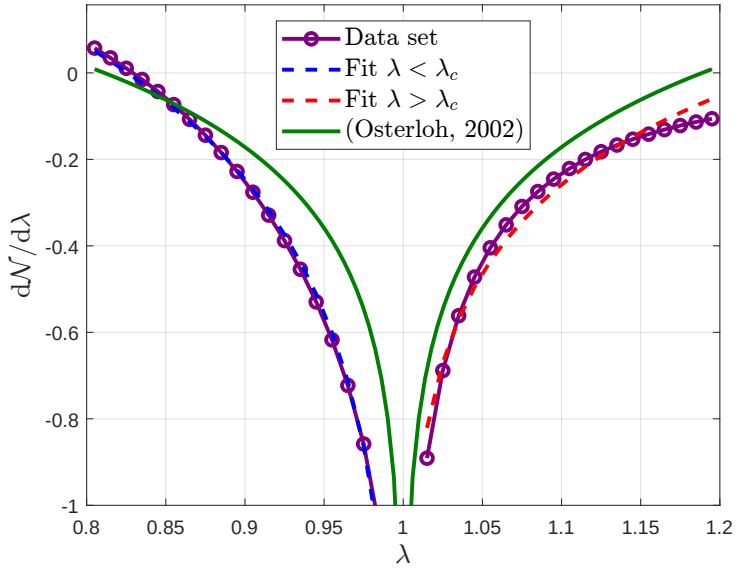

Figure 16 – Numerical derivative of the normalized genuine multipartite negativity $\mathcal{N}(\rho)/\mathcal{N}(\text{Dicke})$ with respect to the Hamiltonian parameter λ. Each data point represents the finite-difference estimate of $d\mathcal{N}/d\lambda$ evaluated from the entanglement data shown in Figure 15. A clear peak emerges near the critical point $\lambda = 1$, consistent with a logarithmic divergence. Linear fits of the form $A \log|\lambda - \lambda_c| + B$ were performed separately for the regions $\lambda < \lambda_c$ and $\lambda > \lambda_c$, and are displayed as dashed lines. The scaling curve reported in Ref. [37] is also shown for comparison, highlighting the structural similarity between bipartite and multipartite entanglement scaling near criticality.

The results of the linear fits (see the caption of Fig. 16) yield the following coefficients: for $\lambda < \lambda_c$, the best-fit parameters are $A = 0.44466$ and $B = 0.77762$, while for $\lambda > \lambda_c$, the corresponding values are $A = 0.29656$ and $B = 0.4246$. These values quantify the rate at which the derivative of the normalized multinegativity diverges as the critical point is approached from either side. More importantly, the emergence of a logarithmic divergence in $d\mathcal{N}/d\lambda$ provides compelling evidence that the genuine multipartite entanglement encoded in the reduced ground state ρ_{cell} becomes increasingly singular in the vicinity of the critical point. This behavior is consistent with the scaling

[5] To enable meaningful quantitative comparisons, the multinegativity values were normalized by the value obtained for the Dicke state $\left|D_4^{(2)}\right\rangle = \frac{1}{\sqrt{6}}(|0011\rangle + |0101\rangle + |0110\rangle + |1001\rangle + |1010\rangle + |1100\rangle)$, which is known to exhibit maximal genuine multipartite entanglement under the fully decomposable witness criterion. This normalization is analogous to the convention adopted in von Neumann entropy calculations, where the entropy of the maximally mixed state is set to unity, thus establishing a natural reference scale for the degree of entanglement.

properties previously documented for bipartite entanglement near quantum phase transitions [37], and extends similar insights into the multipartite regime. Notably, this critical enhancement of multipartite correlations had already been observed in prior investigations employing DMRG techniques and finite-size scaling analysis [78], where it was shown that the geometric entanglement and related multipartite measures also exhibit divergent behavior at criticality. The present findings thus reinforce the interpretation that the peak in multinegativity is not a numerical artifact or a finite-size anomaly, but rather a hallmark of an underlying diverging many-body correlation structure. As such, the multinegativity can be regarded as a robust and physically meaningful indicator of quantum criticality, capable of capturing genuinely multipartite features that transcend the bipartite framework.

Nevertheless, all such approaches rely fundamentally on the operation of partial trace, which—although necessary due to the inaccessibility of full many-body quantum states—may introduce significant interpretive limitations. In particular, this form of reduction can obscure essential global features of the system, as exemplified by the GHZ state, whose reduced density matrices are all separable despite the presence of maximal global entanglement. These limitations motivate the exploration of alternative strategies for quantum state reduction that preserve more faithfully the informational content of the full state. Within this perspective, ongoing research has been directed toward defining an "unbiased" reduction procedure, aiming to identify a reduced state on $N - k$ subsystems that optimally reflects the structure and properties of the original N-partite system.

5.3 Towards Unbiased Quantum State Reductions

As an alternative to the standard reduction scheme, i.e., the partial trace, a different perspective can be adopted: instead of tracing out the degrees of freedom of a subset of k particles, one may consider applying a family of local operations—such as local projections—on those particles, effectively conditioning the resulting state on a particular measurement outcome. In this framework, the reduced state is not defined through marginalization, but rather through the selection of outcomes induced by controlled operations on the discarded part of the system. This raises a natural and fundamental question: which projections should be applied in order to extract the most informative or structurally relevant reduced state?

The choice of such projections is far from arbitrary, as distinct measurement bases or local operations may emphasize different facets of the entanglement structure or reveal specific symmetry properties of the global quantum state. Rather than seeking to maximize a particular informational quantity or entanglement measure, an alternative guiding principle may be adopted: the selected projections should perturb the original state as little as possible. In this context, the notion of *unbiasedness* is understood as the requirement that the reduced state faithfully preserves the intrinsic correlations and structural characteristics of the full N-partite system, without introducing preferential treatment of specific subsystems or artificial asymmetries resulting from the reduction procedure itself.

In a more operational language, consider a global pure state $\left|\psi^N\right\rangle$ represented as a Matrix

Product State (MPS) over N sites, with local tensors $\{A_1, A_2, \ldots, A_N\}$. Rather than tracing out a subset of k sites, one may apply local projective measurements on those sites, each specified by a projection operator $P_j = |u_j\rangle \langle u_j|$. In the MPS formalism, this corresponds to contracting the local tensors A_j with the bra $\langle u_j|$, effectively collapsing the associated physical indices and yielding a new MPS defined on the remaining $N - k$ sites. The figure below illustrates this procedure:

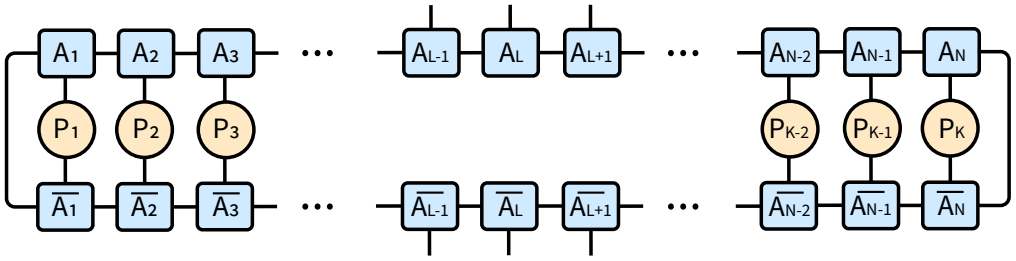

Figure 17 – Schematic representation of a structure-preserving reduction on an MPS. The initial quantum state is encoded in a sequence of local tensors $\{A_1, A_2, \ldots, A_N\}$. A set of local projective measurements, denoted by operators $\{P_1, P_2, \ldots, P_k\}$, is applied to the first k physical sites. Each projection is implemented as a contraction of the corresponding tensor A_j with the conjugate of the local state $\langle u_j|$, effectively collapsing the respective physical index.

To further exemplify the principles discussed above, a more concrete scenario may be considered in which the global quantum state $\left|\psi^N\right\rangle$ is described as a uniform MPS, typically obtained via the VUMPS algorithm. In this setting, additional structural information becomes accessible, allowing the symmetries and interaction terms present in the Hamiltonian to be exploited to guide the identification of local projections that preserve the essential features of the state. Such a formulation is not overly restrictive, as several paradigmatic entangled states can be realized as ground states of simple local Hamiltonians. For instance, the GHZ state can be recovered as the ground state of the QIM in the ordered regime ($\lambda \gg 1$), while the W state can be approximated as the ground state of the XY model under appropriate conditions. In this light, it is natural to consider that the structure of the Hamiltonian may inform the selection of projection directions that minimally disturb the quantum state.

In particular, for the ground state of the QIM, projections in the σ^z or σ^x basis may introduce structural bias. In the limit of large λ, the ground state is known to converge to a GHZ-type state aligned along the z-axis. If local projections are performed in the σ^z basis, a specific classical configuration—such as $|0\rangle^{\otimes N}$ or $|1\rangle^{\otimes N}$—is selected, thereby collapsing the superposition and favoring one symmetry-broken branch. Similarly, projections in the σ^x basis lead to analogous symmetry-breaking effects due to the presence of the interaction term $\sigma_i^x \sigma_{i+1}^x$ in the Hamiltonian.

To avoid such preferential treatment, projections in the σ^y basis may be employed. Since the σ^y operator does not appear in the Hamiltonian and fails to commute with both σ^x and σ^z, its eigenbasis is not aligned with any of the natural symmetry axes of the model. Consequently, a projection in the σ^y basis perturbs the quantum state in a more uniform and nonselective manner. In this sense,

such measurements may be regarded as more *unbiased*, as they tend to preserve the global coherence and entanglement structure inherent to the original state.

This process is schematically illustrated in Fig. 18, where the action of the unbiased local projection is represented through its incorporation into the MPS transfer structure. The contraction with the projectors is absorbed into a modified transfer matrix, and the resulting composition is governed—under spectral decomposition—by its dominant eigenvalue contribution.

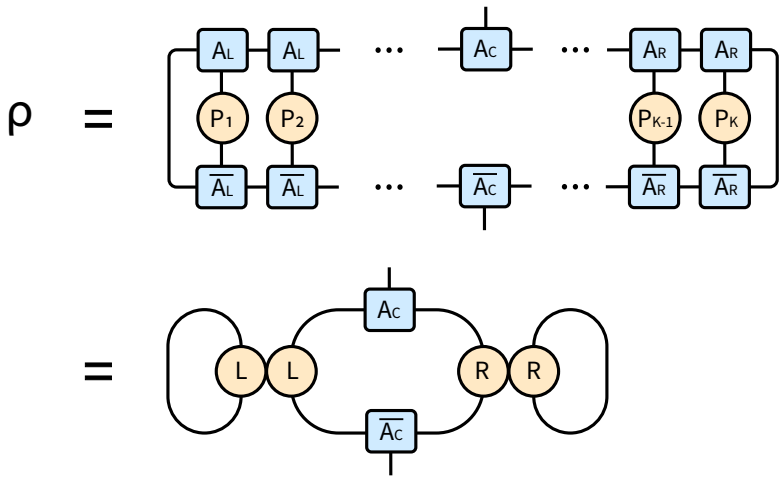

Figure 18 – Diagrammatic representation of a projected transfer matrix structure. The original uniform MPS consists of infinite repetitions of left and right isometric tensors (A_L, A_R) and a central core (A_C). Upon application of the local projector P across all sites, the contractions $P_j A_j$ are absorbed into the transfer structure, yielding a modified transfer operator. In the thermodynamic limit, the dominant behavior is governed by the largest eigenvalue of this operator.

To numerically validate the ideas presented above, the concepts of unbiased reduction were applied to compute two distinct quantities of interest: the *genuine multipartite negativity* and the *quantum coherence* of the reduced state. As demonstrated earlier, the multipartite negativity serves as a robust entanglement-based indicator of quantum phase transitions, exhibiting singular behavior near criticality. In addition, the relative quantum coherence of the reduced state was evaluated as a complementary quantity. This was computed with respect to the computational basis (σ^z-eigenbasis), following the framework introduced by Baumgratz, Cramer, and Plenio in Ref. [113], where coherence is quantified as the relative entropy between the full state and its fully dephased counterpart, i.e.,

$$\mathcal{C}_{\text{rel}}(\rho) = \mathcal{S}(\rho_{\text{diag}}) - \mathcal{S}(\rho),$$

where ρ_{diag} denotes the dephased state of ρ in the reference basis and $\mathcal{S}(\cdot)$ is the von Neumann entropy.

It is worth emphasizing that the post-measurement reduced states obtained through local projections are pure. In this scenario, the relative entropy of coherence reduces to the Shannon entropy of the probability distribution associated with the measurement outcomes in the chosen basis. Since the computational basis is aligned with the eigenstates of the local σ^z operator—which also serves as the order parameter for the model—this entropy directly reflects the uncertainty or information content

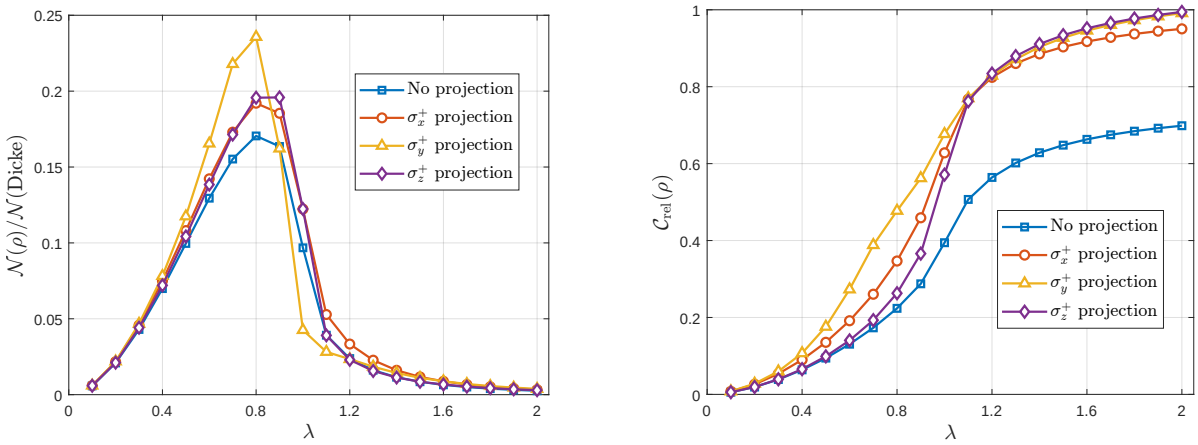

(a) (a) Multinegativity $\mathcal{N}(\lambda)$

(b) (b) Relative quantum coherence $C_{\mathrm{rel}}(\lambda)$

Figure 19 – Comparison of quantum information quantities under different projection bases. Panel (a) shows the multinegativity of the reduced state, while panel (b) displays the relative quantum coherence computed in the σ^z basis. Both quantities are evaluated for the original state and after projections in the σ^x, σ^y, and σ^z bases.

associated with measurements of the order parameter. Consequently, maximizing the coherence of a pure state in a given basis is formally equivalent to maximizing the Shannon entropy of the associated measurement distribution. From an informational perspective, this corresponds to a scenario in which the measurement reveals minimal information about the system, thereby introducing minimal disturbance. In this light, coherence maximization can be interpreted as a principle of unbiased measurement: the more uniformly distributed the outcomes are, the less biased the measurement becomes with respect to the underlying order of the system.

As can be observed in Fig. 19, the choice of projection basis has a significant impact on the ability to preserve relevant structural features of the quantum state. In panel (a), the behavior of the genuine multipartite negativity under different projections reveals a clear advantage for the σ^y-based reduction. Notably, this projection captures the singular behavior in the vicinity of the quantum critical point, as evidenced by the sharp discontinuity in the derivative of $\mathcal{N}(\lambda)$. This observation reinforces the interpretation of the σ^y projection as the most structure-preserving and sensitive to critical phenomena. Panel (b) complements this picture by showing that the same projection also leads to the highest relative coherence among all the projected scenarios. Since coherence in this context is equivalent to the Shannon entropy of the measurement distribution in the σ^z basis—directly related to the order parameter—its maximization indicates that the σ^y projection minimizes information gain and, thus, bias. Importantly, both analyses were performed using the same simulation setup described previously, ensuring consistency and comparability across the results.

In this sense, the above discussion leads naturally to the formulation of a guiding conjecture for structure-preserving reductions in quantum many-body systems. Based on both conceptual arguments and numerical evidence, it is proposed that:

The most unbiased local projection is the one that simultaneously preserves the symmetries

of the Hamiltonian, retains the qualitative type of entanglement present in the original state, and maximizes the local quantum coherence (i.e., the observational entropy) for a given observable.

5.4 Final Remarks and Perspectives

In this dissertation, the intricate interplay between quantum information theory and many-body physics has been thoroughly investigated, with particular emphasis on the role of entanglement in low-dimensional spin systems. The discussion began with a conceptual framework grounded in the formal structure of quantum mechanics. A geometric interpretation of quantum states was advanced, wherein the convex structure of the state space was shown to entail a fundamental classification of quantum states into separable and entangled categories. This perspective not only elucidates the mathematical underpinnings of quantum correlations but also underscores the operational relevance of entanglement as both a physical and informational resource.

From the outset, it was posited that entangled states—once regarded as counterintuitive theoretical constructs—now constitute a cornerstone in the development of quantum technologies, including quantum communication, cryptography, and computation. In light of this, the dissertation was organized to address a comprehensive range of questions concerning entanglement: its formal characterization, the methods by which it can be quantified, and the computational frameworks appropriate for investigating it in physically realistic many-body systems. By systematically integrating theoretical insights, numerical techniques, and analytically tractable models, a cohesive and multifaceted exploration of entanglement was undertaken.

Within this broader context, the principal objective was to examine entanglement as a diagnostic quantity capable of capturing emergent physical properties in structured microscopic systems, particularly one-dimensional quantum spin chains. To anchor this investigation, the concept of quantum phase transitions was introduced. These transitions, as firmly established in the literature, originate from abrupt qualitative changes in the ground state structure driven by quantum fluctuations and mediated by variations in a Hamiltonian control parameter. Special emphasis was placed on analytical and algebraic techniques drawn from mathematical physics, as elaborated in the chapter on quantum phase transitions. A class of exactly solvable models was examined, with particular focus on spin-$\frac{1}{2}$ chains with nearest-neighbor interactions, which stand as paradigmatic systems for probing critical behavior in strongly correlated quantum matter.

Building on this theoretical foundation, the tensor network formalism—particularly the MPS representation—was introduced as a scalable and physically grounded framework for describing quantum many-body systems. By leveraging the entanglement structure characteristic of ground states of local Hamiltonians, especially those obeying area-law scaling, this approach circumvents the exponential growth of the Hilbert space. Within this setting, the VUMPS algorithm was employed as an efficient variational method tailored to the thermodynamic limit, allowing for the accurate approximation of

ground states in translationally invariant one-dimensional models.

In this final chapter, the tools developed throughout the dissertation were employed to probe the entanglement structure encoded in the unit cell of the infinite MPS representation. Particular attention was given to the behavior of the genuine multipartite negativity across the quantum critical point of the transverse-field quantum Ising model. It was found that, in the thermodynamic limit, the multinegativity associated with the unit cell exhibits a logarithmic divergence as the system approaches criticality. These findings highlight that genuinely multipartite entanglement is not merely a formal construct, but a physically relevant quantity capable of capturing the sensitivity of quantum systems to their underlying interactions. In the context of the transverse-field Ising model, the observed critical scaling of the multinegativity reinforces its utility as an entanglement-based diagnostic for quantum phase transitions. This perspective opens new directions for future research, particularly in the exploration of more complex quantum systems that lack conventional local order parameters. In this regard, models such as the extended Hubbard Hamiltonian—characterized by a rich interplay of competing interactions and elusive quantum phases—emerge as natural candidates for the application of multipartite entanglement-based probes [44].

The exploration conducted in the latter part of this dissertation was motivated by a fundamental question: how can one reliably infer structural properties of a global quantum state that remains operationally inaccessible, by performing local operations or reductions to a small number of subsystems? This line of inquiry naturally led to a deeper investigation into the nature of quantum state reduction and the role of unbiased operations. To this end, a framework was proposed in which local projective measurements are selected not arbitrarily, but rather based on principled criteria aimed at preserving the essential informational and structural features of the original state. Numerical results supported the idea that projections in the σ^y basis act as minimally invasive reductions in the transverse-field Ising model, offering a practical realization of the theoretical criteria established.

While preliminary, these results point toward a broader paradigm in which structure-preserving reductions may serve as effective tools for extracting physically meaningful information from complex quantum systems. The formulation of a conjecture linking unbiasedness to the simultaneous preservation of symmetry, coherence, and entanglement provides a conceptual anchor for future investigations. This remains an ongoing line of research, with several open directions: extending the framework to higher-dimensional systems, incorporating noise and decoherence, and exploring experimental realizations in quantum simulation platforms.

Bibliography

[1] EINSTEIN, A., B. PODOLSKY, and N. ROSEN: *Can Quantum-Mechanical Description of Physical Reality Be Considered Complete?* Physical Review, 47:777–780, 1935. Cited on page 11.

[2] BOHR, N.: *Can Quantum-Mechanical Description of Physical Reality be Considered Complete?* Physical Review, 48:696–702, 1935. Cited on page 11.

[3] HOWARD, D.: *Albert Einstein as a philosopher of science*. Physics Today, 58:34–40, 2005. Cited on page 11.

[4] WHITAKER, A.: *Einstein, Bohr and the quantum dilemma: From quantum theory to quantum information*. Cambridge University Press, Cambridge, revised edition, 2006. Cited on page 11.

[5] COSTA, A. and R. ANGELO: *Quantifying the nonclassicality of operations*. Physical Review A, 93:020103, 2016. Cited on page 11.

[6] BILOBRAN, J. and R. ANGELO: *A measure of physical reality*. Europhysics Letters, 112:40005, 2015. Cited on page 11.

[7] ORTHEY JR, A. and R. ANGELO: *Quantum realism: Axiomatization and quantification*. PHYSICAL REVIEW A, 105:052218, 2022. Cited on page 11.

[8] BOHM, D.: *A Suggested Interpretation of the Quantum Theory in Terms of "Hidde" Variables. I*. Physical Review, 85:166–193, 1952. Cited on page 11.

[9] GOLDSTEIN, S.: *Bohmian Mechanics*. The Stanford Encyclopedia of Philosophy, 2001. Available at: https://plato.stanford.edu/entries/qm-bohm/. Cited on page 11.

[10] BELL, J.: *On the Einstein Podolsky Rosen paradox*. Physics Physique Fizika, 1:195–200, 1964. Cited on page 11.

[11] ASPECT, A., J. DALIBARD, and G. ROGER: *Experimental test of Bell's inequalities using time-varying analyzers*. Physical Review Letters, 49:1804–1807, 1982. Cited 2 times on pages 11 and 25.

[12] WEIHS, G. et al.: *Violation of Bell's inequality under strict Einstein locality conditions*. Physical Review Letters, 81:5039–5043, 1998. Cited on page 11.

[13] HENSEN, B. et al.: *Loophole-free Bell inequality violation using electron spins separated by 1.3 kilometres*. Nature, 526:682–686, 2015. Cited on page 11.

[14] BRUNNER, N. et al.: *Bell nonlocality*. Reviews of Modern Physics, 86:419–478, 2014. Cited on page 12.

[15] SCIENCES, THE ROYAL SWEDISH ACADEMY OF: *The Nobel Prize in Physics 2022: Alain Aspect, John F. Clauser and Anton Zeilinger*, 2022. Available at: https://www.nobelprize.org/prizes/physics/2022/summary/. Cited on page 12.

[16] HORODECKI, R. et al: *Quantum entanglement*. Reviews of Modern Physics, 81:865–942, 2009. Cited 2 times on pages 12 and 25.

[17] AMICO, L. et al.: *Entanglement in many-body systems*. Reviews of Modern Physics, 80:517–576, 2008. Cited 4 times on pages 12, 13, 44, and 47.

[18] WERNER, R. F.: *Quantum states with Einstein-Podolsky-Rosen correlations admitting a hidden-variable model*. Physical Review A, 40:4277–4281, 1989. Cited on page 12.

[19] HORODECKI, M., P. HORODECKI, and R. HORODECKI: *Separability of mixed states: necessary and sufficient conditions*. Physics Letters A, 223:1–8, 1996. Cited 3 times on pages 12, 23, and 34.

[20] VIDAL, G.: *Entanglement monotones*. Journal of Modern Optics, 47:355–376, 2000. Cited 2 times on pages 12 and 26.

[21] VEDRAL, V. et al: *Quantifying Entanglement*. Physical Review Letters, 78:2275–2279, 1997. Cited 2 times on pages 12 and 30.

[22] WOOTTERS, W.: *Entanglement of Formation of an Arbitrary State of Two Qubits*. Physical Review Letters, 80:2245–2248, 1998. Cited 2 times on pages 12 and 29.

[23] VIDAL, G. and R. WERNER: *A computable measure of entanglement*. Physical Review A, 65:032314, 2002. Cited 2 times on pages 12 and 32.

[24] BENNETT, C. et al.: *Teleporting an unknown quantum state via dual classical and Einstein-Podolsky-Rosen channels*. Physical Review Letters, 70:1895–1899, 1993. Cited 2 times on pages 12 and 25.

[25] NIELSEN, M. and I. CHUANG: *Quantum Computation and Quantum Information*. Cambridge University Press, Cambridge, 10th anniversary edition, 2010. Cited 3 times on pages 12, 20, and 25.

[26] BARNETT, S.: *Quantum Information*. Oxford University Press, Oxford, 1st edition, 2009. Cited 2 times on pages 12 and 26.

[27] BENNETT, C. and G. BRASSARD: *Quantum cryptography: Public key distribution and coin tossing*. Theoretical Computer Science, 560:7–11, 2014. Cited on page 12.

[28] EKERT, A.: *Quantum cryptography based on Bell's theorem*. Physical Review Letters, 67:661–663, 1991. Cited on page 12.

[29] YIN, J. et al.: *Satellite-based entanglement distribution over 1200 kilometers*. Science, 356:1140–1144, 2017. Cited on page 12.

[30] ARUTE, F. et al.: *Quantum supremacy using a programmable superconducting processor*. Nature, 574:505–510, 2019. Cited on page 13.

[31] ZHONG, H. S. et al.: *Quantum computational advantage using photons*. Science, 370:1460–1463, 2020. Cited on page 13.

[32] Brandão, F. et al.: *Quantum SDP Solvers: Large Speed-ups, Optimality, and Applications to Quantum Learning*, 2019. Cited on page 13.

[33] GILYÉN, A. et al.: *Quantum Singular Value Transformation and Beyond: Exponential Improvements for Quantum Matrix Arithmetics*. Proceedings of the 51st ACM Symposium on Theory of Computing (STOC), pages 193–204, 2019. Cited on page 13.

[34] ORÚS, R., S. MUGUEL, R. SOMMA, and E. LIZASO: *Quantum computing for finance: Overview and prospects*. Reviews in Physics, 4:100028, 2019. Cited on page 13.

[35] REBENTROST, P., B. GUPTA, and T. BROMLEY: *Quantum computational finance: Monte Carlo pricing of financial derivatives*. Physiscal Review A, 98:022321, 2018. Cited on page 13.

[36] WOERNER, S. and D. EGGER: *Quantum risk analysis*. npj Quantum Information, 5:15, 2019. Cited on page 13.

[37] OSTERLOH, A. et al: *Scaling of entanglement close to a quantum phase transition*. Nature, 416:608–610, 2002. Cited 3 times on pages 13, 81, and 82.

[38] VIDAL, G. et al: *Entanglement in quantum critical phenomena*. Physical Review Letters, 90:227902, 2003. Cited 2 times on pages 13 and 44.

[39] Wen-Long, Y., L. Ying-Wai, and Shi Jian G.: *Fidelity, dynamic structure factor, and susceptibility in critical phenomena*. Physical Review E, 76:022101, 2007. Cited on page 13.

[40] KITAEV, A.: *Fault-tolerant quantum computation by anyons*. Annals of Physics, 303:2–30, 2003. Cited on page 14.

[41] KITAEV, A. and J. PRESKILL: *Topological entanglement entropy*. Physical Review Letters, 96:110404, 2006. Cited on page 14.

[42] LEVIN, M. and X. WEN: *Detecting topological order in a ground state wave function*. Physical Review Letters, 96:110405, 2006. Cited on page 14.

[43] Iemini, F., T. Maciel, and R. Vianna: *Entanglement of indistinguishable particles as a probe for quantum phase transitions in the extended Hubbard model.* Physical Review B, 92:075423. Cited on page 14.

[44] Ferreira, D. et al: *Quantum correlations, entanglement spectrum, and coherence of the two-particle reduced density matrix in the extended Hubbard model.* Physical Review B, 105:115145, 2022. Cited 2 times on pages 14 and 87.

[45] ASHCROFT, N. and N. MERMIN: *Solid State Physics.* Cengage Learning, New York, 1976. Cited on page 14.

[46] KITTEL, C.: *Introduction to Solid State Physics.* John Wiley & Sons, Hoboken, 8th edition, 2005. Cited on page 14.

[47] SACHDEV, S.: *Quantum Phase Transitions.* Cambridge University Press, Cambridge, 2nd edition, 2011. Cited 3 times on pages 14, 44, and 46.

[48] GIRVIN, S. and K. YANG: *Modern Condensed Matter Physics.* Cambridge University Press, Cambridge, 2019. Cited on page 14.

[49] ZAUNER-STAUBER, V. et al.: *Variational optimization algorithms for uniform matrix product states.* Physical Review B, 97:045145, 2018. Cited 3 times on pages 15, 69, and 70.

[50] al., ZAUNER STauber V. et: *Topological nature of spinons and holons: Elementary excitations from matrix product states with conserved symmetries.* Cited 2 times on pages 15 and 69.

[51] Laurens VANDESTRAETEN, L., J. HAEGEMAN, and F. VERSTRAETE: *Tangent-space methods for uniform matrix product states.* SciPost Physics Lectures Notes, page 7, 2019. Cited on page 15.

[52] SCHOLLWÖCK, U.: *The density-matrix renormalization group in the age of matrix product states.* Annals of Physics, 326:96–192, 2011. Cited 4 times on pages 15, 47, 63, and 67.

[53] HASTINGS, M. B.: *An area law for one-dimensional quantum systems.* Journal of Statistical Mechanics: Theory and Experiment, 2007:P08024, 2007. Cited on page 15.

[54] OSBORNE, T.: *Efficient approximation of the dynamics of one-dimensional quantum spin systems.* Physical Review Letters, 97:157202, 2006. Cited on page 15.

[55] VERSTRAETE, F. and J. CIRAC: *Matrix product states represent ground states faithfully.* Physical Review B, 73:094423, 2006. Cited on page 15.

[56] EISBERG, R. and R. RESNICK: *Quantum Physics of Atoms, Molecules, Solids, Nuclei, and Particles.* Wiley, New York, 2nd edition, 1985. Cited on page 17.

[57] GRIFFITHS, D. and D. SCHROETER: *Introduction to Quantum Mechanics*. Cambridge University Press, Cambridge, 3rd edition, 2018. Cited on page 17.

[58] SAKURAI, J. and J. NAPOLITANO: *Modern Quantum Mechanics*. Cambridge University Press, Cambridge, 3rd edition, 2021. Cited on page 17.

[59] COHEN-TANNOUDJI, C., B. DIU, and F. LALOË: *Quantum Mechanics*. Wiley-VCH, Weinheim, 2nd edition, 2019. Cited on page 17.

[60] COHEN-TANNOUDJI, C., B. DIU, and F. LALOË: *Quantum Mechanics*. Wiley-VCH, Weinheim, 2nd edition, 2019. Cited on page 17.

[61] BALLENTINE, L.: *Quantum Mechanics: A Modern Development*. World Scientific, Singapore, 2nd edition, 2014. Cited 3 times on pages 17, 18, and 19.

[62] BENGTSSON, I. and K. ŻYCZKOWSKI: *Geometry of Quantum States: An Introduction to Quantum Entanglement*. Cambridge University Press, Cambridge, 1st edition, 2006. Cited 3 times on pages 17, 20, and 26.

[63] BREUER, H. and F. PETRUCCIONE: *The Theory of Open Quantum Systems*. Oxford University Press, Oxford, 2002. Cited on page 17.

[64] KWIAT, P. et al.: *New high-intensity source of polarization-entangled photon pairs*. Physical Review Letters, 75:4337–4341, 1995. Cited on page 25.

[65] BLATT, R. and D. WINELAND: *Entangled states of trapped atomic ions*. Nature, 453:1008–1015, 2008. Cited on page 25.

[66] KJÆRGAARD, M. et al.: *Superconducting Qubits: Current State of Play*. Annual Review of Condensed Matter Physics, 11:369–395, 2020. Cited 2 times on pages 25 and 47.

[67] BLOCH, I., J. DALIBARD, and W. ZWERGER: *Many-body physics with ultracold gases*. Rev. Mod. Phys., 80:885–964, 2008. Cited 2 times on pages 25 and 47.

[68] DOHERTY, M. W., N. B. MAZOUREK, M. MOTTISHOW, T. M. STACE, F. JELEZKO, P. WACHTER, L. T. HALL, R. J. HINDE, and A. D. GREENTREE: *The nitrogen-vacancy colour centre in diamond*. Physics Reports, 528:1–45, 2013. Cited on page 25.

[69] BARENCO, A., C. H. BENNETT, R. CLEVE, D. P. DI VINCENZO, N. MARGOLUS, P. SHOR, T. SLEATOR, J. A. SMOLIN, and H. WEINER: *Elementary gates for quantum computation*. Physical Review A, 52:3457–3467, 1995. Cited on page 25.

[70] PRESKILL, J.: *Quantum Computing in the NISQ era and beyond*. Quantum, 2:79, 2018. Cited on page 25.

[71] PARIS, M. and J. ŘEHÁČEK: *Quantum State Estimation*. Heidelberg, 1st edition, 2010. Cited on page 25.

[72] TSALLIS, C., S. LLOYD, and M. BARANGER: *Canonical density matrix and Rényi entropy*. Physical Review A, 63:042104, 2001. Cited on page 30.

[73] AUDENAERT, K.: *Subadditivity of q-entropies for $q > 1$*. Journal of Mathematical Physics, 48:083507, 2007. Cited on page 30.

[74] MÜLLER-LENNERT, M. et al.: *On quantum Rényi entropies: a new generalization and some properties*. Journal of Mathematical Physics, 54:122203, 2013. Cited on page 30.

[75] VIDAL, G. and R. TARRACH: *Robustness of entanglement*. Physical Review A, 59:141–155, 1999. Cited on page 31.

[76] David A. MEYER, D., NOLAN, and R. Wallach: *Global entanglement in multiparticle systems*. Physical Review A, 66:012327, 2002. Cited on page 39.

[77] JUNGNITSCH, B., T. MORODER, and O. GÜHNE: *Taming multiparticle entanglement*. Physical Review Letters, 106:190502, 2011. Cited on page 40.

[78] HOFMANN, M., T. MORODER, and O. GÜHNE: *Analytical characterization of the genuine multiparticle negativity*. Journal of Physics A: Mathematical and Theoretical, 47:155301, 2014. Cited 2 times on pages 40 and 82.

[79] HOFMANN, M., O. GÜHNE, and T. MORODER: *Genuine multiparticle entanglement from local observables*. Physical Review Letters, 111:060403, 2013. Cited on page 40.

[80] SALINAS, S.: *Introdução à Física Estatística*. EDUSP, São Paulo, 2nd edition, 2008. Cited 3 times on pages 42, 44, and 45.

[81] PATHRIA, R. and P. BEALE: *Statistical Mechanics*. Elsevier, Amsterdam, 4rd edition, 2021. Cited 2 times on pages 42 and 44.

[82] LANDAU, L. and E. LIFSHITZ: *Statistical Physics: Part 1*. Butterworth-Heinemann, Oxford, 3rd edition, 2000. Cited 3 times on pages 42, 44, and 45.

[83] VAN DER WAALS, J.: *Over de Continuïteit van den Gas- en Vloeistoftoestand*. PhD thesis, Universiteit Leiden, Leiden, 1873. PHD dissertation. Cited on page 43.

[84] VAN DER WAALS, J.: *On the Continuity of the Gaseous and Liquid States*. In *Collected Papers of J. D. van der Waals*. Martinus Nijhoff, The Hague, 1959. Cited on page 43.

[85] ISING, E.: *Beitrag zur Theorie des Ferromagnetismus*. Zeitschrift für Physik, 31:253–258, 1925. Cited on page 44.

[86] CALABRESE, P. and J. CARDY: *Entanglement entropy and quantum field theory*. Journal of Statistical Mechanics, page P06002, 2004. Cited on page 44.

[87] BAYAT, A., S. BOSE, and H. JOHANNESSON (editors): *Entanglement in Spin Chains: From Theory to Quantum Technology Applications*. Quantum Science and Technology. Springer Cham, Cham, 2023, ISBN 978-3-031-03998-0. Cited on page 44.

[88] ONSAGER, L.: *Crystal Statistics. I. A Two-Dimensional Model with an Order-Disorder Transition*. Physical Review, 65:117–149, 1944. Cited on page 45.

[89] ZHANG, D.: *Exact Solution for Three-Dimensional Ising Model*. Symmetry, 13:1837, 2021. Cited on page 45.

[90] KARDAR, M.: *Statistical Physics of Fields*. Cambridge University Press, Cambridge, 2007, ISBN 978-0521873413. Cited 2 times on pages 45 and 46.

[91] CARDY, J.: *Scaling and Renormalization in Statistical Physics*. Cambridge University Press, Cambridge, 1996. Cited 2 times on pages 45 and 46.

[92] TONG, D.: *Statistical Physics*, 2012. https://www.damtp.cam.ac.uk/user/tong/statphys.html, Lecture notes, University of Cambridge. Cited on page 45.

[93] TONG, D.: *Statistical Field Theory*, 2014. https://www.damtp.cam.ac.uk/user/tong/sft.html, Lecture notes, University of Cambridge. Cited on page 45.

[94] HSIEH, T.: *Quantum Phase Transitions: Mapping between Classical and Quantum Systems*, 2012. https://web.mit.edu/8.334/www/grades/projects/projects12/TimHsieh.pdf, Project report for MIT course 8.334. Cited on page 46.

[95] SUZUKI, M.: *Relationship between d-dimensional quantal spin systems and $(d+1)$-dimensional Ising systems*. Progress of Theoretical Physics, 56:1454–1469, 1976. Cited on page 46.

[96] WHITE, S. R.: *Density matrix formulation for quantum renormalization groups*. Physical Review Letters, 69:2863–2866, 1992. Cited 2 times on pages 47 and 59.

[97] WHITE, S. R.: *Density-matrix algorithms for quantum renormalization groups*. Physical Review B, 48:10345–10356, 1993. Cited on page 47.

[98] ÖSTLUND, S. and S. ROMMER: *Thermodynamic Limit of Density Matrix Renormalization*. Physical Review Letters, 75:3537–3540, 1995. Cited 2 times on pages 47 and 59.

[99] BLATT, R. and C. F. ROOS: *Quantum simulations with trapped ions*. Nature Physics, 8:277–284, 2012. Cited on page 47.

[100] BROWAEYS, A. and T. LAHARIE: *Many-body physics with individually controlled Rydberg atoms*. Nature Physics, 16:132–142, 2020. Cited on page 47.

[101] VERSTRAETE, F. and J. I. CIRAC: *Renormalization algorithms for quantum-many body systems in two and higher dimensions*. arXiv preprint, 2004. Available at: https://arxiv.org/abs/cond-mat/0407066. Cited on page 59.

[102] VIDAL, G.: *Entanglement renormalization*. Physical Review Letters, 99:220405, 2007. Cited on page 59.

[103] SHI, Y., L. DUAN, and G. VIDAL: *Classical simulation of quantum many-body systems with a tree tensor network*. Physical Review A, 74:022320, 2006. Cited on page 59.

[104] MARKOV, I. and Y. SHAYEBAZANOVA: *Simulating quantum computation by contracting tensor networks*. SIAM Journal on Computing, 38:81–103, 2008. Cited on page 59.

[105] PEDNAULT, E. et al.: *Breaking the 49-qubit barrier in the simulation of quantum circuits*. arXiv preprint, 2017. Available at: https://https://arxiv.org/pdf/1710.05867v1. Cited on page 59.

[106] LEVIN, M. and C. NAVE: *Tensor renormalization group approach to two-dimensional classical lattice models*. Physical Review Letters, 99:120601, 2007. Cited on page 59.

[107] GU, Z. and X. WEN: *Tensor-entanglement-filtering renormalization approach and symmetry-protected topological order*. Physical Review B, 78:205116, 2008. Cited on page 59.

[108] STOUDENMIRE, E. M. and D. J. SCHWAB: *Supervised learning with tensor networks*. Advances in Neural Information Processing Systems (NeurIPS), 29, 2016. Cited on page 59.

[109] CHEN, J. et al: *On the expressive power of deep learning: A tensor analysis*. Journal of Machine Learning Research, 22:1–42, 2021. Cited on page 59.

[110] ORÚS, R.: *A practical introduction to tensor networks: Matrix product states and projected entangled pair states for quantum many-body physics*. Annals of Physics, 349:117–158, 2014. Cited on page 63.

[111] FISHMAN, M. et al.: *The ITensor Software Library for Tensor Network Calculations*. SciPost Phys. Codebases, page 4, 2022. https://scipost.org/10.21468/SciPostPhysCodeb.4. Cited on page 77.

[112] FISHMAN, M. et al.: *Codebase release 0.3 for ITensor*. SciPost Phys. Codebases, pages 4–r0.3, 2022. https://scipost.org/10.21468/SciPostPhysCodeb.4-r0.3. Cited on page 77.

[113] BAUMGRATZ, T., CRAMER M. PLENIO M.: *Quantifying coherence*. Physical Review Letters, 113:140401, 2014. Cited on page 84.

Appendix

APPENDIX A – Digression on the computational problems

This appendix offers a technical digression on the manual implementation of the Variational Uniform Matrix Product States (VUMPS) algorithm, developed in the context of this dissertation, and on the hands-on process of "tightening the bolt" in computational physics problems—where physical insight, numerical methods, and programming intricacies converge.

While the VUMPS algorithm is a well-established and widely adopted method for obtaining ground states in infinite one-dimensional quantum systems, it is typically implemented using advanced tensor network libraries such as `ITensor`, which provide highly optimized routines and efficient contraction schemes. In contrast, the present implementation was deliberately constructed without relying on such high-level libraries. Instead, tensor contractions were explicitly programmed using `TensorOperations`, a Julia package that provides Einstein summation capabilities via the `ncon`-style notation. Additionally, linear algebra operations such as spectral decompositions and iterative solvers were handled via the `Arpack`, `LinearMaps`, and `IterativeSolvers` packages.

A particularly didactic approach following this same philosophy of building tensor network algorithms step by step can be found in the `TensorNet` webpage maintained by Glen Evenbly. That project offers carefully structured implementations of canonical algorithms such as DMRG, TEBD, and MERA, built from first principles and using explicit index contractions. More broadly, this approach highlights a recurring trade-off in computational physics: fully optimized code is often more "unreadable" than readable—that is, performance tends to come at the expense of readability and pedagogical value. In this sense, writing the first version of an algorithm using only low-level `ncon`-style contractions becomes not only instructive, but also foundational for understanding the structure and flow of more abstract or black-box implementations.

To illustrate the contraction syntax, consider a simple example in which two rank-2 tensors A and B are contracted over a shared index. Specifically, the contraction $\sum_m A_i^m B_m^j$ corresponds to a standard matrix multiplication, and can be implemented in Julia using the `ncon` function as follows:

```
ncon((A, B), ([-1, 1], [1, -2])).
```

In this notation, negative integers denote *free indices*, which are preserved in the output tensor, while positive integers represent *contracted indices*, summed over all matching occurrences. In the example above, the index labeled m is internal (shared label `1`) and is contracted, while indices i and j are external and preserved, corresponding to positions `-1` and `-2`, respectively.

A crucial aspect of working directly with `ncon` is the careful bookkeeping of index labels. The `ncon` function contracts tensors by following the numerical ordering of index labels (i.e., contractions

are performed in the order $1 \to 2 \to 3 \to \ldots$). As a result, it becomes essential to assign index labels in a way that both respects the desired contraction order and avoids ambiguities or redundant computations. Incorrect index enumeration may lead to logical errors or severe performance degradation, especially in large or nested contraction sequences.

In practice, the partial trace operation—illustrated in Fig. 3c—can be implemented for a four-leg density tensor by contracting over the degrees of freedom associated with the traced-out subsystem. For example, the one-site reduced density matrix ρ_1 can be obtained from a rank-4 global density tensor ρ using the following `ncon` call:

$$\rho_1 = \texttt{ncon}(\rho, ([-1, 1, -2, 1])) \tag{A.1}$$

Here, the repeated index `1` denotes contraction over the traced subsystem, while the negative indices `-1` and `-2` label the remaining open legs corresponding to the retained site.

Manual Implementation of the VUMPS Algorithm

Here, the algorithm assumes as input a nearest-neighbor Hamiltonian of the form $H = \sum_i h_{i,i+1}$, where $h_{i,i+1}$ acts nontrivially only on two adjacent sites. Given this local structure, one can initialize the MPS ansatz by randomly generating three tensors: a left-isometric tensor A_L, a right-isometric tensor A_R, and a central tensor C encoding the entanglement spectrum between neighboring sites. From these initial tensors, the full center tensor A_C is formed via the contraction:

$$A_C = \texttt{ncon}((A_L, C), ([-1, -2, 1]), ([1, -3])). \tag{A.2}$$

Moreover, it is clear that the transfer matrix can be defined by contracting a tensor A_L with its conjugate $\bar{A}_L$ over the physical leg, resulting in a linear map acting on the virtual space. For instance, the left transfer operator T_L can be implemented as:

$$T_L = \texttt{ncon}((A_L, \bar{A}_L,), ([-1, 1, -2], [-3, 1, -4])). \tag{A.3}$$

With these definitions, one can proceed to compute the effective environment Hamiltonians H_L and H_R by following the procedure detailed in the main text: solving non-homogeneous linear systems defined by the residual equations of the VUMPS fixed-point conditions. These systems are typically addressed using iterative Krylov-space methods such as GMRES, implemented in numerical libraries like `IterativeSolvers.jl`.

However, despite being well-established in the literature, the application of these solvers in practice is far from trivial. Achieving efficient performance requires careful tuning of several optimization parameters, such as the maximum size of the Krylov subspace, convergence tolerances, and initial guesses. These choices can significantly impact both convergence speed and numerical stability. At the same time, introducing such low-level optimizations often comes at the expense of code readability and pedagogical transparency. This trade-off highlights: the more optimized a code becomes, the less accessible it tends to be.

At this stage, all the ingredients are available to reproduce the diagrammatic constructions shown in Figs. 9–12 in fully contracted computational form. The left and right transfer matrices, the effective Hamiltonians H_L and H_R, and their actions on the central tensors C and A_C can all be expressed as combinations of tensor contractions following the indexing rules discussed previously. With these components in place, the full VUMPS algorithm can be implemented as a self-consistent fixed-point iteration:

Algorithm 1 Simplified Pseudocode for the VUMPS Algorithm

Initialize random tensors A_L, A_R, and C
Form center tensor $A_C \leftarrow \texttt{ncon}((A_L, C), (-1, -2, 1), (1, -3))$
for each iteration $p = 1, \ldots, n_{\text{int}}$ do
    Compute transfer matrices and their largest eigenvectors: R from A_L, L from A_R
    Construct effective Hamiltonians h_L, h_R by contracting A_L, A_R, h, and R, L
    Subtract energy densities to define the renormalized energies $\tilde{h}_L$, $\tilde{h}_R$
    Solve for H_L, H_R via GMRES (i.e. solving non-homogeneous linear systems)
    Optimize C by solving $\mathcal{H}_{\text{eff}} C = \lambda C$
    Optimize A_C similarly
    Decompose A_C using SVD to update A_L and A_R
    Check convergence: $\|A_C - A_L C\|$ and $\|A_C - A_R C\|$
    if converged then
        break
    end if
end for
return Optimized tensors A_L, A_R, C